Relationship between degree of branching, carbon number distribution and the low temperature fluidity of jet fuel

TS Joubert

orcid.org/ 0000-0003-4995-3374

Dissertation submitted in fulfilment of the requirements for the degree *Master of Science in Chemistry* at the

North-West University

Supervisor: Prof CA Strydom

Co-supervisor: Dr RJJ Nel

Graduation: May 2018

23527153

Abstract

For the past sixty years, the freeze point specification of jet fuel was considered the most important property for ensuring that jet fuels in the market were fit for use at low temperatures. More recently, Original Equipment Manufacturers (OEMs) in the aviation industry have established that appropriate fuel atomisation within the aircraft Auxiliary Power Unit (APU) can only occur at fuel viscosities below 12 cSt. It was further discovered that some jet fuels currently in the market might exceed the 12 cSt viscosity threshold as the fuel approaches the freeze point specification maximum. As a result of the concerns raised by aviation industry OEMs, ASTM International is currently investigating the validity of these claims, as well as means to mitigate the risk.

It is therefore anticipated that the focus on the low temperature fluidity of jet fuel, which is governed by visocity and freeze point, will grow rapidly in the near future and that specifications that are more stringent may be applied to commercial jet fuel products. The effect of molecular branching and carbon number distribution on the low temperature fluidity characteristics of synthetic jet fuel was thus investigated to gain a better understanding of these relationships.

This research was conducted to prove or disprove the following hypothesis:

> *There exists an ideal i:n ratio and an ideal carbon number distribution that enables the production of jet fuel, which possesses the best low temperature fluidity properties attainable.*

In the literature study, it was observed that the physical properties of the molecules present in jet fuel vary significantly. Molecular modelling techniques were hence used to identify the molecular properties that affect the viscosity and freeze point behaviour of the molecules typically present in jet fuel. The molecular modelling study yielded models for prediction of the viscosities and freeze points of n- and iso-paraffins in the C_4 – C_{20} carbon number range.

Furthermore, statistical mixture design techniques were employed to study the effect of variation in iso-paraffin to n-paraffin (i:n) mass ratio and carbon number distribution on the viscosity and freeze point of synthetic jet fuel. To facilitate the mixture design study, n- and iso-paraffin mixture components in the C_9 – C_{18} carbon number range were produced from existing refinery products by means of fractional distillation.

The viscosity model obtained from the molecular modelling study exhibited satisfactory regression statistics and achieved high viscosity prediction accuracy for all the molecules considered. However, the freeze point model obtained from the molecular modelling study exhibited low regression model precision. Furthermore, the inaccuracy of the freeze point model

also became apparent during the validation process. The poor results with regard to prediction of freeze points were attributed to the inability of the model to account for the crystal formation characteristics of paraffinic molecules.

The viscosity model obtained from the mixture design study exhibited good regression statistics and validation results. It was consequently concluded that the model could be used to predict viscosity as a function of the i:n mass ratio and carbon number distribution for jet fuels in the C_9 – C_{18} carbon number range. The freeze point model obtained from the mixture design studies also exhibited good regression statistics; however, the model could not be validated and it was concluded that the freeze point model must be used with caution.

Similar to the Quantitative Structure-Activity Relationship (QSAR) freeze point model, the mixture design model for freeze point could not account for the crystal formation characteristics of the mixture components. This is ascribed to freeze point being a function of the crystallisation characteristics of individual molecules present in jet fuel, rather than due to the bulk properties of the fuel.

Despite the shortcomings demonstrated for the freeze point model, the mixture design optimisation studies proved that it was possible to determine the ideal i:n mass ratio and carbon number distribution ranges that would enable the production of jet fuel that possesses the best low temperature fluidity properties attainable.

Keywords: Jet fuel; synthetic jet fuel; viscosity; freeze point; molecular branching; molecular modelling; mixture design.

Acknowledgements

I herein express my sincerest gratitude towards:

- Our Heavenly Father for giving me the strength not only to pursue this dissertation, but also to see it through to the end.
- Dr. Reinier Nel for his willingness to walk down this path with me. All the nights and weekends he devoted to this research are much appreciated. Without his guidance and patience, I would never have come this far. He always challenged me and pushed me to do better, and for that, I am extremely grateful.
- Prof. Christien Strydom for her guidance and support throughout this research. She did not know me at all, yet she agreed to be my supervisor without hesitation. I am extremely grateful that our paths crossed.
- Dr. Carl Viljoen for his enthusiasm, help and guidance. He taught me so many things and was always willing to share his knowledge with me. The many debates and discussions opened my eyes to new perspectives and will never be forgotten.
- Dr. Roelof Coetzer for sharing his wealth of knowledge in the field of statistics with me. Without Roelof's contributions and guidance, this dissertation would never have materialized.
- Dr. Johan Coetzee, Energy Technology Management and SASOL for giving me the opportunity to pursue my studies.
- Rudey Brittz for allowing me the time to complete my studies and for his support throughout the whole process.
- My daughter Luanè, for sacrificing our playtime so that I could work on my dissertation, and for the much-needed laughter when I was stressed and sad.
- Last, but not least, my wife Rozanè for her unwavering support throughout all the years. Without her love, devotion and encouragement, I would never have come this far. I truly am the luckiest man on earth for having her as friend, companion and wife.

To my wife and daughter.

Table of Contents

Abstract i
Acknowledgements iii
Table of Contents v
List of Figures ix
List of Tables xi
Abbreviations xiii
Chapter 1 : Introduction 1
1.1. Background 1
1.1.1. Aviation industry history 1
1.1.2. Jet fuel composition overview 3
1.1.3. Low temperature operability of aircraft components 4
1.1.4. Low temperature viscosity of jet fuel 5
1.2. Problem statement 6
1.3. Research aim 7
1.4. Research objectives 7
1.5. Dissertation outline 7
Chapter 2 : Literature Review 10
2.1. Introduction 10
2.2. Crude oil refineries 10
2.2.1. Paraffins 10
2.2.2. Olefins 10
2.2.3. Naphthenes 10
2.2.4. Aromatics 11
2.2.5. Heteroatomic compounds 11
2.2.6. Crude oil refining 11
2.2.7. Separation 12
2.2.8. Conversion 14
2.2.9. Purification 15
2.2.10. Blending refined petroleum products 16
2.3. Synthetic fuel refineries 16
2.3.1. Synthesis gas production 18
2.3.2. Fischer-Tropsch synthesis 19
2.3.3. Product upgrading 19
2.3.4. Blending of fully refined Fischer-Tropsch products 20
2.4. Introduction to jet fuel as refining distillate 20
2.4.1. Volatility 22
2.4.2. Fluidity 22

2.4.3. Combustion 23
2.4.4. Corrosion 24
2.4.5. Thermal stability 24
2.4.6. Contaminants 24
2.4.7. Additives 25
2.4.8. Composition 25
2.4.9. Additional requirements for jet fuel containing synthesised hydrocarbons 25
2.5. Effect of chemical composition on jet fuel properties 26
2.5.1. Physical properties of hydrocarbon classes 26
2.5.2. Intermolecular forces 33
2.6. Conclusion 34
Chapter 3 : Experimental Procedures 36
3.1. Introduction 36
3.2. Molecular modelling 36
3.2.1. Establish datasets 37
3.2.2. Drawing of molecular structures and geometry optimisation 40
3.2.3. QSAR molecular properties 40
3.2.4. Model development 41
3.2.5. Model validation 42
3.3. Fractional distillation 43
3.3.1. Refinery products distilled 43
3.3.2. Distillation apparatus 43
3.3.3. Reference distillation points 44
3.3.4. n-Paraffin distillation 45
3.3.5. iso-Paraffin distillation 46
3.4. Analytical techniques 46
3.4.1. Freeze point analysis 46
3.4.2. Kinematic viscosity and density analysis 47
3.4.3. GCxGC analysis 47
3.5. n-Paraffin and iso-paraffin mixture design 48
3.5.1. Design-Expert® parameters 49
3.5.2. Specification of model type 50
3.5.3. Candidate mixture set 50
3.5.4. Mixture design 51
3.5.5. Mixture preparation and analyses 51
3.5.6. Statistical evaluation of the model 53
3.5.7. Model validation 53
3.5.8. Ideal jet fuel mixtures 54

Chapter 4 : QSAR Models for Viscosity Prediction 57
4.1. Introduction 57
4.2. Definition of statistical terms 57
4.2.1. Coefficient of determination 58
4.2.2. Adjusted R^2 58
4.2.3. Standard error 58
4.2.4. P-values 58
4.2.5. Confidence intervals 58
4.2.6. Standardised residuals 58
4.3. Viscosity prediction models 59
4.3.1. Viscosity prediction model: Four molecular descriptors 59
4.3.2. Viscosity prediction model validation: Four molecular descriptors 61
4.3.3. Viscosity prediction model: Three molecular descriptors 65
4.3.4. Viscosity prediction model validation: Three molecular descriptors 68
4.3.5. Final viscosity model discussion 70
4.4. Conclusion 72
4.5. Recommendations 73
Chapter 5 : QSAR Model for Freeze Point Prediction 74
5.1. Introduction 74
5.2. Freeze point prediction model 74
5.3. Freeze point prediction model validation 77
5.3.1. Standardised residuals 77
5.3.2. LMO validation 79
5.3.3. Freeze point prediction of non-dataset molecules 81
5.4. Final freeze point model discussion 82
5.4.1. Total molecular mass 82
5.4.2. Molecular density 82
5.4.3. Topological indices 82
5.5. Conclusion 84
Chapter 6 : Fractional Distillation Results 85
6.1. Introduction 85
6.2. n-Paraffin mixture components 85
6.2.1. Fractionation results 85
6.2.2. n-Paraffin mixture component GCxGC results 86
6.2.3. n-Paraffin mixture component physical properties 88
6.3. iso-Paraffin mixture components 89
6.3.1. Fractionation results 89
6.3.2. iso-Paraffin mixture component GCxGC results 90

6.3.3. iso-Paraffin mixture component physical properties 92
6.4. n-Paraffin/iso-paraffin viscosity and freeze point comparison 93
6.5. Conclusion 95
6.6. Recommendations 96
Chapter 7 : Mixture Design Results 97
7.1. Introduction 97
7.2. Definition of statistical terms 97
7.2.1. Cross-validated R^2 97
7.2.2. Significance level 97
7.3. Mixture design 98
7.4. Mixture models 100
7.4.1. Model for viscosity 101
7.4.2. Model for freeze point 104
7.5. Model validation 107
7.6. Ideal jet fuel mixtures 111
7.6.1. Ideal ASTM jet fuel mixture 111
7.6.2. Ideal jet fuel mixture for minimum viscosity and freeze point 113
7.6.3. Ideal jet fuel mixture for best low temperature fluidity properties attainable 115
7.7. Conclusion 116
Chapter 8 : Conclusions and Recommendations 118
8.1. Introduction 118
8.2. QSAR models for viscosity and freeze point prediction 118
8.2.1. Viscosity prediction model 118
8.2.2. Freeze point prediction model 119
8.3. Fractional distillation 119
8.4. n-Paraffin and iso-paraffin mixture design 120
8.4.1. Viscosity model 120
8.4.2. Freeze point model 121
8.4.3. Optimisation studies 122
8.5. Recommendations for future studies 122
8.5.1. QSAR models for viscosity prediction 122
8.5.2. Fractional distillation results: iso-Paraffin freeze points 123
Bibliography 124
Appendix A 130
Appendix B 140

List of Figures

Figure 1.1. Comparison of jet fuel composition (Brittz, 2012). 4
Figure 1.2. Viscosity graph for different jet fuels (Adapted from Viljoen (2015)). 6
Figure 2.1. Schematic of a typical crude oil refinery (Adapted from Colwell (2009)). 12
Figure 2.2. Schematic of a bubble cap fractionating column (Adapted from Laidler et al. (2003)). 13
Figure 2.3. Schematic of a typical synthetic crude oil refinery (Adapted from Van der Laan (1999)). 18
Figure 2.4. Boiling point data for C_8 and C_9 hydrocarbons (ASTM DS 4B, 1991). 29
Figure 2.5. Specific gravity data for C_8 and C_9 hydrocarbons (ASTM DS 4B, 1991). 30
Figure 2.6. Viscosity data for C_8 and C_9 hydrocarbons (ASTM DS 4B, 1991). 31
Figure 2.7. Freeze point data for C_8 and C_9 hydrocarbons (ASTM DS 4B, 1991). 32
Figure 3.1. Flow diagram of development of molecular modelling prediction model. 37
Figure 3.2. Pilodist 104 (PD104) distillation apparatus (Pilodist GmbH, n.d.). 44
Figure 3.3. Flow diagram of mixture model development. 49
Figure 4.1. Predicted viscosity versus literature viscosity scatter plot (Four descriptors). 61
Figure 4.2. Graph of standardised residuals versus predicted viscosity (Four descriptors). 62
Figure 4.3. Normal probability plot of four-descriptor regression model. 63
Figure 4.4. Predicted viscosity versus literature viscosity scatter plot (Three descriptors). 68
Figure 4.5. Three-dimensional view of the Van der Waal's surface of n-butane. 71
Figure 5.1. Freeze point parity plot. 77
Figure 5.2. Graph of standardised residuals versus predicted freeze point. 78
Figure 5.3. Normal probability plot of prediction model. 79
Figure 6.1. n-Paraffin average carbon number versus desired carbon number. 87
Figure 6.2. Compositional graph of n-paraffin GCxGC results. 88
Figure 6.3. iso-Paraffin average carbon number versus desired carbon number. 91
Figure 6.4. Compositional graph of iso-paraffin GCxGC results. 92
Figure 6.5. n-Paraffin versus iso-paraffin viscosity graph. 94
Figure 6.6. n-Paraffin versus iso-paraffin freeze point graph. 95
Figure 7.1. Predicted viscosity versus measured viscosity scatter plot. 102
Figure 7.2. Predicted contours as a function of changing C_{11} and C_{12} components with an i:n mass ratio of 84:16. 103
Figure 7.3. Predicted contours as a function of changing C_{11} and C_{12} components with an i:n mass ratio of 5:95. 104
Figure 7.4. Predicted freeze point versus measured freeze point scatter plot. 105
Figure 7.5. Predicted contours as a function of changing C_9 and C_{10} components with an i:n mass ratio of 84:16. 106

Figure 7.6. Predicted contours as a function of changing C_9 and C_{10} components with an i:n mass ratio of 5:95. 107
Figure 7.7. Predicted viscosity versus measured viscosity scatter plot for validation mixtures. 109
Figure 7.8. Predicted freeze point versus measured freeze point scatter plot for validation mixtures. 110
Figure 7.9. Measured viscosity at 20°C versus viscosity at -20°C scatter plot for the validation mixtures. 111
Figure 7.10. Compositional comparison of ideal jet fuels. 115

List of Tables

Table 2.1. Specifications for the physical properties of aviation turbine fuels (ASTM D1655-16c, 2016). 21
Table 2.2. Requirements for aviation turbine fuels containing synthesised hydrocarbons (ASTM D7566-15c, 2015). 26
Table 2.3. Physical properties of hydrocarbons in the jet fuel regime (ASTM DS 4B, 1991). 27
Table 3.1. Viscosity dataset. 38
Table 3.2. Freeze point dataset. 39
Table 3.3. Boiling points of n-Paraffins (ASTM DS 4B, 1991). 45
Table 3.4. n-Paraffin initial distillation parameters. 45
Table 3.5. iso-Paraffin initial distillation parameters. 46
Table 3.6. Mixture design for variation of i:n mass ratio and carbon number distribution. 52
Table 3.7. Validation mixtures. 54
Table 3.8. Ideal ASTM jet fuel mixture. 54
Table 3.9. Optimum blends for minimised freeze point and viscosity. 55
Table 3.10. Ideal i:n jet fuel mixture for minimising freeze point and viscosity. 55
Table 3.11. Ideal i:n mass ratio and carbon number distribution for optimum jet fuel blends. 56
Table 4.1. Statistics of viscosity prediction model: Four molecular descriptors. 60
Table 4.2. Statistics of viscosity prediction model (Four molecular descriptors): Dataset 1 + 2 (Predicting subset 3). 64
Table 4.3. Statistics of viscosity prediction model (Four molecular descriptors): Dataset 2 + 3 (Predicting subset 1). 64
Table 4.4. Statistics of viscosity prediction model (Four molecular descriptors): Dataset 1 + 3 (Predicting subset 2). 65
Table 4.5. Statistics of viscosity prediction model: Three molecular descriptors. 66
Table 4.6. Results of viscosity prediction model: Three molecular descriptors. 67
Table 4.7. Viscosity prediction of non-dataset molecules. 70
Table 5.1. Statistics of freeze point prediction model. 75
Table 5.2. Results of freeze point prediction model. 76
Table 5.3. Statistics of freeze point prediction model: Dataset 1 + 2 (Predicting subset 3). 80
Table 5.4. Statistics of freeze point prediction model: Dataset 2 + 3 (Predicting subset 1). 80
Table 5.5. Statistics of freeze point prediction model: Dataset 1 + 3 (Predicting subset 2). 81
Table 5.6. Freeze point prediction of non-dataset molecules. 82
Table 6.1. Results of n-paraffin fractionation. 86
Table 6.2. Physical properties of n-paraffin mixture components. 89
Table 6.3. Results of iso-paraffin fractionation. 90
Table 6.4. Physical properties of the iso-paraffin mixture components. 93
Table 7.1. Mixture design for variation of i:n mass ratio and carbon number distribution. 99

Table 7.2. Validation results. 108
Table 7.3. Ideal ASTM jet fuel mixture results. 112
Table 7.4. Optimum blends for minimised freeze point and viscosity. 113
Table 7.5. Ideal i:n jet fuel mixture for minimising freeze point and viscosity..... 114
Table 7.6. Ideal i:n mass ratio and carbon number distribution for optimum jet fuel blends..... 116

Abbreviations

AET	Atmospheric Equivalent Temperature
APU	Auxiliary Power Units
ASTM	American Society for Testing and Materials
BDL	Below Detection Limit
BTL	Biomass-to-Liquids
CNM	Could Not Measure
CRC	Coordinating Research Council
CTL	Coal-to-Liquids
ETOPS	Extended range twin-engine operations
FCC	Fluid Catalytic Cracking
FID	Flame Ionisation Detector
GCxGC	Two-dimensional Gas Chromatography
GFA	Genetic Function Approximation
GTL	Gas-to-Liquids
HTFT	High Temperature Fischer-Tropsch
LMO	Leave Many Out
LOO	Leave One Out
LTFT	Low Temperature Fischer-Tropsch
Merox	Mercaptan oxidation
MLR	Multiple Linear Regression
NDDO	Neglect of Diatomic Differential Overlap
OEM	Original Equipment Manufacturer
QSAR	Quantitative Structure-Activity Relationship
SCF	Self-Consistent Field method
TOF-MS	Time-of-Flight Mass Spectrometer

Chapter 1 : Introduction

1.1. Background

1.1.1. Aviation industry history

Humankind has been fascinated by the concept of flight for centuries. In 1783, the Montgolfier brothers launched the first untethered balloon into the air, sparking excitement across Europe and America. Balloons were filled with gaseous hydrogen and hot air in order to achieve the dream of flight (Fortier, 2004).

Balloons remained the only means of flying until 1804, when Sir George Cayley designed, built and flew the first known glider in the world. Cayley conducted many experiments, some of which form the fundamental building blocks of flight as it is known today (NASA, 2002).

The Wright brothers became interested in the concept of powered flight in 1899 and built numerous gliders in order to determine how best to control a glider in the air. After perfecting their glider control system, the Wright brothers built and designed a four-cylinder spark-ignition internal combustion engine and fitted it to their glider. They successfully tested their engine-powered glider, fuelled by automotive gasoline, on 17 December 1903, flying a distance of 260 metres after 59 seconds in the air. This marked the first time that an engine-powered, pilot-controlled flight took place. The Wright brothers improved on their initial design with the Wright Flyer II and the Wright Flyer III, and in 1909 became the world's largest airplane manufacturer (NASA, 2003).

Airplanes played a significant reconnaissance role in World War I (1914 – 1918). Trenches and military positions, as well as military targets, were identified by observation planes, and these planes were also used to control ground troops. The importance of controlling the air by means of armed aircraft led to the development of the Fokker Eindecker fighter plane. Airplanes were also being converted to bombers during this period and, by the end of the war, every possible purpose that the airplane could serve during wartime had been explored (NASA, 2002). Airplanes of this time still made use of automotive gasoline-powered piston engines.

Aviation gasoline was first differentiated on its anti-knock properties in 1930, when the U.S. Army Air Corps specified a fighting grade gasoline with a minimum octane number requirement of 87 (Chevron Corporation, 2007). The Douglas DC-3, introduced in 1935, was an aviation gasoline-powered, fixed-wing propeller-driven airliner. It had a cruising speed of 333 km/h and a range of 2400 km, which signalled the beginning of the modern era of passenger airline services (Boeing, 2017).

Aircraft played a significant role in many aspects of World War II (1939 – 1945). Spitfires terrorised the German army, whilst bombers targeted German cities, industrial hubs and transportation systems, devastating the Nazi transportation system and oil production infrastructure (Maier, 2005). Aviation gasoline used by the U.S Army Air Corps had an anti-knock rating of 100 by the time the U.S. entered the war, which gave their aircraft superior performance capabilities (Chevron Corporation, 2006a).

Pioneering efforts in Germany led to the development of the direct coal liquefaction technology by Friedrich Bergius (1913), as well as the indirect coal liquefaction process developed by Franz Fischer and Hans Tropsch (1923) (Andrews & Logan, 2008). In order to fuel the German war machine, 12 Bergius process plants and 9 Fischer-Tropsch plants were constructed, producing ±100 000 barrels of synthetic transportation fuels per day by the end of the war (Stranges, 2001), (Maier, 2005). Germany developed the Messerschmitt Me 262, which was introduced in 1944. This was the world's first fully operational turbine-powered fighter plane (NASA, 2002). The Messerschmitt was faster than any of the Allied aircraft, and it used synthetic kerosene produced by the Coal-to-Liquid process, among other conventional fuels.

After World War II, thousands of surplus airplanes were converted for use by civilian airlines and, because of the war effort, there were sufficient pilots to fly these aircraft. Development of kerosene as aviation turbine fuel also accelerated after the World War II period.

In 1952, British Airways developed the world's first jet airliner, named the DH 106 Comet, which used kerosene as fuel. The Boeing 707 followed in 1954 and improved on the flaws and design limitations of the Comet. The first Boeing 747 was built in 1968, and it became the world's first and largest commercial jumbo jet, with a seating capacity of 550 passengers (NASA, 2002).

Fuelled by the desire to build faster, more efficient and comfortable commercial jets, aircraft manufacturers continue to adapt their aircraft. The Boeing 777, Boeing 787 and Airbus A380 are prime examples of the advances that have been made in recent years.

Jet fuel specifications for civilian use were first published in 1959 by the American Society for Testing and Materials (ASTM) in the form of ASTM D1655. The original version of the specification included three jet fuel grades, namely Jet A, Jet A-1 and Jet B. Jet B, which is a wide-cut kerosene, has since been removed from ASTM D1655, and forms part of a separate ASTM specification.

Specifications for jet fuel are regularly adapted and updated in order to ensure that these fuels conform to technological advances being made in the aviation industry. ASTM D7566 was

brought into existence due to the increased presence in the market of alternative and synthetic jet fuels, including those produced from Fischer-Tropsch synthesis.

1.1.2. Jet fuel composition overview

Jet fuel is a mixture of a multitude of different hydrocarbons. As can be seen in Figure 1.1, these hydrocarbons can generally be divided into four groups: paraffins, naphthenes (also known as cycloparaffins), aromatics and olefins.

Each of these groups differs in terms of (Chevron Corporation, 2007):

- The ratio of carbon atoms to hydrogen atoms;
- The manner in which atoms are bonded to each other.

The mass contribution of each of these four groups to the overall chemical composition of the fuel dictates the bulk physical properties of the fuel. The refining technique used to produce jet fuel, in turn, dictates the overall composition of the fuel.

Fischer-Tropsch derived jet fuels consist mainly of linear (n-paraffins) and branched (iso-paraffins) paraffins, as well as smaller quantities of aromatics. Aromatics are required to meet the minimum density specification limits and are set by ASTM International. The availability of aromatics in a Fischer-Tropsch refinery is dependent on the type of Fischer-Tropsch refining technology employed. Crude oil derived jet fuels consist of n-paraffins, iso-paraffins, aromatics and naphthenes, as well as minute quantities of undesired olefins.

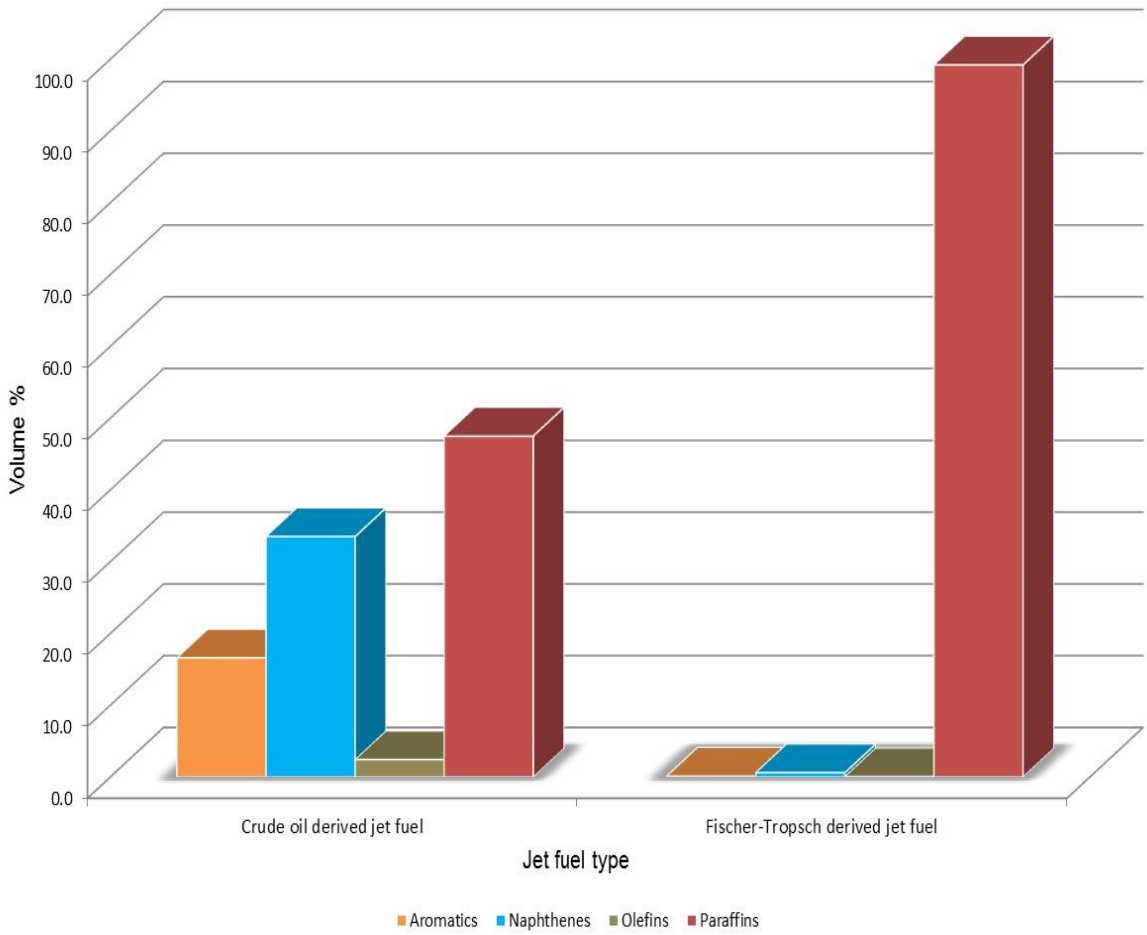

Figure 1.1. Comparison of jet fuel composition (Brittz, 2012).

Even though chemical composition determines the bulk physical properties of fuels, boiling point values are conventionally used to estimate these properties (Chevron Corporation, 2007). Until now, the conventional practice of jet fuel refining was sufficient for the petroleum refining industry; however, global refining operations are constantly under pressure due to new legislation being passed by governments, pressure from environmental groups and technological advances being made by Original Equipment Manufacturers (OEMs). Ignoring these parties will result in refiners producing fuels that may not be deemed fit for use in the future, which will in turn be detrimental to the sustainability of petroleum refineries.

1.1.3. Low temperature operability of aircraft components

Auxiliary power units (APUs) are small turbine engines that are used as power source to start the main aircraft engine. In order for the main turbine engines to achieve self-sustaining operation, the engines must be accelerated to a high rotational speed to provide sufficient air compression, which is achieved through the aircraft APU. APUs also serve as a safety device in case of main engine failure, providing electricity to critical aircraft components; they are thus considered essential safety components for extended range twin-engine operations (ETOPS)

flights. APUs are also used as power sources for aircraft air conditioners and electrical systems during ground operations (Novillo, et al., 2010). High altitude and low temperature start requirements of APUs are very harsh; APUs have to be able to start up after extended periods of exposure to low temperatures at altitudes above 40 000 feet.

Honeywell Aerospace, which is the world's largest APU manufacturer (Honeywell Aerospace, 2016), sets the low temperature fuel viscosity limit of their APUs at 12 cSt, which is the maximum viscosity where adequate APU fuel atomisation still occurs, thereby ensuring satisfactory jet fuel flame stability. At viscosities higher than 12 cSt, APUs will have trouble starting, or may not start at all. Repeated start attempts may result in hot section distress (Coordinating Research Council, 2010).

Based on the above findings, the Coordinating Research Council (CRC) concluded that current jet fuel viscosity and freeze point specifications do not address the potential hazards associated with APU performance, since these specifications do not ensure that fuels have viscosities lower than 12 cSt at -40℃ for Jet A or -47℃ for Jet A-1 (Coordinating Research Council, 2010).

As a result of the concerns raised by aviation industry OEMs, the ASTM International organization is currently investigating the need for jet fuels to possess low temperature viscosities not exceeding 12 cSt, as well as the means by which these concerns can be addressed, e.g. through fuel specification changes, operational changes, or APU design changes (ASTM D1655-16c, 2016).

Furthermore, Annexure X1.6.2 of ASTM D1655-16c (2016) states that jet fuel can exceed the 12 cSt viscosity maximum specified by APU manufacturers as the fuel approaches the freeze point specification limit (-40℃ for Jet A or -47℃ for Jet A-1), when the viscosity at -20℃ exceeds 5.5 cSt for Jet A or 4.5 cSt for Jet A-1.

1.1.4. Low temperature viscosity of jet fuel

In order to determine whether current jet fuels available in the market would adhere to such future specifications, viscosity curves were compiled for a typical crude derived Jet A-1, as well as for two different types of Fischer-Tropsch kerosenes. This was done according to ASTM D341, whereby kinematic viscosity values can be predicted within a limited range, if viscosity values at two temperatures are known (ASTM D341-09, 2009). The results are displayed in Figure 1.2.

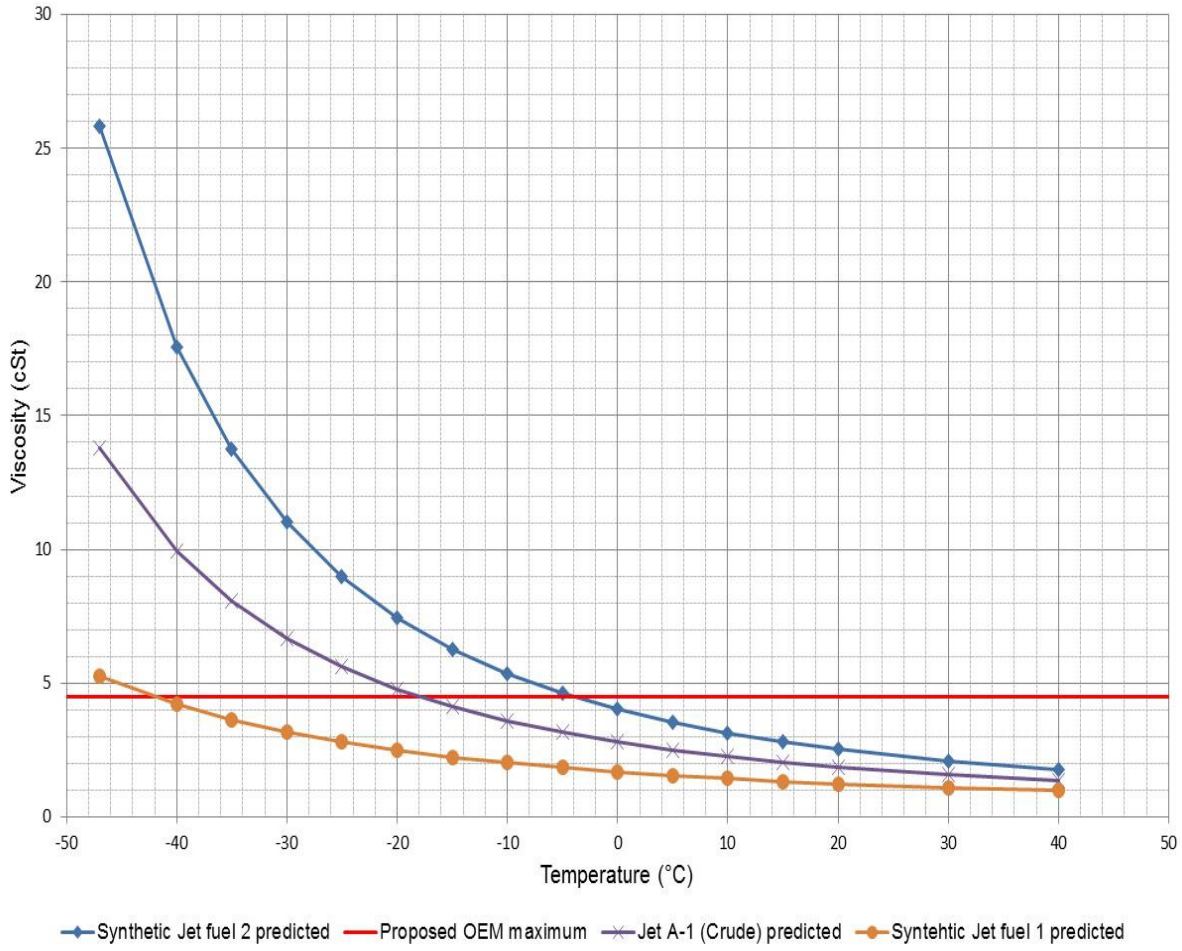

Figure 1.2. Viscosity graph for different jet fuels (Adapted from Viljoen (2015)).

When considering the data obtained from Figure 1.2, it can be observed that the conventional crude derived Jet A-1 fuel exceeded the proposed low temperature viscosity limit of 4.5 cSt at -20℃. However, the results for the different types of synthetic jet fuels varied significantly; one type of synthetic fuel was well within the proposed -20℃ viscosity limit, whereas the second type of synthetic fuel exceeded this maximum viscosity limit. From the graph, it can be seen that the three fuels, while complying with the current jet fuel specification, have completely different viscosity curves. These differences are ascribed to the differences in chemical composition of the respective jet fuels.

1.2. Problem statement

For more than sixty years, the freeze point specification of jet fuel was considered the most critical property in order to ensure that these fuels were fit for use in the aviation industry. However, as mentioned previously, aviation industry OEMs recently determined that appropriate fuel atomisation within the aircraft APUs can only occur with fuels having low temperature viscosities below 12 cSt; the validity of these claims are currently being investigated by the ASTM International organization.

It is anticipated that the focus on fluidity of jet fuel at low temperatures will grow rapidly in the near future and that stringent specification limits, similar to those mentioned by the CRC and aviation industry OEMs, as well as by the ASTM International organization, may be applied to jet fuel products. The effect of molecular branching and carbon number distribution on the low temperature fluidity characteristics of synthetic jet fuel was thus investigated in this research to gain a better understanding of this relationship.

1.3. Research aim

The aim of this research was to vary both the iso-paraffin to n-paraffin (i:n) mass ratio and the carbon number distribution of synthetic jet fuel components in the C_9 - C_{18} range in such a manner as to obtain a fuel that would meet the freeze point requirements of Jet A-1, whilst maintaining a viscosity profile that was not readily susceptible to changes in temperature, as discussed in Annexure X1.6.2 of ASTM D1655-16c.

This research was conducted to prove or disprove the following hypothesis:

> *There exists an ideal i:n ratio and an ideal carbon number distribution that enables the production of jet fuel, which possesses the best low temperature fluidity properties attainable.*

1.4. Research objectives

The objectives of this study were as follows:

- To determine the molecular properties that affect the freeze point and viscosity behaviour of n- and iso-paraffins by means of molecular modelling;
- To isolate n-paraffins and iso-paraffins from refinery streams by means of fractional distillation;
- To determine the effect that various i:n mass ratios and carbon number distributions would have on the fluidity properties of jet fuel; and
- To attempt production of jet fuel that possesses the best possible low temperature fluidity properties attainable.

1.5. Dissertation outline

Chapter 1: Introduction

An overview is given of the history of the aviation industry as well as of the fuels used to power aircraft, showing how the industry developed since the first balloon carrying humans was launched. A brief overview is provided of jet fuel composition, followed by an examination of the

challenges regarding possible future fluidity specifications for synthetic jet fuels. Finally, the aim and objectives of this study are discussed, along with a brief outline of the dissertation.

Chapter 2: Literature review
This chapter presents a brief discussion of crude oil refining and Fischer-Tropsch refining, introducing the importance of different refining techniques and their influence on the chemical composition of fuels. Furthermore, the physical properties of jet fuels will be discussed. In the last section of the literature study, emphasis will be placed on the effect of chemical composition on jet fuel properties, as well as on the molecular properties that give rise to these physical properties.

Chapter 3: Experimental procedures
The molecular modelling procedures for the prediction of the freeze point and the viscosity properties of various n- and iso-paraffin molecules will be presented. The approach followed to isolate n- and iso-paraffins from refinery streams by means of fractional distillation, as well as the methodology followed to blend these fractionated components in different ratios by means of a statistical mixture design, will be discussed. Details of the various analytical techniques used to analyse these fractions and mixtures will also be described in this section.

Chapter 4: QSAR models for viscosity prediction
In this chapter, the molecular modelling results obtained with regard to the prediction of kinematic viscosities of n- and iso-paraffin molecules will be discussed.

Chapter 5: QSAR model for freeze point prediction
The molecular modelling results obtained with regard to the prediction of freeze points of n- and iso-paraffin molecules will be discussed.

Chapter 6: Fractional distillation results
Results obtained from the fractional distillation of various refinery products in order to produce n- and iso-paraffin mixture components with specific carbon chain lengths will be presented in this chapter.

Chapter 7: Mixture design results
In this chapter, the statistical mixture design for estimation of the low temperature viscosity and freeze point properties of jet fuel, by variation of the i:n mass ratio, in conjunction with variation of the carbon number distribution, will be presented. In the last section of this chapter, the results obtained with regard to the ideal jet fuel that was produced by means of the statistical mixture design will be discussed.

Chapter 8: Conclusions and recommendations

This chapter summarises the conclusions that were reached, as well as the recommendations for further work to be done.

Chapter 2 : Literature Review

2.1. Introduction

The first part of this literature review describe the most common refining techniques used for the production of transportation fuels, namely conventional crude oil refining and synthetic fuel refining. The second part focuses on the physical properties of jet fuel, while the final part looks at the effect of chemical composition and intermolecular forces on these physical properties.

2.2. Crude oil refineries

The key purpose of a crude oil refinery is to transform raw crude oil into valuable end products that meet market demands. Crude oils are essentially a mixture of a multitude of hydrocarbons and lower amounts of heteroatomic compounds (Demirbas & Bamufleh, 2017), which can be divided into five categories. The categories are described below.

2.2.1. Paraffins

Also known as alkanes, these saturated hydrocarbons consist of carbon atoms linked by single bonds. They have the general formula C_nH_{2n+2}, where n is the number of carbon atoms. Paraffins can be divided into two distinct sub-categories:

- Linear alkanes, or normal paraffins. Examples of n-paraffins are hexane (C_6H_{14}) and octane (C_8H_{18});
- Branched alkanes, or iso-paraffins. Examples of branched paraffins are 2-methylpentane (C_6H_{14}) and 2,2,4-trimethylpentane (C_8H_{18}).

2.2.2. Olefins

Olefins or alkenes are unsaturated hydrocarbons that contain one or more double bonds. These hydrocarbons have the general formula C_nH_{2n}. Propylene (C_3H_6) is an example of a typical olefin. During crude oil refining, butene is reacted with iso-butane to produce high-octane mixture components for the production of gasoline.

2.2.3. Naphthenes

Naphthenes or cycloparaffins, for example cyclohexane (C_6H_{12}), are saturated single bond hydrocarbons, which are arranged in a ring formation. They have the general formula C_nH_{2n}. In a crude oil refinery, these compounds are converted to aromatic compounds, which have much higher octane numbers.

2.2.4. Aromatics

Aromatics are unsaturated hydrocarbons, which are arranged in a ring formation. Benzene (C_6H_6) is the most simple one-ring aromatic compound with the general formula C_nH_{2n-6}. Polycyclic aromatics, also known as naphthalenes, consist of two or more aromatic rings, which share some of the carbon atoms. Aromatics such as benzene and toluene exhibit high octane numbers, which is a desired gasoline property.

2.2.5. Heteroatomic compounds

Heteroatomic compounds contain sulphur, nitrogen and oxygen (Robson, et al., 2017). Molecules containing heteroatoms are not classified as hydrocarbons. Various refining techniques are employed to minimise the presence of these compounds in fully refined fuels.

2.2.6. Crude oil refining

Crude oils vary greatly in composition, ranging from light crude oil to heavy crude oil. Light crude oil contains more low molecular weight components, which reduce the complexity associated with refining processes. Heavy crude oil contains a larger portion of high molecular weight components, rendering them more complex to refine due to the additional refining processes required to produce suitable products (Chevron Corporation, 2007). The refining process is described below.

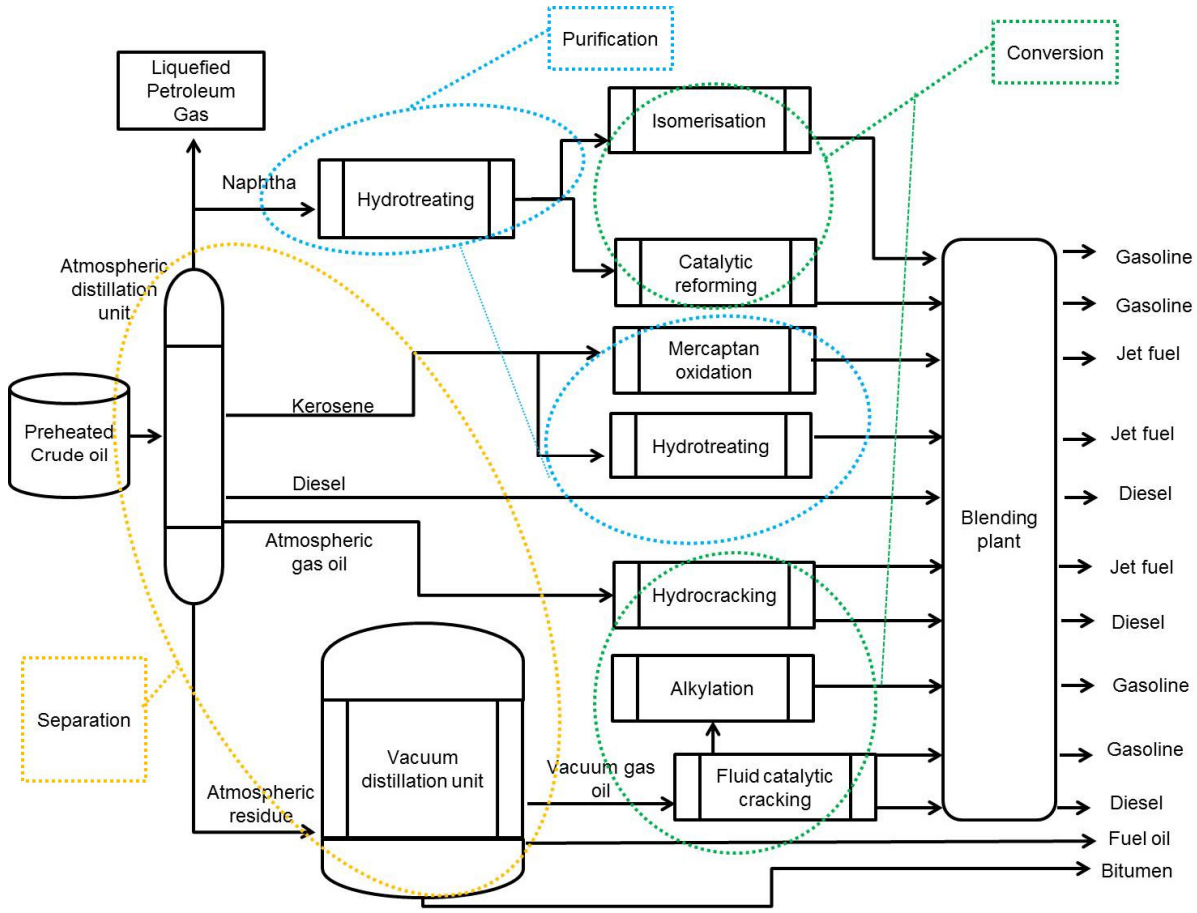

Figure 2.1. Schematic of a typical crude oil refinery (Adapted from Colwell (2009)).

A typical crude oil refinery (Figure 2.1) utilises a variety of refining processes to produce liquid fuels and all of these processes can be arranged into three fundamental refining categories (Wansbrough, n.d.), each of which is discussed further below:

- Separation;
- Conversion; and
- Purification.

2.2.7. Separation

Distillation is defined as the means by which a mixture of components is separated, based on the differences in volatilities of the components contained within the mixture. This separation process forms the foundation of any crude oil refinery.

According to Raoult's law, the vapour pressure of a component in a mixture contributes to the total vapour pressure, based on the percentage of the component in the mixture, as well as its vapour pressure when pure (Laidler, et al., 2003). Dalton's law of partial pressures state that the total vapour pressure of a mixture is equal to the sum of the vapour pressure of each component in the mixture (Laidler, et al., 2003). When a liquid mixture is heated, the vapour

pressure of each component in the mixture will increase, subsequently increasing the total vapour pressure of the mixture. Boiling (bubble formation) occurs when the total vapour pressure of the mixture is equal to the pressure of the atmosphere surrounding the mixture. Lower molecular weight components will be present in higher concentrations in the gas phase, with higher molecular weight boiling point components being present at lower concentrations.

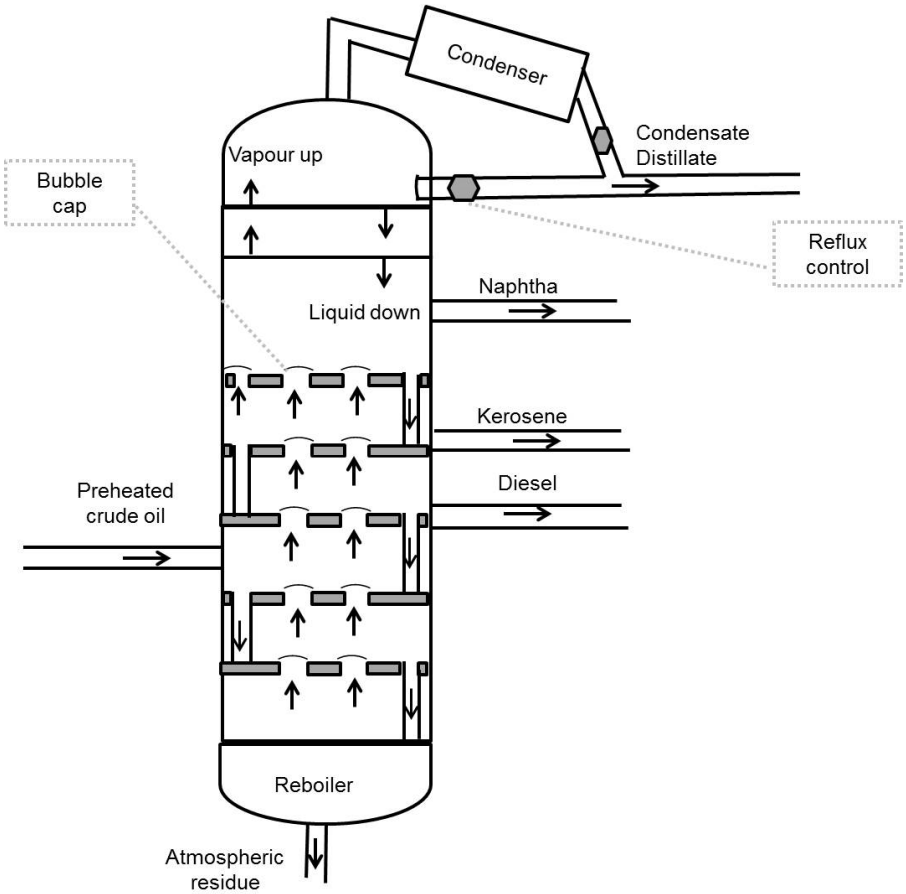

Figure 2.2. Schematic of a bubble cap fractionating column (Adapted from Laidler et al. (2003)).

The function of a distillation column (Figure 2.2) is to provide a contact surface for the mass transfer that needs to occur between liquid and vapour. Preheated crude oil is pumped into the distillation column at ambient pressure, approximately halfway up the column. The liquefied petroleum gas consists of low boiling point components, which consequently rise to the top of the distillation column, where an externally cooled condenser chills the vapour back into the liquid phase. The liquid phase is then collected as a distillate. The higher boiling point components descend to levels lower down in the column, where they are reheated. As the crude oil vapour rises in the column, the higher boiling point components start to condense, whilst the lower boiling point components continue to rise, thereby establishing a temperature gradient in the column. The highest boiling point components, such as fuel oil and bitumen (atmospheric column residue), are consequently located at the bottom of the column in the

reboiler. Diesel, kerosene and naphtha can be located at increasingly higher stages in the column, and are drawn off from the side of the column. At each successive level in the column, vapour from the plate below bubbles through a thin film of liquid, consisting of a mixture of components present in the crude oil; the temperature of this liquid is slightly lower than the temperature of the vapour rising through the bubble cap. Partial condensation of the vapour occurs, after which the vapour of the lower boiling point components continues to rise to the next plate. The vapour rising in the column is therefore continuously enriched with the lowest boiling point components present in the column (Laidler, et al., 2003).

The residue from the atmospheric distillation unit cannot vaporize under atmospheric distillation conditions and is therefore removed from the bottom of the distillation column. The residue obtained at atmospheric pressure is further fractionated by a secondary distillation process, namely vacuum distillation. Vacuum distillation units operate at reduced pressures and therefore enable higher boiling point components to vaporize and be collected as distillates. Examples of distillates collected at higher stages of the column are vacuum gas oil and fuel oil, whilst the product collected at the bottom of the column is vacuum residue or bitumen.

2.2.8. Conversion

Distillation does not alter the chemical composition of crude oil, but only separates the crude oil into partially refined products. Conversion processes are employed to bridge the gap between crude oil feed characteristics and desired product properties, by altering the molecular structure of distillates. The various conversion processes are described below.

2.2.8.1. Catalytic cracking

Catalytic cracking produces middle distillates by breaking long carbon chain length components into multiple short carbon chain length components, whilst making use of heat and a catalyst. Fluid catalytic cracking (FCC) is the most widely used catalytic process in the petrochemical industry. The FCC catalyst promotes the reaction that breaks longer carbon chain length hydrocarbon molecules in the appropriate position to produce gasoline and diesel.

2.2.8.2. Hydrocracking

Hydrocracking is similar to catalytic cracking; however, this type of cracking makes use of high-pressure hydrogen to convert longer chain length hydrocarbons into diesel and jet fuel. The catalyst of the hydrocracker is fixed in place, whereas the catalyst of the FCC is finer and moves with the longer chain length hydrocarbons. Hydrocracking breaks the carbon-carbon bonds whilst adding hydrogen atoms to the fragmented molecular ends. During the

hydrocracking process, denitrogenation and desulphurisation also occur, producing diesel and jet fuel with lower nitrogen and sulphur contents.

2.2.8.3. Catalytic reforming

The catalytic reformer converts low octane naphthas into high-octane aromatic molecules. The reforming reaction occurs at elevated temperatures in the presence of hydrogen and a catalyst. An increase in aromatic content within the gasoline will bring about an increase in the octane number of the gasoline, which is an important property of gasoline (Ramanathan & Turaga, 2003). Hydrogen is a by-product of the reforming process, and is routed to the refinery hydrotreaters for use in desulphurization, deoxygenation, olefin saturation, and denitrification reactions.

2.2.8.4. Alkylation

During the alkylation process, iso-butane is chemically reacted with the olefins in the crude oil to produce a high-octane refinery product that is blended into gasoline. The alkylation reaction occurs in the presence of a catalyst. Alkylate is a high quality product with low volatility, containing neither aromatics nor sulphur (Olsen, 2014).

2.2.8.5. Isomerisation

Isomerisation converts linear paraffins to branched paraffins. This process substantially increases the octane number of the paraffins that are used as mixture components during gasoline production. Light naphtha compounds ($C_5 - C_6$) or butane usually serve as feedstock for this conversion process. A portion of the iso-butane required by the alkylation process is also produced in the isomerisation unit.

2.2.9. Purification

After completion of the separation and conversion processes, the partially refined petroleum products need to pass through various purification processes to remove undesired components, such as sulphur and surfactants. Petroleum products that contain these undesired components are of lower quality, both from an end-user point of view, as well as from an environmental point of view, and may thus not be fit for use. The various purification processes are described below.

2.2.9.1. Hydrotreating

The partially refined products are reacted with hydrogen at elevated temperature and pressure. The reaction occurs in the presence of a catalyst. Furthermore, the hydrotreating process removes sulphur from refinery products in the form of hydrogen sulphide. This process also removes impurities such as nitrogen, oxygen and olefins. Although hydrotreating may sound

similar to hydrocracking, the hydrotreating process does not break long carbon chain length molecules into shorter carbon chain length molecules.

2.2.9.2. Mercaptan oxidation (Merox)

Known as the sweetening process, mercaptan oxidation removes the mercaptans from partially refined petroleum products by oxidising these undesired components to form disulphides. This process does not remove sulphur; it merely converts undesirable mercaptans into less reactive disulphides. The resultant heavier disulphide compounds are then removed by distillation.

2.2.9.3. Clay treatment

Surfactants are undesired compounds that are present in fuel. It is essential that these polar compounds be removed from jet fuel since the coalescing process is disrupted when they attach to the interface between fuel and water. The most commonly used practice to remove surfactants from jet fuel is to pump the jet fuel through clay filters, as surfactants readily adhere to the surface of clay (Chevron Corporation, 2006a).

2.2.10. Blending refined petroleum products

Even though separation, conversion and purification processes are employed to refine crude oil, the composition of petroleum products is essentially dictated by the composition of the crude oil that serves as the refinery feed material. Consequently, the composition of crude oil also dictates the use of all refinery products in order to produce fully refined fuels. Sophisticated computer software enables the refinery blending plant to combine the various refinery products in such a manner as to obtain fully refined fuels that meet both end user and environmental specifications (Demirbas & Bamufleh, 2017).

2.3. Synthetic fuel refineries

Fischer-Tropsch synthesis utilises carbon monoxide (CO) and hydrogen (H_2), named synthesis gas, to produce synthetic liquid fuels. The synthesis gas can be obtained from virtually any carbon source. The most widely used materials for synthesis gas production is (Chevron Corporation, 2006b):

- Coal: Coal-to-Liquids (CTL);
- Natural gas: Gas-to-Liquids (GTL); and
- Biomass: Biomass-to-Liquids (BTL).

Fischer-Tropsch refineries are conventionally classified according to the feed material used during synthesis gas production; however, the feed material dictates neither the Fischer-Tropsch refining technology employed nor the composition of the synthetic crude oil. The feed

material simply influences the type of gasifier utilised during the refining process (De Klerk, 2008).

Historically, CTL technology was employed during synthetic fuel production; however, government legislation and continuous pressure from environmental groups regarding CO_2 (g) emissions, which is produced in abundance during CTL refining, render this type of Fischer-Tropsch refining much less attractive than in the past (Marano & Ciferno, 2001).

Natural gas reserves around the world have remained unexploited for many years, and these reserves can potentially provide the GTL industry with an abundance of feed material. The GTL refining process produces significantly less CO_2 (g) than the CTL refining process (Marano & Ciferno, 2001).

Products produced by Fischer-Tropsch synthesis are considered more environmentally friendly than their crude oil counterparts, as such products contain no sulphur, or metals, and consist mainly of linear paraffins and branched paraffins (Agee, n.d.). The presence of aromatic compounds in these fuels depends on the type of Fischer-Tropsch technology employed during the refining process.

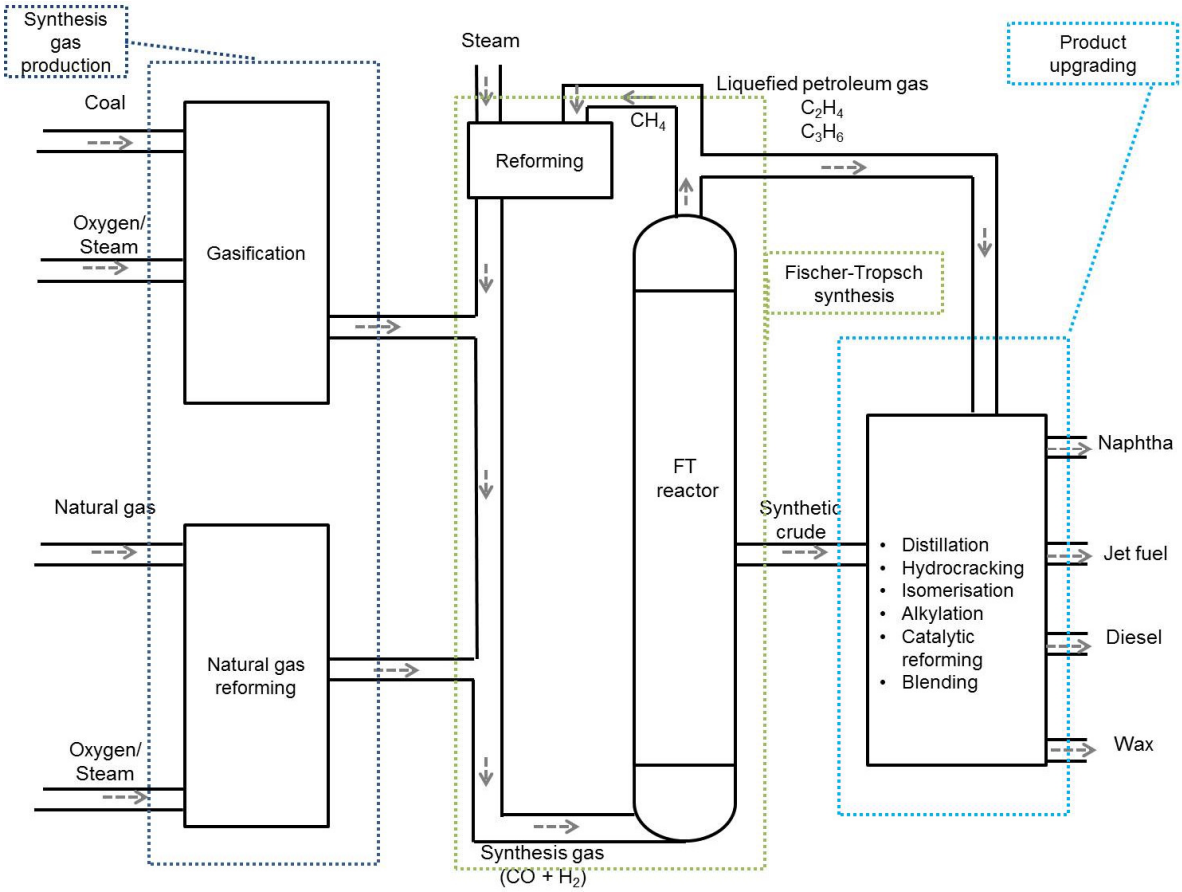

Figure 2.3. Schematic of a typical synthetic crude oil refinery (Adapted from Van der Laan (1999)).

Synthetic crude oil refineries (Figure 2.3) utilise a wide variety of refining processes; however, all of these can be organised into three fundamental categories:

- Synthesis gas production;
- Fischer-Tropsch synthesis; and
- Product upgrading.

2.3.1. Synthesis gas production

Synthesis gas is produced by the gasification of coal or by the reforming of natural gas. These conversion processes utilise steam, oxygen or carbon dioxide (auto-thermal processes). The most important reactions that occur during synthesis gas production are (Wood, et al., 2012):

- Steam reforming: $CH_4(g) + H_2O(g) \rightarrow CO(g) + 3H_2(g)$
- Partial oxidation: $2CH_4(g) + O_2(g) \rightarrow 2CO(g) + 2H_2(g)$
- CO_2 reforming: $CH_4(g) + CO_2(g) \rightarrow 2CO(g) + 2H_2(g)$
- Water gas shift reaction: $CO(g) + H_2O(g) \leftrightarrow CO_2(g) + H_2(g)$

The water gas shift reaction is critical for Fischer-Tropsch synthesis, since this reaction balances the CO/H_2 ratio of the synthesis gas that feeds into the reactor, thereby increasing reaction yields.

2.3.2. Fischer-Tropsch synthesis

Fischer-Tropsch synthesis is essentially a catalytic polymerisation process, whereby CO(g) and H_2(g) are converted to longer carbon chain length hydrocarbon molecules, which are predominantly linear:

$$CO + H_2 \rightarrow -(CH_2)_n- + H_2O$$

There are three main types of reactors utilised for synthesis:

- Slurry phase reactors: These yield linear hydrocarbons consisting of carbon chain lengths in the diesel regime. This type of reactor is considered a low temperature Fischer-Tropsch (LTFT) reactor.
- Tubular fixed bed reactors: As with the slurry phase reactor, tubular fixed bed reactors yield linear hydrocarbons with carbon chain lengths in the diesel regime. These are also considered to be LTFT reactors.
- Fluidised bed reactors: These reactors yield shorter carbon chain length hydrocarbons in the gasoline range and are considered high temperature Fischer-Tropsch (HTFT) reactors. The HTFT process also produces aromatic compounds.

LTFT reactors function at lower temperatures (180 - 250°C) and pressures (±20 bar) than HTFT reactors, which function at 330 - 350°C and ±25 bar (Parmaliana, et al., 1998). HTFT makes use of an iron-based catalyst, whilst LTFT can use either iron- or cobalt-based catalysts, with cobalt being the preferred catalyst.

2.3.3. Product upgrading

The hydrocarbon mixture produced during Fischer-Tropsch synthesis is a raw material, called synthetic crude oil, which needs to be further refined into products that meet market demands; the synthetic crude oil is subjected to similar processes as those found in a crude oil refinery:

- Distillation;
- Hydrocracking;
- Alkylation;
- Catalytic reforming; and

- Isomerisation: Isomerisation is of vital importance during synthetic fuel refining, since products consisting of mostly linear paraffins would not meet all the required performance criteria.

2.3.4. Blending of fully refined Fischer-Tropsch products

Similar to crude oil refineries, Fischer-Tropsch refineries also employ computer software that enables the blending plant to combine the various refinery products in such a manner as to obtain fully refined fuels that meet market demands.

2.4. Introduction to jet fuel as refining distillate

The earliest propeller-driven aircraft used automotive gasoline as fuel. Aviation gasoline was later developed to enhance aircraft engine performance. The first turbine engine was developed in the late 1930s, and the first turbine engine-powered flight took place in 1944. Kerosene was chosen as fuel for turbine engines because all the gasoline produced during the 1940s was needed to fuel World War II. Kerosene was also used as turbine engine fuel, since it was believed that turbine engines were insensitive to fuel properties (Chevron Corporation, 2006a).

Wide boiling point distribution kerosene, known as Jet B, consisting of both gasoline and kerosene components, was developed on an unknown date for use by the American military. Due to the high volatility of Jet B, it is not ideal for general use though; today, it is only used in extremely cold climates (Carhart, et al., 1976).

The commercial aviation industry developed rapidly during the 1950s and chose kerosene-type jet fuel for the following reasons:

- Safety: Superior flash point and freeze point properties;
- Performance: Less evaporation than Jet B; and
- Energy density: Range versus fuel consumption.

Jet A-1 is used by the aviation industry throughout the world, with the exception of the United States, which makes use of Jet A. The main difference between Jet A-1 and Jet A is the maximum freezing point specification of the fuels, which is -47℃ and -40℃ respectively (ASTM D7566-15c, 2015).

Table 2.1. Specifications for the physical properties of aviation turbine fuels (ASTM D1655-16c, 2016).

Property	Limit	Specification value	Test method
Volatility			
Distillation			ASTM D86
Distillation temperature (℃):			
10% recovered (T10)	Maximum	205.0	
50% recovered (T50)	Maximum	Report	
90% recovered (T90)	Maximum	Report	
Final boiling point	Maximum	300.0	
Distillation residue (%)	Maximum	1.5	
Distillation loss (%)	Maximum	1.5	
Flash point (℃)	Minimum	38.0	ASTM D56
Density at 15℃ (g/cm^3)		0.775 – 0.840	ASTM D4052
Fluidity			
Freeze point (℃)	Maximum	-40 (Jet A) or -47 (Jet A-1)	ASTM D5972
Viscosity at -20℃ (mm^2/s)	Maximum	8.0	ASTM D7042
Combustion			
Net heat of combustion	Minimum	42.8	ASTM D4529
Smoke point (mm)	Minimum	18.0	ASTM D1322
Naphthalenes (vol %)	Maximum	3.0	ASTM D1840
Corrosion			
Copper strip, 2h at 100℃	Maximum	No. 1	ASTM D130
Thermal stability			
Filter pressure drop (mm Hg)	Maximum	25.0	ASTM D3241
VTR, VTR colour code		< 3 (No peacock or abnormal colour deposits)	
Contaminants			
Existent gum (mg/100mL)	Maximum	7.0	ASTM D381
Microseparometer rating			ASTM D3948
Without electrical	Minimum	85.0	
With electrical conductivity	Minimum	70.0	
Additives			
Electrical conductivity (pS/m)	Maximum	600	ASTM D2624
Composition			
Acidity, total (mg KOH/g)	Maximum	0.10	ASTM D3242
Aromatics (vol %)	Maximum	26.5	ASTM D6379
Sulphur, mercaptan (mass	Maximum	0.003	ASTM D3227
Sulphur, total (mass %)	Maximum	0.30	ASTM D2622

The quality requirements of jet fuel (Table 2.1) can be arranged into eight categories:

- Volatility;
- Fluidity;
- Combustion;
- Corrosion;
- Thermal stability;
- Contaminants;
- Additives; and

- Composition.

These categories are discussed below.

2.4.1. Volatility

Volatility, as indicated by the distillation profile, flash point and density, is used to describe the tendency of fuel to vaporise (SAPIA, 2008). Volatility increases as density, flash point and initial boiling point decrease.

Blakey et al. (2011) concluded that synthetic jet fuels, which are less dense than conventional crude oil derived fuels, offer greater flight range capabilities per fuel tank when aircraft operate at their maximum load capacity (payload). However, they also concluded that more dense conventional jet fuels offer greater flight range capabilities at lower payloads. During storage, transfer and handling of jet fuel, volatility must also be taken into consideration, since the fuel can easily ignite. The flash point of jet fuel is thus also considered an important safety factor. Since jet fuel is a mixture of different hydrocarbons, the boiling point profile is a temperature range, known as a boiling point distribution, rather than a single temperature; hence, the various means by which volatility can be measured.

2.4.2. Fluidity

Each hydrocarbon compound present in jet fuel possesses its own freezing point and, as the fuel is cooled, these hydrocarbons begin to form wax crystals, which increase in size as the fuel temperature decreases. Increased crystal dimensions result in increased contact between such crystals, ultimately producing a fuel structure similar to that of a gel (Zhuze, 1951). As the fuel temperature decreases, jet fuel essentially changes from a homogenous liquid to a liquid containing a few hydrocarbon crystals, to a slurry of liquid and wax crystals, and at sufficiently low temperatures, to a solid hydrocarbon wax. The aircraft turbine engines would thus be starved of fuel and unable to reignite whilst in flight, if the fuel cannot be pumped due to the formation of wax crystals.

Moses et al. (2009) studied the effects of isomerisation on the properties of synthetic jet fuel and mixtures with Jet A. It was observed that the carbon number distribution of synthetic fuels composed mainly of n-paraffins had to be narrower in order to adhere to freeze point specification criteria. Their study further found that the carbon number distribution of more hydro-isomerised synthetic fuels could be extended without any detrimental effects on the freeze point properties of the fuel.

The viscosity of a fuel is dependent on temperature; as the temperature of the fuel decreases, the viscosity of the fuel increases. It becomes increasingly difficult for the aircraft fuel pump to maintain a constant fuel flow rate, as the viscosity of the fuel increases. Beyond a certain viscosity threshold, the turbine engines will be deprived of fuel.

Shi and Tao (2013) studied the effect of iso-paraffin content on jet fuel properties and found that longer carbon chain length iso-paraffins increased the viscosity of jet fuel. Beyond a certain viscosity threshold, high fuel viscosity may lead to poor fuel atomisation at lower flight temperatures, since the droplet size of vaporised fuel increases with an increase in fuel viscosity (Blakey, et al., 2011), (Coordinating Research Council, 2010).

In order to ensure the fluidity of jet fuel during flight, the pilot must ensure that the fuel temperature remains at least 3℃ above the fuel freezing point (Lawicki, 2002). This can be achieved by:

- Descending to lower altitudes: The ambient temperature increases as the plane descends; and
- Diverting the airplane around cold air masses.

2.4.3. Combustion

Heat of combustion is defined as the quantity of energy released when a substance is burned (McMurry & Fay, 2004). The energy released during combustion of the fuel is what powers the turbine engines; hence the importance of jet fuel energy content. Combustion is a chemical reaction; if complete combustion is possible, it may be described as follows:

$$\text{Fuel} + O_2(\text{from air}) \rightarrow CO_2 + H_2O + N_2$$

Incomplete fuel combustion may lead to the formation of carbonaceous material, which is responsible for the visible smoke that turbine engines occasionally emit. These carbonaceous materials may, in turn, cause erosion of turbine blades. Complete combustion is thus essential:

- To ensure optimal turbine engine performance;
- To minimise the release of unwanted pollutants into the atmosphere; and
- To prolong engine lifetime.

Fuels that possess high concentrations of aromatic compounds tend to form carbonaceous material during combustion, thereby affecting the combustion process as described above. Crude oil derived jet fuels contain larger quantities of aromatics, hence the maximum specification limit for aromatics.

Corporan et al. (2005) studied the impact of synthetic jet fuel on the emissions of turbine engines and noted that synthetic jet fuels, which are free of aromatics and sulphur, showed significant reductions in particle number distributions, as well as particle mean diameters, when compared to conventional jet fuels. Furthermore, lower concentrations of sulphur oxides, as well as minor increases in water vapour, were observed, which the authors attributed to the sulphur-free nature and higher hydrogen/carbon ratio of synthetic jet fuel.

2.4.4. Corrosion

Sulphur may be present in jet fuel in any of the following forms:

- Free sulphur;
- Sulphides;
- Disulphides; and
- Mercaptans.

These sulphur compounds can be corrosive toward material that the fuel comes into contact with during handling, storage and flight. Corrosion is an undesired chemical reaction, which must be minimised to protect aircraft fuel systems.

2.4.5. Thermal stability

Thermal stability is a measure of the tendency of jet fuel to degrade at elevated temperatures, forming gum and carbonaceous material.

Jet fuel stability is an important fuel property since the fuel also serves as a coolant for the turbine engine lubricant, as well as for other critical aircraft equipment. Since jet fuel also serves as a cooling medium, it is subjected to elevated temperatures for extended periods. Gums and carbonaceous materials that form due to the chemical instability of such fuel may clog fuel filters and disrupt the spray pattern of the fuel injector nozzle.

Olefins are highly reactive and may contribute toward jet fuel instability. Fortunately, neither crude oil nor Fischer-Tropsch synthesised jet fuel contain significant quantities of these hydrocarbons.

2.4.6. Contaminants

As discussed previously, surfactants are polar compounds that attach to the interface of fuel and water to form an emulsion. Surfactants may also reduce the efficiency of the water removal systems by adhering to surfaces of the coalescer. Even though surfactants are removed during

the refining process, jet fuel is analysed for the presence of these compounds throughout the various phases of the fuel distribution system as a precautionary measure.

2.4.7. Additives

Additives are compounds that are blended with jet fuel during the refining process and that serve to enhance fuel properties, as prescribed by regulatory authorities. The most important additives are listed below.

Fuel performance improvement additives:

- Antioxidants;
- Metal deactivators; and
- Fuel system icing inhibitors.

Fuel handling and maintenance additives:

- Electrical conductivity improvers;
- Leak detection additives;
- Biocidal additives; and
- Corrosion inhibitors/Lubricity improvers.

2.4.8. Composition

The importance of the maximum allowable quantities of aromatic compounds and sulphur compounds were discussed in Sections 2.4.3 and 2.4.4.

2.4.9. Additional requirements for jet fuel containing synthesised hydrocarbons

Jet fuels that contain synthetic hydrocarbons produced by the Fischer-Tropsch process must adhere to additional requirements. These requirements are described below.

Table 2.2. Requirements for aviation turbine fuels containing synthesised hydrocarbons (ASTM D7566-15c, 2015).

Property	Limit	Specification value	Test method
Volatility			
Distillation			D86
Distillation profile (°C):			
T50 – T10	Minimum	15.0	
T90 – T10	Minimum	40.0	
Fluidity			
Viscosity at -40°C (mm^2/s)	Maximum	12.0	ASTM D445
Lubricity			
Lubricity (mm)	Maximum	0.85	ASTM D5001
Composition			
Aromatics (vol %)	Minimum	8.4	ASTM D6379

Even though aromatics are unfavourable in terms of jet fuel combustion and emission characteristics, these compounds also increase the bulk density of the fuel. The absence of aromatic compounds in jet fuel may result in fuels that do not meet the minimum ASTM density requirements, hence the minimum aromatics specification for jet fuels that contain synthesised hydrocarbons (Table 2.2).

Moses and et al. (2009) offered isomerisation as a potential solution to increase the density of synthetic jet fuels; increased density can be achieved by increasing the carbon number distribution of these fuels without negatively affecting their freeze point behaviour. The mentioned study did not, however, investigate the effects of increased low temperature viscosity, which would also be brought about when increasing the carbon number distribution of synthetic jet fuels. The viscosity of synthetic jet fuels at -40°C is important when considering proper fuel atomisation, combustion, and low temperature fuel pumpability.

2.5. Effect of chemical composition on jet fuel properties

2.5.1. Physical properties of hydrocarbon classes

Jet fuel consists of a multitude of different hydrocarbon molecules blended together in the C_8 – C_{16} carbon number range. Table 2.3 displays the physical properties of the different hydrocarbons, which are representative of those found in jet fuel. Behaviour of each of the hydrocarbon groups in terms of their physical properties determines the bulk properties of jet fuel as a whole.

Comprehensive physical property data for longer carbon chain length molecules, e.g. C_{18} iso-paraffins, are scarce; hence, it was decided to evaluate the physical properties of molecules in the C_8 – C_9 range.

Table 2.3. Physical properties of hydrocarbons in the jet fuel regime (ASTM DS 4B, 1991).

Octane  Formula: C_8H_{18} Class: n-Paraffin Boiling point: 126.0℃ Freeze point: -57.0℃ Density at 15.6℃: 0.7070 g/cm^3 Viscosity at 37.8℃: 0.6371 cSt	2,3,4-Trimethylpentane 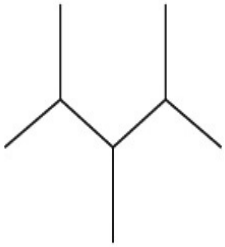 Formula: C_8H_{18} Class: iso-Paraffin Boiling point: 113.0℃ Freeze point: -109.0℃ Density at 15.6℃: 0.7240 g/cm^3 Viscosity at 37.8℃: 0.6823 cSt	Ethylcyclohexane 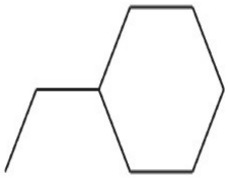 Formula: C_8H_{16} Class: Naphthene Boiling point: 132.0℃ Freeze point: -111.0℃ Density at 15.6℃: 0.7921 g/cm^3 Viscosity at 37.8℃: 0.8634 cSt	p-Xylene 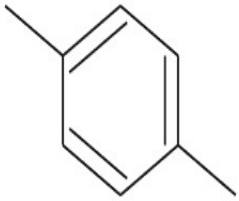 Formula: C_8H_{10} Class: Aromatic Boiling point: 138.0℃ Freeze point: 13.3℃ Density at 15.6℃: 0.8666 g/cm^3 Viscosity at 37.8℃: 0.6152 cSt
Nonane  Formula: C_9H_{20} Class: n-Paraffin Boiling point: 151.0℃ Freeze point: -53.0℃ Density at 15.6℃: 0.7219 g/cm^3 Viscosity at 37.8℃: 0.8070 cSt	2,2,3,4- Tetramethylpentane 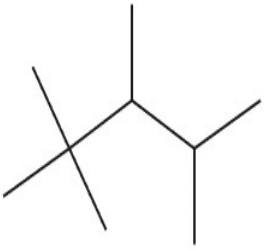 Formula: C_9H_{20} Class: iso-Paraffin Boiling point: 133.0℃ Freeze point: -121℃ Density at 15.6℃: 0.7236 g/cm^3 Viscosity at 37.8℃: 0.8119 cSt	Isopropylcyclohexane 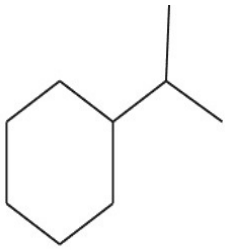 Formula: C_9H_{18} Class: Naphthene Boiling point: 155.0℃ Freeze point: -89.0℃ Density at 15.6℃: 0.8064 g/cm^3 Viscosity at 37.8℃: 1.0920 cSt*	1,3,5- Trimethylbenzene 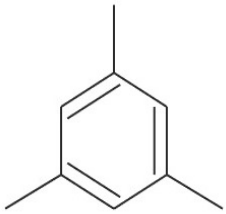 Formula: C_9H_{12} Class: Aromatic Boiling point: 165.0℃ Freeze point: -45.0℃ Density at 15.6℃: 0.8699 g/cm^3 Viscosity at 37.8℃: 0.8449 cSt
2-Methyloctane 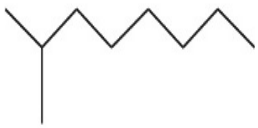 Formula: C_9H_{20} Class: iso-Paraffin Boiling point: 143.0℃ Freeze point: -80℃ Density at 15.6℃: 0.7177 g/cm^3 Viscosity at 37.8℃: 0.6582 cSt	2,2,5-Trimethylhexane 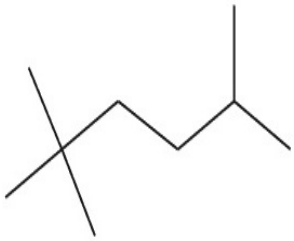 Formula: C_9H_{20} Class: iso-Paraffin Boiling point: 124.0℃ Freeze point: -105℃ Density at 15.6℃: 0.7154 g/cm^3 Viscosity at 37.8℃: 1.3067 cSt	3,3-Diethylpentane 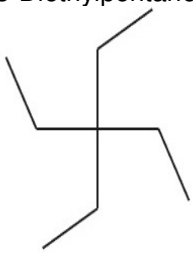 Formula: C_9H_{20} Class: iso-Paraffin Boiling point: 146.0℃ Freeze point: -33℃ Density at 15.6℃: 0.7587 g/cm^3 Viscosity at 37.8℃: 1.5876 cSt	2,2,3,3- Tetramethylpentane 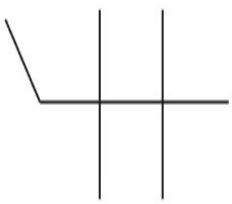 Formula: C_9H_{20} Class: iso-Paraffin Boiling point: 140.0℃ Freeze point: -10℃ Density at 15.6℃: 0.7607 g/cm^3 Viscosity at 37.8℃: 0.8146 cSt

Isopropylbenzene	o-Ethyltoluene	m-Ethyltoluene	p-Ethyltoluene
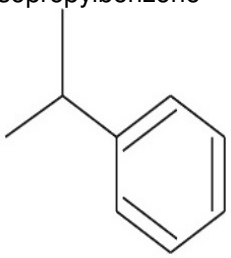	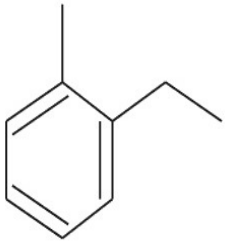	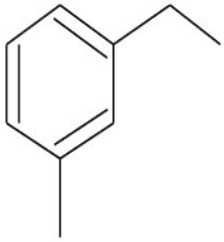	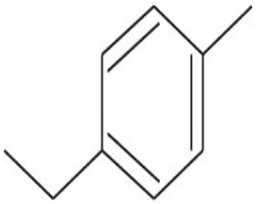
Formula: C_9H_{12} Class: Aromatic Boiling point: 152.0℃ Freeze point: -96.0℃ Density at 15.6℃: 0.8685 g/cm^3 Viscosity at 37.8℃: 0.7376 cSt	Formula: C_9H_{12} Class: Aromatic Boiling point: 165.0℃ Freeze point: -81.0℃ Density at 15.6℃: 0.8847 g/cm^3 Viscosity at 37.8℃: 0.8354 cSt	Formula: C_9H_{12} Class: Aromatic Boiling point: 161.0℃ Freeze point: -95.0℃ Density at 15.6℃: 0.8685 g/cm^3 Viscosity at 37.8℃: 0.7870 cSt	Formula: C_9H_{12} Class: Aromatic Boiling point: 162.0℃ Freeze point: -62.0℃ Density at 15.6℃: 0.8652 g/cm^3 Viscosity at 37.8℃: 0.6717 cSt

*Actual viscosity measured in the laboratory, not the literature value.

The following tendencies were observed upon evaluation of the physical property data in Table 2.3:

- Boiling point increases as the carbon chain length increases for molecules of the same hydrocarbon class;
- For molecules of the same carbon chain length, the order of increasing boiling point for the hydrocarbon classes is iso-paraffins, n-paraffins, naphthenes and aromatics;
- Density and viscosity increase as the carbon chain length of molecules of the same hydrocarbon class increase; and
- n-Paraffins exhibit higher freeze points than iso-paraffins.

In order to validate the observations made, additional hydrocarbon data from ASTM DS 4B were also considered. The data are graphically represented by Figure 2.4 – Figure 2.7 and discussed below.

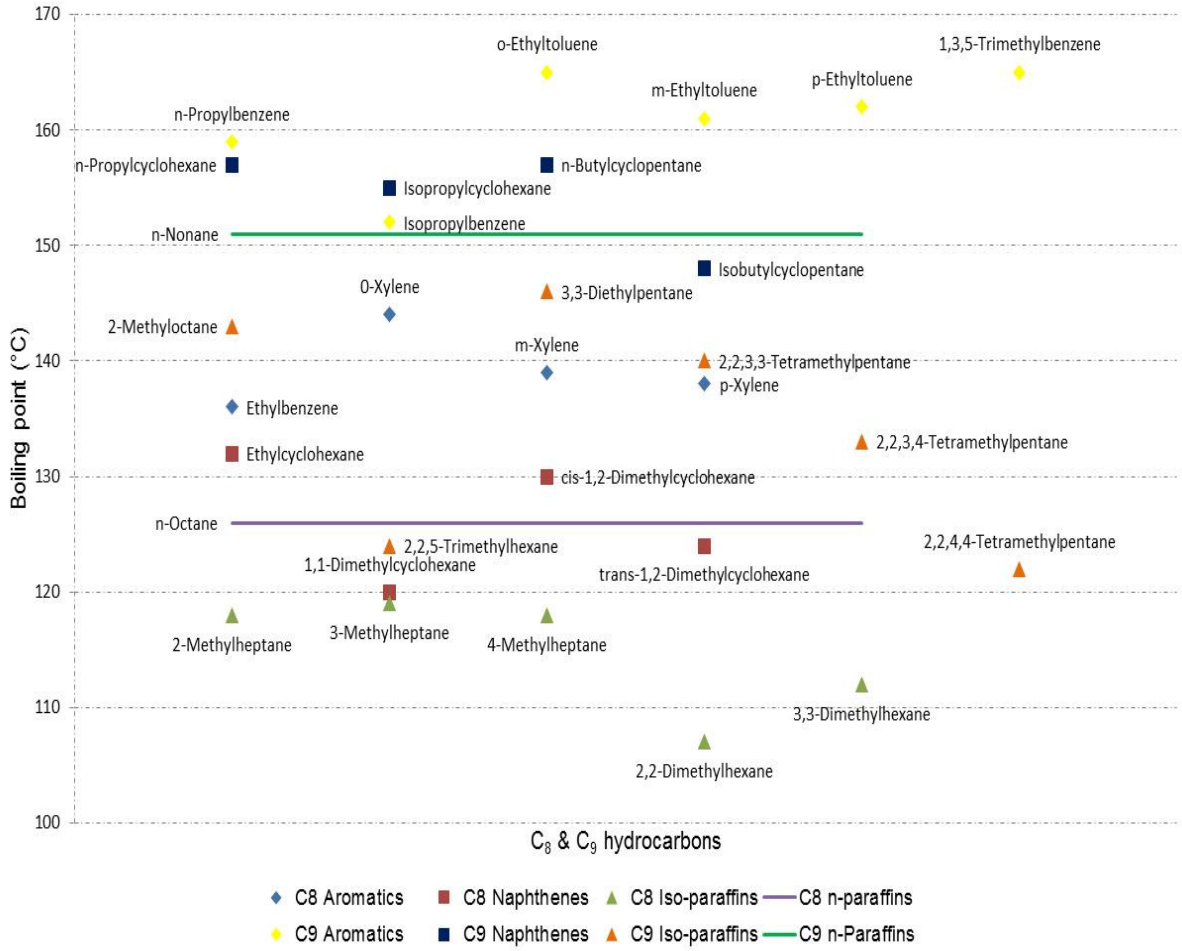

Figure 2.4. Boiling point data for C_8 and C_9 hydrocarbons (ASTM DS 4B, 1991).

According to Figure 2.4, iso-paraffins exhibit lower boiling points than n-paraffins, naphthenes and aromatics of the same carbon chain length, which corresponds well with previous observations made.

In general, aromatic compounds exhibit higher boiling points than naphthenes of the same carbon chain length; however, there are instances where the contrary is true, as indicated by the boiling points of isopropylcyclohexane and isopropylbenzene. Furthermore, aromatic compounds possess higher boiling points than n-paraffins of the same carbon chain length; however, there are instances where the boiling points of these hydrocarbon classes are similar, as indicated by the boiling points of isopropylbenzene and n-nonane.

The boiling points of naphthenes are higher than the boiling points of n-paraffins of the same carbon chain length; however, there are naphthenes that possess lower boiling points than n-paraffins, as indicated by the boiling points of isobutylcyclopentane and n-nonane.
The boiling points of 2,2,4,4-tetramethylpentane and 2,2,5-trimethylhexane, which are C_9 iso-paraffins, are lower than the boiling points of C_8 molecules, such as n-octane and ethylcyclohexane.

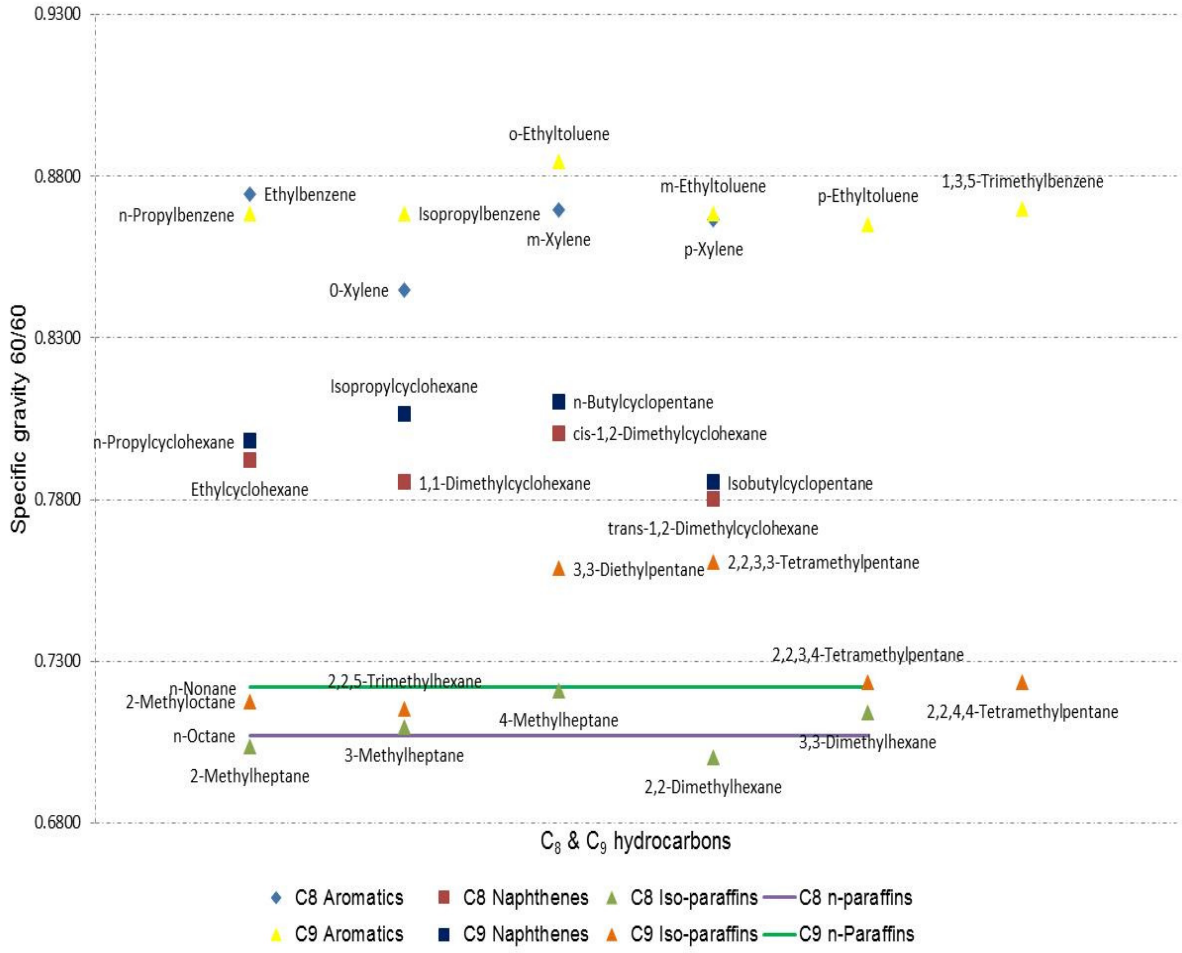

Figure 2.5. Specific gravity data for C_8 and C_9 hydrocarbons (ASTM DS 4B, 1991).

As can be observed in Figure 2.5, iso-paraffins possess lower specific gravities than naphthenes and aromatics of the same carbon chain length.

Naphthenes possess higher specific gravities than n-paraffins and iso-paraffins of the same carbon chain length. The specific gravities of naphthenes are lower than the specific gravities of aromatics of the same carbon chain length.

Ethylbenzene, a C_8 aromatic, possesses a higher specific gravity than n-propylbenzene, a C_9 aromatic. 2,2,5-Trimethylhexane is a C_9 iso-paraffin with a lower specific gravity than that of the C_8 iso-paraffin, 4-methylheptane.

Aromatic compounds possess much higher specific gravities than any of the other hydrocarbon classes, which is indicative of the fact that aromatic compounds are considered important contributors toward jet fuel bulk density.

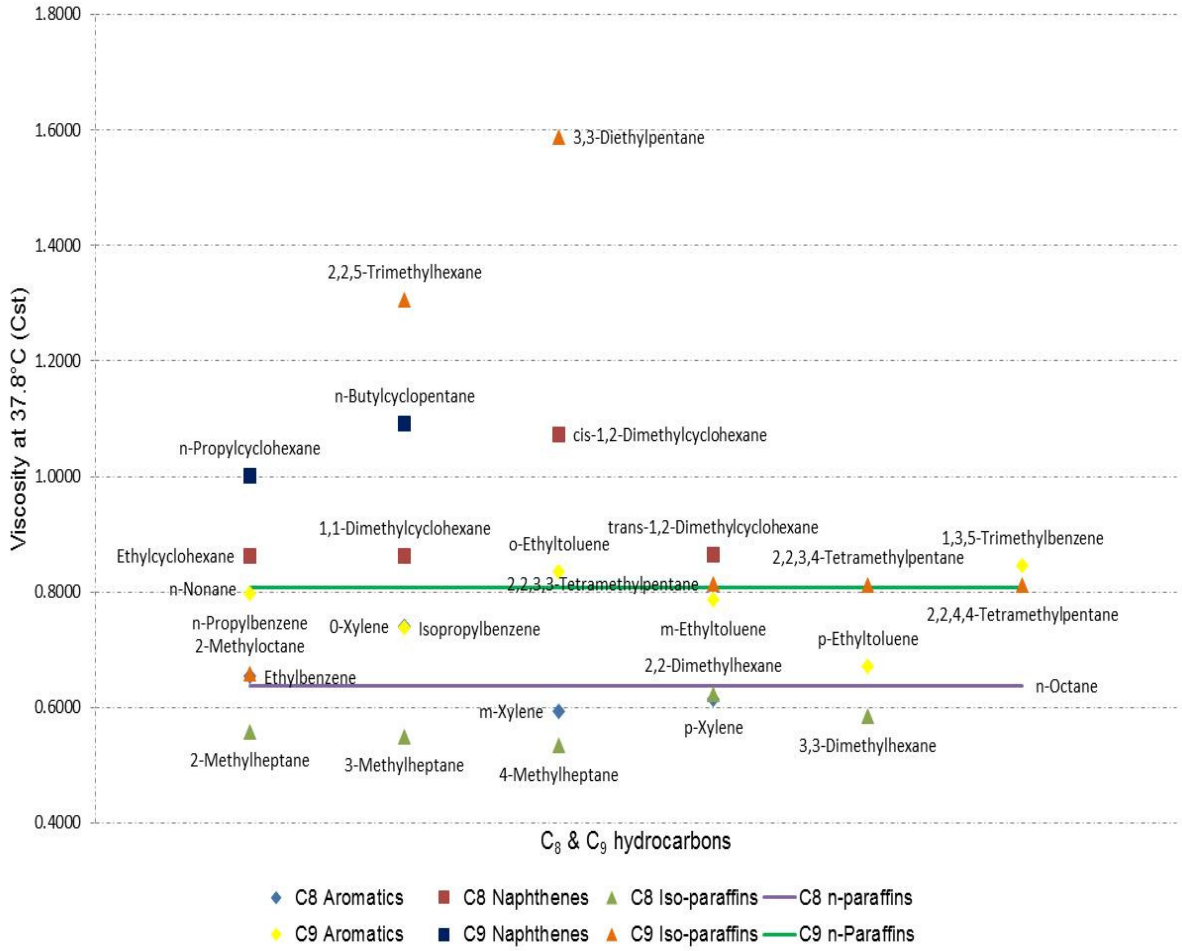

Figure 2.6. Viscosity data for C_8 and C_9 hydrocarbons (ASTM DS 4B, 1991).

As can be observed in Figure 2.6, naphthenes are more viscous than aromatics and n-paraffins of the same carbon chain length. The C_8 naphthenes are more viscous than n-nonane, which is a C_9 n-paraffin. The C_8 naphthenes are also more viscous than the C_9 aromatics; however, when considering the viscosity values of 1,1-dimethylcyclohexane and 1,3,5-trimethylbenzene, it can be observed that these two hydrocarbon classes may also exhibit viscosity values that are within a close range of one another.

iso-Paraffins exhibit unexpected viscosity behaviour; certain iso-paraffins are less viscous than aromatics and n-paraffins of the same carbon chain length, whilst other iso-paraffins are more viscous than any other hydrocarbon class. Examples of unexpected iso-paraffin viscosity behaviour are:

- Ethylcyclohexane, a C_8 naphthene, is more viscous than 2-methyloctane, a C_9 iso-paraffin;
- 2-Methyloctane (C_9 iso-paraffin) is less viscous than isopropylbenzene (C_9 aromatic) and n-nonane (C_9 n-paraffin);
- 3,3-Diethylpentane is ±45% more viscous than n-butylcyclopentane; and

- 2,2,5-Trimethylhexane is ±60% more viscous than 2,2,3,4-tetramethylpentane, which is also a C_9 iso-paraffin.

Jet fuel may contain longer carbon chain length iso-paraffins that exhibit similar viscosity behaviour to that of 3,3-diethylpentane and 2,2,5-trimethylhexane. These iso-paraffins may negatively affect the fluidity of jet fuel at low temperatures.

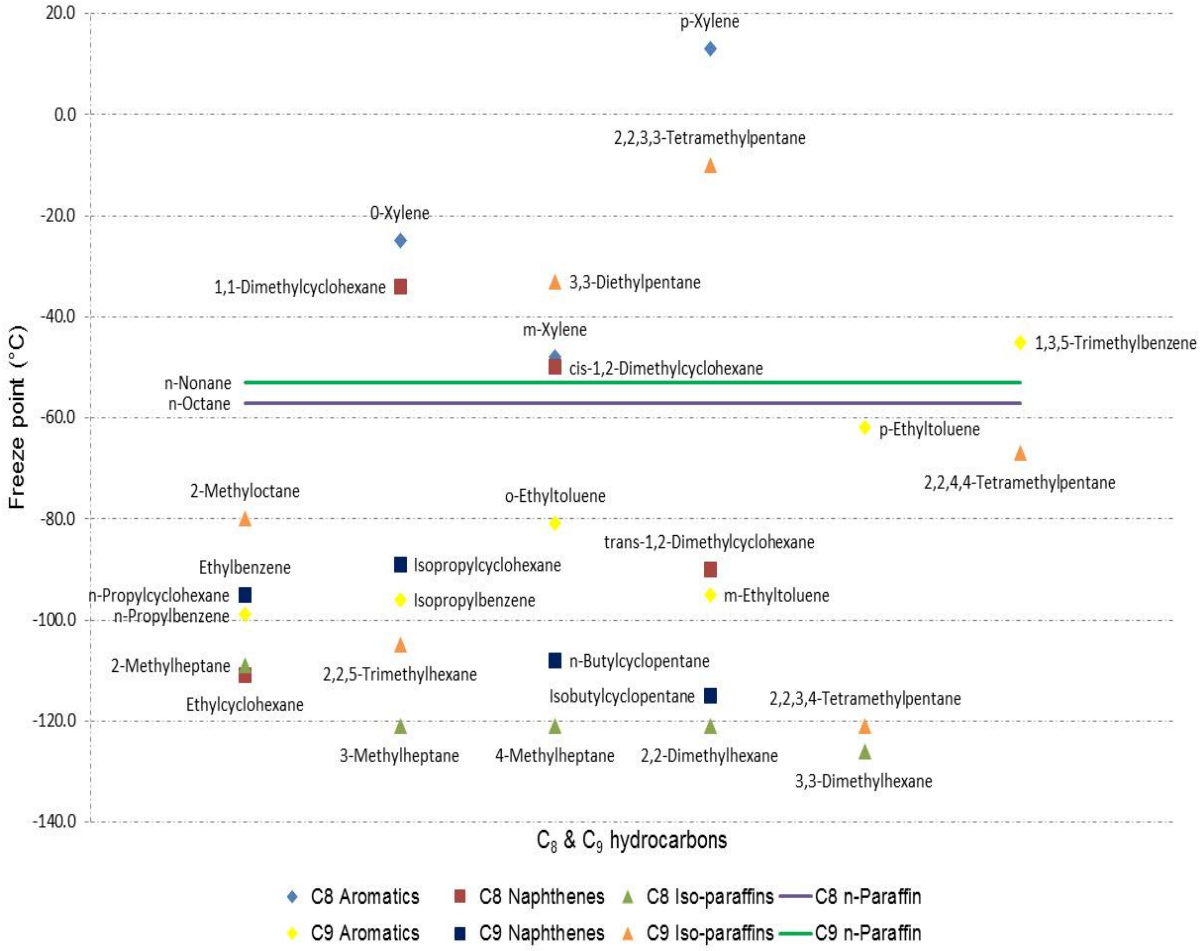

Figure 2.7. Freeze point data for C_8 and C_9 hydrocarbons (ASTM DS 4B, 1991).

As can be observed in Figure 2.7, the freeze point behaviour of the various hydrocarbon classes is mostly erratic, as no clear freeze point behavioural trends could be identified.

Jet fuel may contain longer carbon chain length iso-paraffins and aromatics that exhibit similar freeze point behaviour to that of 2,2,3,3-tetramethylpentane and p-xylene. Compounds such as these may negatively affect the freeze point characteristics of jet fuel.

2.5.2. Intermolecular forces

Intermolecular forces, or Van der Waal's forces, are the attractive forces that hold molecules together at certain temperatures. These forces are quite weak when compared to intramolecular forces, but they are strong enough to control physical properties, such as boiling and freezing points, vapour pressures and viscosities (Brown, et al., 2006).

Intermolecular forces can be divided into the following categories (McMurry & Fay, 2004):

- Dipole-dipole forces: Occur between neutral polar molecules;
- Ion-dipole forces: Occur between ions and polar molecules;
- London dispersion forces: Occur between nonpolar molecules; and
- Hydrogen bonds: Occur between hydrogen atoms and electronegative atoms.

Since the hydrocarbon classes present in jet fuel are mainly nonpolar, only London dispersion forces are applicable to the interactions occurring in jet fuel. London dispersion forces occur when there are temporary distortions in the electron cloud of a molecule. Such a distortion creates a temporary dipole, in other words, a molecule with opposite positive and negative ends. The temporary dipole of one molecule causes a second temporary dipole to occur in an adjacent molecule. Weak attractive forces then form between the two molecules, causing them to move closer together. The ease with which a molecule's electron cloud can be distorted by a nearby electric field, called polarizability, also affects the strength of these forces (McMurry & Fay, 2004).

London dispersion force trends:

- The strength of London dispersion forces increase with the number of electrons in a molecule.
- Smaller molecules are less polarizable, since it is more difficult to distort the electron cloud surrounding these molecules, thus resulting in smaller dispersion forces.
- Larger molecules contain more electrons than smaller molecules and are more polarizable, since it is easier to distort the electron cloud surrounding the molecules. This results in higher dispersion forces.
- Molecules with larger molecular surface areas experience higher dispersion forces than smaller molecules with smaller molecular surface areas. Furthermore, more spread-out shapes allow for greater contact between molecules, whereas smaller molecules minimise molecular contact.
- Spheres have the lowest surface area to volume ratio of any shape and are thus more compact than other molecular shapes. Spherical molecules can thus pack more closely together.

Espinosa et al. (2001) developed models describing the relationship between the boiling point and the molecular properties of a variety of organic compounds. Molecular properties used for this study included both the sum of atomic numbers and the dipole moments.

Riazi and Al-Roomi (2000) conducted a study to estimate the physical properties of petroleum products. The authors established a mathematical relationship between the boiling point distribution, specific gravity and refractive index of petroleum products in order to estimate a variety of physical properties, including viscosity. The estimated physical properties differed by 1 – 2% from the experimental property measurements. The polarizability of molecules can be related to refractive indices by the Lorentz–Lorenz equation. The authors thus utilised intermolecular forces in combination with boiling point distribution and specific gravity to estimate the physical properties of petroleum products (Born & Wolf, 1999).

Burch and Whitehead (2004) studied the freeze point characteristics of C_{10} – C_{20} iso-paraffins with a single methyl branch. In order to estimate the freeze points of these molecules, the authors established a mathematical relationship between freeze point, number of carbon atoms, location of the methyl group, Wiener path numbers, and Wiener index.

Rawat and Sati (2014) conducted similar studies to that of Burch and Whitehead (2004) and were able to establish a mathematical relationship between eight molecular properties and the freeze points of 30 paraffins ranging from C_1 to C_{10}. Even though the aforementioned authors did obtain satisfactory freeze point prediction results, both studies were limited to a narrow range of paraffins. As indicated by the studies conducted by Needham et al. (1988), as well as Charton and Charton (1994), currently there still exists insufficient understanding of the correlation between the freeze points of more complex molecules and the molecular properties that give rise to the freeze point behaviour of these molecules.

2.6. Conclusion

Crude oil refining and Fischer-Tropsch refining are the two most widely used production techniques to produce the liquid fuels that power the economies of the world. Crude oil refineries make use of complex separation, conversion and purification techniques. Distillation is a separation technique that forms the foundation of the crude oil refinery. Thereafter, conversion and purification processes are employed to bridge the gap between crude oil properties and desired product properties.

Fischer-Tropsch refineries convert coal or natural gas into synthesis gas, which in turn is converted into synthetic crude oil by making use of the Fischer-Tropsch synthesis process.

Synthetic crude oil produced during the synthesis process is converted into fully refined fuel products by making use of refining processes similar to those found in a conventional crude oil refinery.

Petroleum products produced in crude oil refineries consist of a mixture of paraffins, naphthenes, olefins, aromatics and heteroatomic compounds. Fuels produced in Fischer-Tropsch refineries consist mostly of linear- and branched paraffins. Fischer-Tropsch products are preferred from both a quality and an environmental perspective, since there are no sulphur compounds present in these fuels.

The physical properties of jet fuel are strictly controlled by aviation authorities to ensure that only jet fuels of the highest quality are approved for use in the aviation industry. Stringent quality control ensures:

- Optimum performance of turbine engines over a wide temperature range;
- Prolonged turbine engine lifespan;
- No blockages of fuel line components due to fuel instability; and
- Safety during storage and handling of the fuel.

The focus has always been on the physical properties of jet fuel as a whole; however, it is evident that the chemical composition of jet fuel is an important aspect to consider. The behaviour of individual molecules present in jet fuel, in terms of boiling point, density, viscosity and freeze point, have a profound effect on the performance of jet fuel.

From the literature studied, it is clear that the functional groups present in jet fuel vary in terms of their behaviour for each of the physical properties discussed. In fact, this physical property behaviour varied to such an extent that it was not possible to define principles that could fully explain the behaviour of these molecules. The literature suggests that the physical properties of molecules present in jet fuel are affected by London dispersion forces and hence polarizability. It was found that the relationship between molecular properties, such as London dispersion forces, and the physical properties of molecules is remarkably complex. It is anticipated that molecular modelling would provide more clarity as to which molecular properties could give rise to the physical property behaviour of the molecules present in jet fuel.

Chapter 3 : Experimental Procedures

3.1. Introduction

This chapter describes the molecular modelling procedures followed to develop viscosity and freeze point prediction models for n- and iso-paraffins with carbon chain lengths ranging from C_4 to C_{20}. Furthermore, the distillation procedures used for production of n- and iso-paraffin distillates are described. Since these distillates served as mixture components for the subsequent mixture design, the analytical techniques used to characterise these fractions are also discussed. The last section of this chapter explains the mixture design technique applied to study the effect of different i:n mass ratios and carbon number distributions on the viscosity and freeze point of jet fuel.

3.2. Molecular modelling

Molecular modelling software was used to develop viscosity and freeze point prediction models for n- and iso-paraffins with carbon chain lengths ranging from C_4 to C_{20}. The software used for this part of the study was Accelrys Materials Studio^{TM}. The steps followed to develop these models are outlined in Figure 3.1.

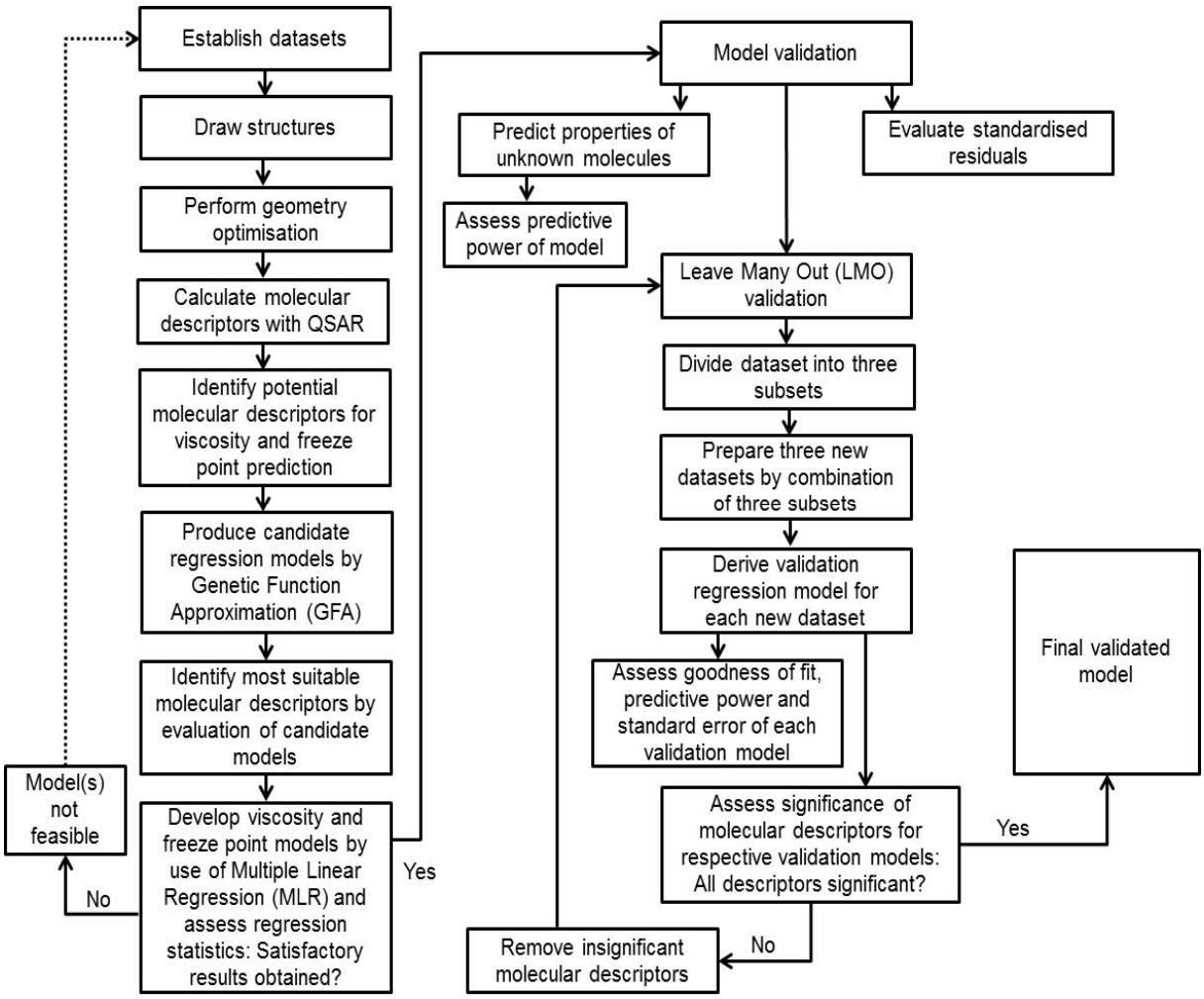

Figure 3.1. Flow diagram of development of molecular modelling prediction model.

3.2.1. Establish datasets

Two datasets were constructed for development of the viscosity and freeze point prediction models. The types of molecules chosen were representative of those typically present in synthetic jet fuel, namely n- and iso-paraffins. The smaller quantities of naphthenes and aromatics which may also be present in these fuels were excluded from the study. Data were obtained from ASTM DS 4B (1991) and the respective datasets are shown in Table 3.1 and Table 3.2. Molecules with carbon chain lengths shorter than C_8 and longer than C_{15} were included in the study since the size of the datasets were restricted by the limited amount of literature data available, particularly for iso-paraffins.

Table 3.1. Viscosity dataset.

Molecule	**Carbon number**	**Kinematic Viscosity (cSt)**
n-Butane	n-C_4	0.26
iso-Butane	iso-C_4	0.28
n-Pentane	n-C_5	0.34
2-Methylbutane	iso-C_5	0.32
n-Hexane	n-C_6	0.41
2-Methylpentane	iso-C_6	0.39
3-Methylpentane	iso-C_6	0.39
2,2-Dimethylbutane	iso-C_6	0.47
2,3-Dimethylbutane	iso-C_6	0.44
n-Heptane	n-C_7	0.51
2-Methylhexane	iso-C_7	0.48
3-Methylhexane	iso-C_7	0.45
3-Ethylpentane	iso-C_7	0.44
2,2-Dimethylpentane	iso-C_7	0.54
2,3-Dimethylpentane	iso-C_7	0.53
2,4-Dimethylpentane	iso-C_7	0.53
3,3-Dimethylpentane	iso-C_7	0.56
2,2,3-Trimethylbutane	iso-C_7	0.69
n-Octane	n-C_8	0.64
2-Methylheptane	iso-C_8	0.56
3-Methylheptane	iso-C_8	0.55
4-Methylheptane	iso-C_8	0.53
3-Ethylhexane	iso-C_8	0.53
2,2-Dimethylhexane	iso-C_8	0.62
2,3-Dimethylhexane	iso-C_8	0.58
2,4-Dimethylhexane	iso-C_8	0.71
3,3-Dimethylhexane	iso-C_8	0.59
3,4-Dimethylhexane	iso-C_8	0.57
2-Methyl-3-ethylpentane	iso-C_8	0.53
2,2,3-Trimethylpentane	iso-C_8	0.68
2,2,4-Trimethylpentane	iso-C_8	0.60
2,3,3-Trimethylpentane	iso-C_8	0.70
2,3,4-Trimethylpentane	iso-C_8	0.68
n-Nonane	n-C_9	0.81
2,2,3,3-Tertamethylpentane	iso-C_9	0.81
n-Decane	n-C_{10}	1.01
n-Undecane	n-C_{11}	1.26
n-Dodecane	n-C_{12}	1.54
n-Tridecane	n-C_{13}	1.75
n-Tetradecane	n-C_{14}	2.25
n-Pentadecane	n-C_{15}	2.49
n-Hexadecane	n-C_{16}	2.92
n-Heptadecane	n-C_{17}	3.58
n-Octadecane	n-C_{18}	4.13
n-Nonadecane	n-C_{19}	4.70
n-Eicosane	n-C_{20}	5.39

Table 3.2. Freeze point dataset.

Molecule	Carbon number	Freeze point (℃)
n-Butane	n-C_4	-138.4
n-Pentane	n-C_5	-129.7
2-Methylbutane	iso-C_5	-159.9
n-Hexane	n-C_6	-95.3
2-Methylpentane	iso-C_6	-153.7
n-Heptane	n-C_7	-90.6
2-Methylhexane	iso-C_7	-118.3
3-Methylhexane	iso-C_7	-119.4
3-Ethylpentane	iso-C_7	-118.6
2,2-Dimethylpentane	iso-C_7	-123.8
2,4-Dimethylpentane	iso-C_7	-119.2
3,3-Dimethylpentane	iso-C_7	-134.5
n-Octane	n-C_8	-56.8
2-Methylheptane	iso-C_8	-109.0
3-Methylheptane	iso-C_8	-120.5
4-Methylheptane	iso-C_8	-121.0
2,2,-Dimethylhexane	iso-C_8	-121.2
3,3-Dimethylhexane	iso-C_8	-126.1
2-Methyl-3-ethylpentane	iso-C_8	-115.0
2,2,3-Trimethylpentane	iso-C_8	-112.3
2,2,4-Trimethylpentane	iso-C_8	-107.4
2,3,3-Trimethylpentane	iso-C_8	-100.9
2,3,4-Trimethylpentane	iso-C_8	-109.2
n-Nonane	n-C_9	-53.5
2-Methyloctane	iso-C_9	-80.4
3-Methyloctane	iso-C_9	-107.6
2,2-Dimethylheptane	iso-C_9	-113.0
2,6-Dimethylheptane	iso-C_9	-102.9
2,2,5-Trimethylhexane	iso-C_9	-105.8
2,3,3-Trimethylhexane	iso-C_9	-116.8
2,3,5-Trimethylhexane	iso-C_9	-127.8
2,4,4-Trimethylhexane	iso-C_9	-113.4
3,3,4-Trimethylhexane	iso-C_9	-101.2
2,2-Dimethyl-3-ethylpentane	iso-C_9	-99.5
2,4-Dimethyl-3-ethylpentane	iso-C_9	-122.4
2,2,4,4-Tetramethylpentane	iso-C_9	-66.5
2,3,3,4-Tetramethylpentane	iso-C_9	-102.1
n-Decane	n-C_{10}	-29.6
2-Methylnonane	iso-C_{10}	-74.7
3-Methylnonane	iso-C_{10}	-84.8
5-Methylnonane	iso-C_{10}	-87.7
2,2,3,3-Tetramethylhexane	iso-C_{10}	-54.0
2,4-Dimethyl-3-isopropylpentane	iso-C_{10}	-81.7
n-Undecane	n-C_{11}	-25.6
n-Dodecane	n-C_{12}	-9.6
n-Tridecane	n-C_{13}	-5.4
n-Tetradecane	n-C_{14}	5.9
n-Pentadecane	n-C_{15}	9.9
n-Hexadecane	n-C_{16}	18.6
n-Heptadecane	n-C_{17}	22.0
n-Octadecane	n-C_{18}	28.2
n-Nonadecane	n-C_{19}	31.9
n-Eicosane	n-C_{20}	36.4

3.2.1.1. Viscosity dataset

A collection of 46 n- and iso-paraffins was selected. The kinematic viscosity values are reported at 37.8℃ (100℉).

3.2.1.2. Freeze point dataset

A collection of 53 n- and iso-paraffin molecules was selected.

3.2.2. Drawing of molecular structures and geometry optimisation

Structures of the molecules comprising the respective datasets were drawn by using the Materials Studio™ software. Molecules that are drawn using molecular modelling software need to be reconfigured in order to establish a stable geometry. This iterative reconfiguration process is known as geometry optimisation. Geometry optimisation adjusts the coordinates of all atoms so that the forces acting on the atoms are zero (Dassault Systemes, 2005b).

Geometry optimisation of the molecules was conducted with the VAMP module of the Materials Studio™ software. This is a semi-empirical molecular orbital program. VAMP was chosen to optimise the molecular structures since semi-empirical methods are capable of performing fast and reliable predictions of structural and electronic properties of organic molecules, thereby significantly reducing computational times (Dassault Systemes, 2014).

After selecting the VAMP module, the following parameters were specified in the software to perform the geometry optimisation of the individual molecules (Dassault Systemes, 2005c):

- Neglect of Diatomic Differential Overlap (NDDO) Hamiltonian: AM1;
- Convergence tolerance: Fine;
- Convergence scheme: Standard;
- Self-Consistent Field method (SCF) quality: Fine; and
- Maximum SCF cycles: 500.

3.2.3. QSAR molecular properties

After completion of the geometry optimisation procedure, molecular properties that may potentially describe the viscosity and freeze point behaviour of the dataset were identified and calculated using the Quantitative Structure-Activity Relationship (QSAR) module of Materials Studio™. In this study, molecular properties are referred to as molecular descriptors.

3.2.3.1. Viscosity prediction model: Molecular descriptors

Viscosity is defined as a liquid's resistance to flow (McMurry & Fay, 2004). According to the literature reviewed in Chapter 2, viscosity is influenced by intermolecular forces. The literature

further suggests that intermolecular forces are influenced by polarizability and by the spatial orientation of molecules. The following molecular descriptors were consequently evaluated as candidates for use in the viscosity prediction model:

- Molecular area (Van der Waal's area);
- Molecular volume (Van der Waal's volume);
- Molecular density;
- Moments of inertia;
- Molecular shadow indices;
- Molecular dipole moments;
- Balaban index; and
- Mean polarizability.

The most suitable molecular descriptors identified during evaluation of the viscosity prediction model will be discussed in Chapter 4.

3.2.3.2. Freeze point prediction model: Molecular descriptors

Freeze point is defined as the temperature at which a substance changes from the liquid phase to the solid phase (ASTM D5972-16, 2016). According to the literature reviewed in Chapter 2, freeze point is influenced by intermolecular forces. The literature further suggests that intermolecular forces are influenced by molecular size and shape. The following molecular descriptors were consequently selected as candidates for the freeze point prediction model:

- Zagreb index;
- Molecular density;
- Kappa-2;
- Molecular volume (Van der Waal's volume);
- Balaban index;
- Mean polarizability;
- Total molecular mass; and
- Wiener index.

The most suitable molecular descriptors identified during evaluation of the freeze point prediction model will be discussed in Chapter 5.

3.2.4. Model development

Statistical analyses were used to identify the most suitable models for prediction of viscosity and freeze point as a function of the specified molecular descriptors.

The Genetic Function Approximation (GFA) tool of Materials Studio™ was used to produce candidate models consisting of different combinations of the molecular descriptors mentioned above. The software performed this function automatically after being selected, and yielded five candidate models for the respective physical properties being studied. The molecular descriptors, which occurred most often in these candidate models, were identified. These descriptors were then used to develop the most suitable viscosity and freeze point models obtainable by application of Multiple Linear Regression (MLR). MLR was conducted by means of the data analysis function of Microsoft® Excel.

The regression statistics of the respective models were assessed to determine the quality of fit of the models. Emphasis was placed on evaluation of the R^2, adjusted R^2 and standard error values. The P-values associated with each model were also evaluated. The statistical terminology associated with this study will be discussed in Chapter 4.

3.2.5. Model validation

After a model has been developed, it needs to be validated to determine the accuracy of the model. The models developed above were validated by the following procedures:

- Leave Many Out (LMO) validation;
- Viscosity/freeze point prediction of unknown molecules; and
- Evaluation of the standardised residuals.

3.2.5.1. Leave Many Out (LMO) validation

The models were validated by following the leave a third ($\frac{1}{3}$) out validation procedure. This validation procedure utilises two thirds ($\frac{2}{3}$) of the original dataset to develop a validation model comprising of the molecular descriptors identified during development of the initial model. The resultant model is then used to predict the physical properties of the remaining $\frac{1}{3}$ of the dataset. This process is repeated until the physical properties of all the molecules in the original dataset have been predicted. The significance of the molecular descriptors for each validation model is also assessed. The LMO validation procedure is outlined below (Katrizky, et al., 2010):

1. The dataset was divided into three subsets by selecting each third molecule.
   1.1. The 1st, 4th, 7th, etc. molecules comprised the 1st subset.
   1.2. The 2nd, 5th, 8th, etc. molecules comprised the 2nd subset.
   1.3. The 3rd, 6th, 9th, etc. molecules comprised the 3rd subset.
2. Three datasets were prepared by combination of subsets 1 and 2, 1 and 3, and, lastly, 2 and 3.

3. Molecular descriptors identified during the development phase of the initial model were used to derive validation models for each dataset in step 2.
    3.1. The predictive power of the validation models was determined by assessing the goodness of fit and the standard error of each model. The accuracy of the viscosity/freeze point predictions for each validation model was assessed by means of the remaining $\frac{1}{3}$ of the dataset.
    3.2. The significance of the molecular descriptors for the respective validation models was determined by evaluation of the relevant P-values.
    3.3. Insignificant descriptors were removed from the original model, producing a reduced model.
4. The LMO validation procedure was repeated until all descriptors remaining in the models were significant. Once all the insignificant descriptors had been eliminated, the LMO validation process was used to determine the significance of the remaining molecular descriptors.

3.2.5.2. Viscosity/freeze point prediction of unknown molecules

The validated models were used to predict the viscosity/freeze point properties of molecules that did not form part of the datasets used during model development. The accuracy of the predictions was assessed.

3.3. Fractional distillation

In order to produce jet fuel with the desired low temperature fluidity characteristics as described in Chapter 1, refinery products were separated into their respective carbon numbers by means of fractional distillation. These fractions were in the C_9 – C_{18} carbon number range, and served as mixture components for the subsequent mixture design investigation.

3.3.1. Refinery products distilled

Two refinery products were distilled to produce the mixture components:

- C_8 – C_{20} product: Rich in n-paraffins; and
- C_8 – C_{27} product: Rich in iso-paraffins.

3.3.2. Distillation apparatus

A Pilodist PD104 distillation apparatus (Figure 3.2) was used to conduct the distillations. The distillation apparatus consists of a 30 theoretical plate wire gauze glass trickling column equipped with a reflux divider and 20 L reboiler flask. The maximum operating temperature of the apparatus is 400℃ and it operates at pressures ranging from 750.0 to 1.0 torr. The

apparatus makes use of a DCD 4001 control unit to monitor and adjust distillation parameters (Pilodist GmbH, n.d.).

Figure 3.2. Pilodist 104 (PD104) distillation apparatus (Pilodist GmbH, n.d.).

For each distillation, 10 kg of refinery product was loaded into the reboiler flask of the distillation apparatus. The flask was attached to the apparatus as illustrated in Figure 3.2, and the integrity of all other glass fixtures was verified. The appropriate distillation parameters were then entered into the distillation software and the distillation sequence was initialised. The reboiler flask was heated until the refinery product started boiling and vapours started rising into the distillation column. The distillation parameters were adjusted in such a manner as to obtain stable distillation conditions, whereafter the reflux divider was opened and the distillate was collected. The refinery product was separated into individual distillates by use of fractionation temperatures.

3.3.3. Reference distillation points

Literature boiling point values of C_8 – C_{18} n-paraffins served as reference points for the fractionation temperatures of the individual carbon numbers. The literature values are shown in Table 3.3. The Atmospheric Equivalent Temperature (AET) is the boiling point temperature of

substances at sea level (760 torr). Conventionally, the boiling points of all substance are converted to atmospheric equivalent temperatures to standardise reporting of these values.

Table 3.3. Boiling points of n-Paraffins (ASTM DS 4B, 1991).

n-Paraffin	Carbon number	Boiling point [AET] (℃)
n-Octane	C_8H_{18}	125.7
n-Nonane	C_9H_{20}	150.8
n-Decane	$C_{10}H_{22}$	174.2
n-Undecane	$C_{11}H_{24}$	195.9
n-Dodecane	$C_{12}H_{26}$	216.3
n-Tridecane	$C_{13}H_{28}$	235.5
n-Tetradecane	$C_{14}H_{30}$	253.6
n-Pentadecane	$C_{15}H_{32}$	270.7
n-Hexadecane	$C_{16}H_{34}$	286.9
n-Heptadecane	$C_{17}H_{36}$	302.0
n-Octadecane	$C_{18}H_{38}$	316.3

3.3.4. n-Paraffin distillation

The initial parameters used for distillation of the C_8 – C_{20} product are shown in Table 3.4. The distillation was commenced under atmospheric conditions; however, as the distillation progressed, the vacuum was adjusted to maintain optimum distillation conditions.

Table 3.4. n-Paraffin initial distillation parameters.

Distillation parameter	Parameter values
Reflux ratio	5:1
Vacuum (torr)	640.0
ΔT (℃)	16.0
Heating power (%)	8.0
Initial boiling point: Flask temperature (℃)	138.0

3.3.4.1. n-Paraffin distillation procedure

The initial fractionation temperature was set 4℃ below the literature boiling point value of n-octane (121.7℃). Individual distillates were collected at fractionation temperature intervals of 2℃ as the distillation progressed. Distillates were collected up to a fractionation temperature of 10℃ above the literature boiling point value of n-octadecane (326.3℃). The chemical composition of each distillate was determined by use of two-dimensional gas chromatography (GCxGC). The GCxGC results were then used to combine the appropriate distillates in such a manner as to obtain C_9 – C_{18} mixture components containing the highest concentration of desired molecules. In order for the fractions to remain representative of the entire refinery product, none of the fractions collected in the 121.7 - 324.3℃ temperature range were discarded; fractions were blended in a sequential manner to produce the mixture components.

3.3.5. iso-Paraffin distillation

The initial distillation parameters for the C_8 – C_{27} product are shown in Table 3.5. The distillation was initially conducted under a vacuum of 80.0 torr; however, as the distillation progressed, the vacuum also had to be adjusted to maintain optimum distillation conditions.

Table 3.5. iso-Paraffin initial distillation parameters.

Distillation parameter	Parameter values
Reflux ratio	5:1
Vacuum (torr)	80.0
ΔT (℃)	33.5
Heating power (%)	6.0
Initial boiling point: Flask temperature (℃)	127.0

3.3.5.1. iso-Paraffin distillation procedure

The procedure followed was similar to that of the n-paraffin distillation; the only difference was the initial fractionation temperature, which was set 9℃ below the literature boiling point value of n-octane (116.7℃). The initial fractionation temperature was lowered due to the iso-paraffins having lower boiling points than their n-paraffin counterparts.

3.4. Analytical techniques

The mixture components obtained from the distillation process were analysed in the laboratory to determine whether they were suitable for use in the subsequent mixture design study. The analyses conducted were:

- Freeze point;
- Kinematic viscosity at -20℃ and 20℃;
- Density at 20℃
- GCxGC.

3.4.1. Freeze point analysis

Freeze point measurements were conducted with a Phase Technology® FP-70X freeze point analyser conforming to the requirements of the ASTM D5972 method. The integrity of the instrument was verified by use of primary references with freeze points ranging from -57℃ to 0℃.

3.4.1.1. Freeze point analyser principle of operation

The sample was monitored for initial hydrocarbon crystal formation whilst being cooled by a Peltier device. After detection of crystals, the sample was reheated until the last crystals returned to the liquid phase. The instrument recorded the temperature at which the last crystals returned to the liquid phase as the freeze point (ASTM D5972-16, 2016).

A light source was positioned in such a manner that the light beam passed through the sample at an acute angle. If the sample was a homogeneous liquid, the beam was reflected from the bottom of the sample chamber and absorbed by the chamber lid; however, if the sample was non-homogeneous, the light beam was scattered by the solid-liquid phase boundaries and detected by the optical detector (ASTM D5972-16, 2016).

3.4.2. Kinematic viscosity and density analysis

Viscosity and density measurements were conducted with an Anton Paar Stabinger SVM3000 viscometer that conformed to the requirements of the ASTM D7042 method. The integrity of the instrument was verified by means of two primary references. The first primary reference possessed a viscosity of 4.5 cSt and a density of 0.8187 g/cm^3 at 20℃. The second reference possessed a viscosity of 8.0 cSt at -20℃.

3.4.2.1. Principle of viscosity measurement

The sample was introduced into the measurement cell by means of a syringe. The measurement cell consists of a pair of rotating concentric cylinders along with an oscillating U-tube. The instrument measured the dynamic viscosity from the rotational speed of the inner cylinder under the influence of the shear stress of the sample and an eddy current brake in combination with adjustment data. The density of the sample was measured by means of the oscillation frequency of the U-tube in combination with adjustment data. The kinematic viscosity was calculated by dividing the dynamic viscosity by the density (ASTM D7042-14, 2014).

3.4.3. GCxGC analysis

GCxGC measurements were conducted with a Pegasus 4D instrument equipped with both a Time-of-Flight Mass Spectrometer (TOF-MS) and a flame ionisation detector (FID). GCxGC is a powerful analytical technique used for comprehensive characterisation of complex volatile matrices. Calibration of the instrument was verified with a suitable set of primary references before sample analysis commenced.

3.4.3.1. GCxGC principle of operation

In order to enhance analyte separation, the sample was subjected to a double separation process achieved by two separate GC columns. Analytes that eluted from the first, non-polar column were transferred to the second, polar column. A modulator served as interface between the columns, and was located between the outlet of the fist column and the inlet of the second column (Van der Westhuizen, 2016), (Shimadzu Corporation, 2012).

Samples were injected at the inlet of the first column where they underwent separation based on boiling point differences. The modulator then transferred the separated analytes to the second column where they underwent further separation based on polarity. After eluting from the second column, analytes reached the detectors, which produced an electronic signal that was sent to the computer software for generation of a chromatogram (Shimadzu Corporation, 2012).

3.5. n-Paraffin and iso-paraffin mixture design

The Stat-Ease Design-Expert® software was employed to produce an experimental design for mixtures that varied both the i:n mass ratio and the carbon number distribution. The responses of interest were kinematic viscosity and freeze point. The relevance of these two physical properties was discussed previously in Chapter 1.

Mixture designs are employed when the response changes as a function of the relative proportions of the components present in the mixture. Since both the i:n mass ratio and the carbon number distribution for the mixtures had to vary, a custom optimal design had to be implemented. Custom optimal designs can accommodate both unequal mixture component ranges and multicomponent constraints (Stat-Ease, Inc., 2014).

Cornell (2002) provides a comprehensive overview of the design of mixture experiments and model development. A brief overview of the design parameters, as well as of the model development, validation and optimisation procedures, is given below. The steps followed to develop the freeze point and viscosity models are outlined in Figure 3.3.

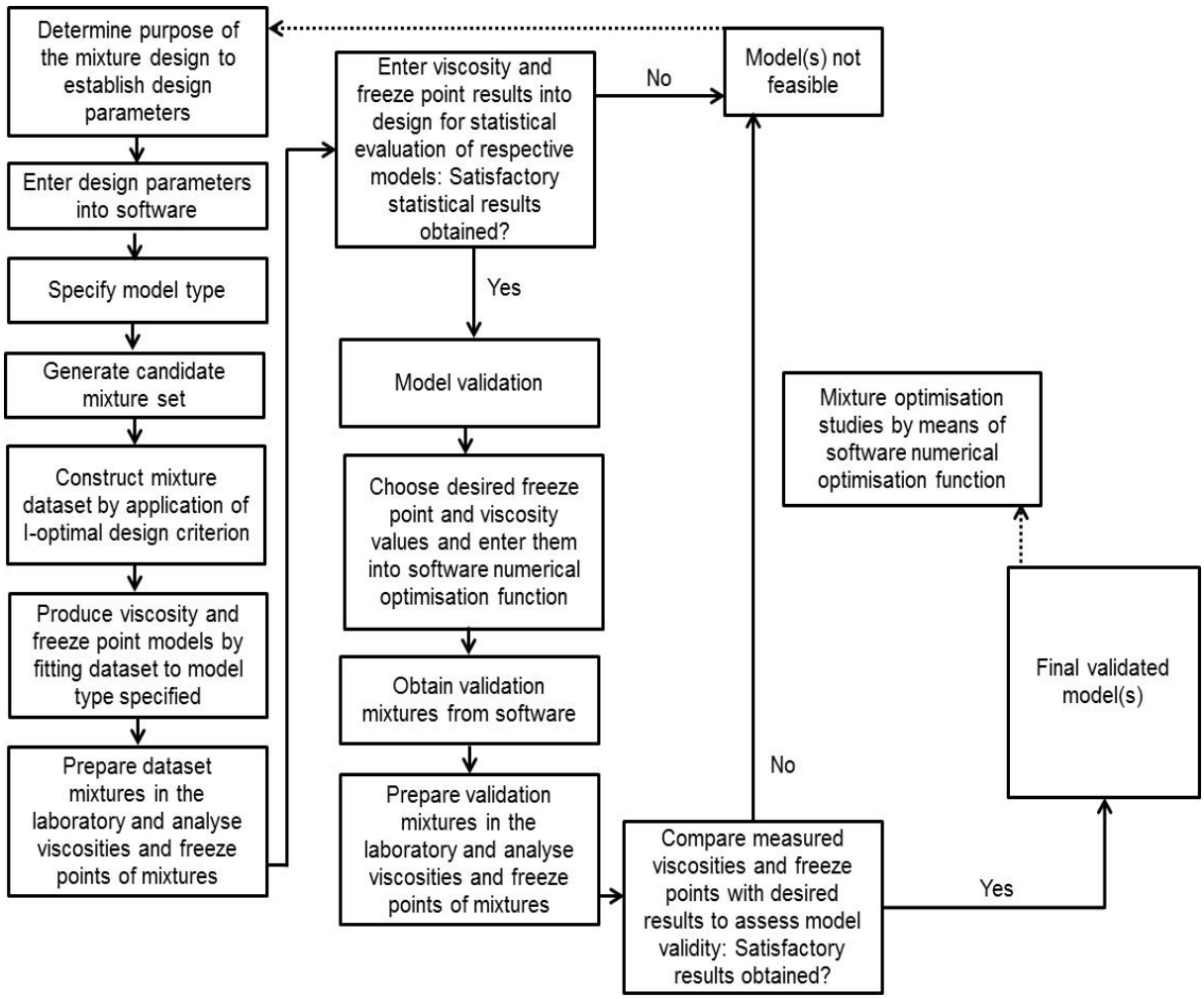

Figure 3.3. Flow diagram of mixture model development.

3.5.1. Design-Expert® parameters

After establishing the purpose of the mixture design (0), the following required parameters were selected:

- Number of mixture components: 2;
- Mixture components low value (Mass percent): 0;
- Mixture components high value (Mass percent): 100;
- Number of numeric factors: 9;
- Numeric factor low value (Mass percent): 0; and
- Numeric factor high value (Mass percent): 40.

3.5.1.1. Number of mixture components

This parameter was specified as 2 in order to vary the i:n mass ratio of the mixtures.

3.5.1.2. Mixture components low and high values

The i:n mass ratio was varied between 0 and 100 mass percent to determine the full effects brought about by the presence of n- and iso-paraffins in jet fuel mixtures. The number of the mixture components, as well as the low and high value parameters of such components, should theoretically enable determination of the ideal i:n mass ratio, as discussed in Chapter 1.

3.5.1.3. Number of numeric factors

In order to vary the carbon number distribution of mixtures in the C_9 – C_{18} range, this parameter was initially set at 10; however, due to the design space being too constrained, no feasible candidate mixture set could be obtained. The design was therefore simplified by omitting the C_{18} mixture component from the design construction. This value was consequently set at 9.

3.5.1.4. Numeric factor low and high values

These values were specified as 0 and 40 mass percent respectively to vary the mass contribution of the C_9 – C_{17} mixture components. To prevent exclusion of C_{18} components from the design, the sum of the C_9 – C_{17} mixture components was restricted in the software to allow for the presence of 0 – 40 mass percent C_{18} components in the mixtures.

The range of the numeric factors was chosen in order for the carbon number distribution to correspond approximately to that of a conventional crude oil derived jet fuel. The number of numeric factors, as well as the low and high value parameters of such numeric factors, should theoretically enable determination of the ideal carbon number distribution.

3.5.2. Specification of model type

After entering the design parameters into the Design-Expert® software, the type of model used for the experimental design was specified in the software. A quadratic model was chosen to determine the effect of the i:n mass ratio on the viscosity and freeze point properties of the mixtures. Use of the quadratic model allowed for identification of possible interactions between the n- and iso-paraffins. Due to the wide carbon number distribution range being studied, only the linear effect of the carbon numbers on viscosity and freeze point was evaluated. The model specified for freeze point and viscosity prediction was thus a quadratic x linear crossed model.

3.5.3. Candidate mixture set

After specifying both the design parameters and the model type, the Design-Expert® software automatically generated a candidate mixture set using the quadratic x linear crossed model. A candidate set is a comprehensive set of mixtures that can potentially be used in the mixture design. The crossed model produced a candidate set consisting of 3605 mixtures.

3.5.4. Mixture design

Optimal designs are functions used to construct model datasets. I-optimal designs provide lower average prediction variance across the region of the design space. Furthermore, I-optimal designs are desirable where the goal is to optimise the mixture components and numeric factors to estimate a preferred response, which requires greater precision in the estimated model (Stat-Ease, Inc., 2014).

The I-optimal design criterion was specified in the software for construction of the dataset since the aim of the study was to optimise both the i:n mass ratio and the carbon number distribution of jet fuels. Following construction of the candidate set, the 50 most suitable mixtures from the candidate set were used to create the dataset. The dataset was constituted as follows: 29 mixtures for model estimation, 12 mixtures for lack-of-fit testing and 9 replicates for estimation of the experimental error.

Once the dataset had been constructed, the Design-Expert® software automatically fitted the 50 mixtures to the quadratic x linear model to create two separate models for viscosity and freeze point prediction.

3.5.5. Mixture preparation and analyses

Following construction of the respective models, the aforementioned 50 mixtures were prepared in the laboratory by making use of the n- and iso-paraffin mixture components produced by means of fractional distillation. A calibrated Sartorius balance with 0.01 g accuracy was used to ensure precise sample preparation. Furthermore, 50.0 g of each mixture was prepared to ensure that sufficient sample quantities were available for response analyses. The viscosities and freeze points of the resultant mixtures were measured. The final mixture design and values of the measured properties are depicted in Table 3.6.

Table 3.6. Mixture design for variation of i:n mass ratio and carbon number distribution.

	Mixture components (Mass %)		Numeric factors (Mass %)										Blend properties (Responses)	
Run	iso-Paraffin	n-Paraffin	C_9	C_{10}	C_{11}	C_{12}	C_{13}	C_{14}	C_{15}	C_{16}	C_{17}	C_{18}	Freeze point (℃)	Viscosity at 20℃ (cSt)
1	50	50	10.0	10.0	10.0	10.0	10.0	10.0	10.0	10.0	10.0	10.0	-10.3	2.4
2	100	0	0.0	0.0	0.0	0.0	20.0	0.0	0.0	40.0	40.0	0.0	-37.9	4.0
3	50	50	40.0	20.0	0.0	0.0	40.0	0.0	0.0	0.0	0.0	0.0	-33.8	1.4
4	0	100	0.0	0.0	40.0	0.0	0.0	0.0	0.0	20.0	40.0	0.0	8.1	3.0
5	50	50	0.0	0.0	40.0	0.0	20.0	0.0	0.0	0.0	40.0	0.0	-2.9	2.6
6	0	100	0.0	0.0	0.0	0.0	0.0	40.0	0.0	20.0	0.0	40.0	14.4	4.5
7	50	50	40.0	0.0	0.0	0.0	0.0	0.0	20.0	0.0	40.0	0.0	-5.1	2.2
8	100	0	0.0	40.0	0.0	20.0	0.0	0.0	0.0	0.0	40.0	0.0	-43.0	2.1
9	50	50	20.0	0.0	40.0	40.0	0.0	0.0	0.0	0.0	0.0	0.0	-34.2	1.5
10	50	50	0.0	0.0	0.0	40.0	20.0	0.0	0.0	40.0	0.0	0.0	-4.2	2.7
11	50	50	0.0	0.0	0.0	0.0	40.0	20.0	40.0	0.0	0.0	0.0	-12.7	2.9
12	100	0	0.0	0.0	0.0	40.0	0.0	0.0	0.0	0.0	20.0	40.0	-37.3	3.5
13	100	0	0.0	0.0	20.0	40.0	0.0	0.0	40.0	0.0	0.0	0.0	-56.6	2.2
14	0	100	0.0	20.0	0.0	0.0	0.0	0.0	40.0	0.0	0.0	40.0	11.8	3.5
15	50	50	0.0	0.0	0.0	40.0	0.0	20.0	0.0	0.0	40.0	0.0	-2.6	3.0
16	100	0	0.0	0.0	0.0	40.0	20.0	0.0	0.0	40.0	0.0	0.0	-52.3	2.6
17	75	25	0.0	40.0	20.0	0.0	40.0	0.0	0.0	0.0	0.0	0.0	-42.5	1.6
18	0	100	40.0	0.0	0.0	0.0	0.0	40.0	20.0	0.0	0.0	0.0	-9.7	1.9
19	50	50	20.0	0.0	0.0	0.0	0.0	40.0	0.0	40.0	0.0	0.0	-9.9	2.5
20	100	0	40.0	0.0	0.0	0.0	0.0	0.0	0.0	40.0	0.0	20.0	-44.0	2.1
21	50	50	0.0	20.0	0.0	40.0	0.0	0.0	0.0	0.0	0.0	40.0	0.5	2.6
22	100	0	20.0	0.0	0.0	0.0	0.0	0.0	40.0	0.0	40.0	0.0	-42.6	2.8
23	50	50	0.0	40.0	20.0	0.0	0.0	40.0	0.0	0.0	0.0	0.0	-19.6	1.7
24	0	100	40.0	0.0	20.0	0.0	0.0	0.0	0.0	0.0	0.0	40.0	6.6	2.1
25	50	50	0.0	40.0	0.0	0.0	0.0	0.0	40.0	20.0	0.0	0.0	-12.4	2.2
26	50	50	20.0	0.0	40.0	0.0	0.0	0.0	40.0	0.0	0.0	0.0	-19.0	1.8
27	50	50	0.0	0.0	0.0	0.0	20.0	40.0	0.0	0.0	0.0	40.0	2.3	3.8
28	100	0	20.0	0.0	0.0	0.0	40.0	40.0	0.0	0.0	0.0	0.0	-53.6	2.0
29	0	100	0.0	0.0	0.0	40.0	0.0	0.0	40.0	20.0	0.0	0.0	0.4	2.9
30	100	0	40.0	20.0	0.0	40.0	0.0	0.0	0.0	0.0	0.0	0.0	BDL	1.2
31	50	50	0.0	0.0	20.0	0.0	0.0	0.0	0.0	40.0	0.0	40.0	4.1	4.0
32	0	100	0.0	40.0	0.0	40.0	0.0	0.0	0.0	0.0	20.0	0.0	-5.1	1.9
33	0	100	0.0	40.0	0.0	40.0	0.0	0.0	0.0	0.0	20.0	0.0	-5.2	1.9
34	50	50	10.0	10.0	10.0	10.0	10.0	10.0	10.0	10.0	10.0	10.0	-10.4	2.4
35	50	50	10.0	10.0	10.0	10.0	10.0	10.0	10.0	10.0	10.0	10.0	-10.4	2.4
36	50	50	0.0	0.0	0.0	0.0	40.0	20.0	40.0	0.0	0.0	0.0	-12.6	2.9
37	50	50	40.0	0.0	0.0	0.0	0.0	0.0	20.0	0.0	40.0	0.0	-5.3	2.2
38	0	100	0.0	40.0	0.0	0.0	20.0	0.0	0.0	40.0	0.0	0.0	2.7	2.2
39	0	100	0.0	40.0	0.0	0.0	20.0	0.0	0.0	40.0	0.0	0.0	2.4	2.2
40	50	50	0.0	0.0	40.0	0.0	20.0	0.0	0.0	0.0	40.0	0.0	-3.7	2.6
41	0	100	20.0	0.0	0.0	40.0	40.0	0.0	0.0	0.0	0.0	0.0	-17.5	1.8
42	100	0	20.0	0.0	0.0	0.0	0.0	40.0	0.0	0.0	40.0	0.0	-45.2	2.6
43	100	0	0.0	0.0	40.0	0.0	40.0	0.0	0.0	20.0	0.0	0.0	-62.5	2.1
44	0	100	0.0	0.0	40.0	0.0	40.0	20.0	0.0	0.0	0.0	0.0	-14.7	2.1
45	50	50	0.0	0.0	20.0	0.0	0.0	0.0	0.0	40.0	0.0	40.0	4.2	4.0
46	100	0	0.0	0.0	40.0	0.0	0.0	40.0	0.0	20.0	0.0	0.0	-55.6	2.2
47	100	0	0.0	0.0	0.0	0.0	20.0	0.0	40.0	40.0	0.0	0.0	-43.5	3.5
48	50	50	40.0	20.0	0.0	0.0	40.0	0.0	0.0	0.0	0.0	0.0	-34.6	1.4
49	100	0	0.0	40.0	0.0	0.0	0.0	0.0	20.0	0.0	0.0	40.0	-40.4	2.5
50	0	100	0.0	0.0	0.0	0.0	40.0	0.0	0.0	0.0	40.0	20.0	13.9	4.0

*BDL: Below Detection Limit.

3.5.6. Statistical evaluation of the model

The viscosity and freeze point results of the mixtures prepared in the laboratory were entered into the Design-Expert® software for statistical evaluation of the respective models. The software then automatically produced a set of statistical parameters, which were evaluated to determine the significance of the models developed. Emphasis was placed on evaluation of the R^2, adjusted R^2 and cross-validated R^2 values. The standard error of each model was also evaluated. The statistical terminology associated with this study will be discussed in Chapter 4 and Chapter 7.

3.5.7. Model validation

After satisfactory results had been obtained from the statistical evaluation of models, they were validated. The freeze point and viscosity models were validated by means of the dual surface optimisation technique. This technique must be employed to optimise multiple blend properties simultaneously. The Design-Expert® software applies the desirability function approach developed by Derringer and Suich (1980) for dual surface optimisations. The desirability value of the predicted response is interpreted as the degree to which the predicted response satisfies the desired response. The resultant desirability value ranges between 0 and 1, with 1 being the highest degree of satisfaction (Coetzer, et al., 2008). The Design-Expert® dual surface optimisation technique is an automated process that uses the desired responses entered into the software to predict optimised mixture recipes.

The desired viscosity and freeze point values were entered into the Design-Expert® software and converted to individual desirability functions. The individual desirability functions were then combined to produce a single desirability value. The resultant desirability value was lastly used by the software to predict the optimised i:n mass ratio and carbon number distribution mixtures that would theoretically meet the desired viscosity and freeze point criteria. Table 3.7 depicts nine validation mixtures obtained from the numerical optimisation function of the Design-Expert® software. The desired freeze point value was kept constant at -50°C for all validation mixtures, whilst the desired viscosity values ranged from 1.4 to 2.2 cSt at 20°C. The mixtures were prepared in the laboratory, after which the viscosity and freeze point of each mixture was measured. The predicted blend properties were lastly compared to the measured blend properties to validate the models.

Table 3.7. Validation mixtures.

Mixture	1	2	3	4	5	6	7	8	9
n-Paraffin mixture component (Mass %)	0	2	2	4	5	5	7	10	11
iso-Paraffin mixture component (Mass %)	100	98	98	96	95	95	93	90	89
C_9 (Mass %)	13.6	20.8	4.5	3.8	4.3	28.6	15.3	6.4	13.2
C_{10} (Mass %)	33.3	20.5	25.0	3.6	20.3	24.4	17.0	4.2	1.4
C_{11} (Mass %)	9.2	6.3	1.2	39.4	5.0	0.7	22.5	27.1	34.0
C_{12} (Mass %)	4.2	2.9	13.1	4.0	35.1	18.2	13.3	2.8	35.4
C_{13} (Mass %)	3.5	7.4	12.3	3.3	6.6	0.0	4.3	39.4	1.0
C_{14} (Mass %)	4.7	12.4	26.3	39.4	8.0	13.0	7.9	2.8	1.0
C_{15} (Mass %)	3.7	16.5	17.7	2.8	20.7	2.3	4.9	3.7	1.4
C_{16} (Mass %)	10.7	2.5	0.0	1.1	0.0	6.1	4.1	9.9	1.2
C_{17} (Mass %)	1.9	2.9	0.0	1.0	0.0	4.9	5.4	1.5	0.9
C_{18} (Mass %)	15.1	7.8	0.0	1.6	0.0	1.7	5.5	2.1	10.4
Measured freeze point (°C)	-52.2	-50.0	-51.9	-51.6	-49.0	-46.3	-36.9	-42.7	-29.7
Measured viscosity at 20°C (cSt)	1.8	1.8	1.9	1.9	1.9	1.5	1.7	2.0	1.7
Desired/predicted freeze point (°C)	-50.0	-50.0	-50.0	-55.0	-50.0	-50.0	-50.0	-50.0	-50.0
Desired/predicted viscosity at 20°C (cSt)	1.8	1.8	1.8	1.8	1.8	1.4	1.7	2.2	1.8

3.5.8. Ideal jet fuel mixtures

Since the nine validation mixtures in Table 3.7 were obtained by means of the numerical optimisation function of Design-Expert®, these mixtures were also used to determine the ideal i:n mass ratio and carbon number distribution of jet fuels that possess viscosities lower than 4.5 cSt at -20°C and freeze points below -47°C, as discussed in Chapter 1. This was achieved by calculating the average i:n mass ratio and carbon number distribution of the nine mixtures by means of Microsoft® Excel. The resultant i:n mass ratio and carbon number distribution was used to prepare and analyse a final blend to confirm the validity of the theoretical ideal i:n mass ratio and carbon number distribution. As before, the sample was analysed for viscosity and freeze point. Table 3.8 depicts the results of the final blend prepared in the laboratory.

Table 3.8. Ideal ASTM jet fuel mixture.

n-Paraffin mixture component (Mass %)	5
iso-Paraffin mixture component (Mass %)	95
C_9 (Mass %)	12.3
C_{10} (Mass %)	16.6
C_{11} (Mass %)	16.1
C_{12} (Mass %)	14.3
C_{13} (Mass %)	8.7
C_{14} (Mass %)	12.8
C_{15} (Mass %)	8.2
C_{16} (Mass %)	3.9
C_{17} (Mass %)	2.1
C_{18} (Mass %)	4.9
Measured freeze point (°C)	-47.1
Measured viscosity at 20°C (cSt)	1.8
Measured viscosity at -20°C (cSt)	4.3

Furthermore, the numerical optimisation function of the software was used to produce 10 theoretical blends, which minimised both viscosity and freeze point. The 10 optimised mixtures are depicted in Table 3.9.

Table 3.9. Optimum blends for minimised freeze point and viscosity.

Mixture	**1**	**2**	**3**	**4**	**5**	**6**	**7**	**8**	**9**	**10**
n-Paraffin mixture component (Mass %)	0	0	0	0	0	0	0	0	0	0
iso-Paraffin mixture component (Mass %)	100	100	100	100	100	100	100	100	100	100
C_9 (Mass %)	30.0	22.0	22.0	30.0	24.0	5.0	32.0	31.0	30.0	32.0
C_{10} (Mass %)	2.0	20.0	15.0	4.0	24.0	33.0	10.0	6.0	16.0	12.0
C_{11} (Mass %)	32.0	34.0	30.0	32.0	30.0	40.0	35.0	27.0	27.0	33.0
C_{12} (Mass %)	33.0	10.0	9.0	21.0	2.0	2.0	2.0	26.0	0.0	3.0
C_{13} (Mass %)	1.0	5.0	6.0	2.0	10.0	5.0	1.0	1.0	13.0	9.0
C_{14} (Mass %)	0.0	2.0	9.0	4.0	0.0	7.0	1.0	1.0	0.0	0.0
C_{15} (Mass %)	1.0	2.0	8.0	0.0	2.0	2.0	13.0	5.0	13.0	1.0
C_{16} (Mass %)	1.0	2.0	0.0	2.0	6.0	2.0	6.0	3.0	1.0	7.0
C_{17} (Mass %)	0.0	1.0	0.0	4.0	0.0	3.0	0.0	1.0	0.0	1.0
C_{18} (Mass %)	0.0	2.0	1.0	1.0	2.0	1.0	0.0	-1.0	0.0	2.0
Predicted freeze point (°C)	-65.9	-63.9	-62.5	-64.1	-62.8	-62.6	-63.0	-62.8	-62.6	-63.5
Predicted viscosity at 20°C (cSt)	1.1	1.1	1.2	1.2	1.1	1.2	1.2	1.2	1.2	1.2

The 10 mixtures in Table 3.9 were also used to determine the ideal i:n mass ratio and carbon number distribution of jet fuels that minimised viscosity and freeze point. This was achieved by calculating the average i:n mass ratio and carbon number distribution of the 10 mixtures by means of Microsoft® Excel. The resultant i:n mass ratio and carbon number distribution was used to prepare and analyse a final blend in the laboratory. Table 3.10 depicts the results of the final blend prepared in the laboratory.

Table 3.10. Ideal i:n jet fuel mixture for minimising freeze point and viscosity.

n-Paraffin mixture component (Mass %)	0
iso-Paraffin mixture component (Mass %)	100
C_9 (Mass %)	25.8
C_{10} (Mass %)	14.2
C_{11} (Mass %)	32.0
C_{12} (Mass %)	10.8
C_{13} (Mass %)	5.3
C_{14} (Mass %)	2.4
C_{15} (Mass %)	4.7
C_{16} (Mass %)	3.0
C_{17} (Mass %)	1.0
C_{18} (Mass %)	0.8
Measured freeze point (°C)	-79.1
Measured viscosity at 20°C (cSt)	1.3
Measured viscosity at -20°C (cSt)	2.9

The results from Table 3.8 and Table 3.10 were lastly combined to produce ideal i:n mass ratio and carbon number distribution ranges for jet fuel that possesses the best low temperature fluidity properties attainable. The ideal i:n mass ratio and carbon number distribution ranges are depicted in Table 3.11.

Table 3.11. Ideal i:n mass ratio and carbon number distribution for optimum jet fuel blends.

n-Paraffin mixture component (Mass %)	0 - 5
iso-Paraffin mixture component (Mass %)	95 - 100
C_9 (Mass %)	12 - 26
C_{10} (Mass %)	14 -17
C_{11} (Mass %)	16 - 32
C_{12} (Mass %)	11 - 14
C_{13} (Mass %)	5 - 9
C_{14} (Mass %)	2 - 13
C_{15} (Mass %)	5 - 8
C_{16} (Mass %)	3 - 4
C_{17} (Mass %)	1 - 2
C_{18} (Mass %)	0 - 5
Freeze point (°C)	-79.1 to -47.1
Viscosity at 20°C (cSt)	1.3 – 1.8
Viscosity at -20°C (cSt)	2.9 – 4.3

Chapter 4 : QSAR Models for Viscosity Prediction

4.1. Introduction

All of the chemical, physical and biological properties displayed by organic molecules can be attributed to their molecular structure and vary with the structure in a systematic way (Katrizky, et al., 2010). Over the last couple of decades, significant progress has been made to correlate physical properties successfully with molecular structures (Katrizky, et al., 1999).

The aim of QSAR studies is to establish a mathematical relationship between the property of interest and the structure of the molecule. Numerous QSAR models have been developed for the prediction of various properties, such as octane and cetane numbers, boiling points, flash points, viscosities and freeze points.

A multitude of QSAR viscosity models were found in the literature (Katrizky, et al., 2010). These models differ in terms of:

- The methodology followed to develop the model, including the type of molecular descriptors selected;
- The magnitude of the dataset used to develop the model; and
- The quality of the fit of the model to the data (R^2).

The molecular descriptors for viscosity models obtained from the literature include molar refraction, molecular weight, and Randic branching index. The R^2 values for these models varied from 0.87 to 0.93 and were considered suitable for their intended purpose (Katrizky, et al., 2010). The kinematic viscosity of petroleum products, including jet fuel, needs to be reported accurately to 0.1 cSt (ASTM D1655-16c, 2016), (ASTM D7042-14, 2014). Viscosity models, which exhibit R^2 values between 0.87 and 0.93, are expected to predict viscosities that vary by more than the required 0.1 cSt.

This chapter presents the results of the QSAR methodology applied to develop viscosity prediction models for n- and iso-paraffins in the C_4 – C_{20} carbon number range.

4.2. Definition of statistical terms

Since the statistics associated with regression models are of vital importance, the statistical terms used to evaluate the model results are discussed below.

4.2.1. Coefficient of determination

The coefficient of determination (R^2) is a measure of the goodness of fit (also known as the quality of fit) of the model to the observed data. The coefficient of determination provides the fraction of the variability in the response variable, which is explained by the model. R^2 values range from 0 to 1, with values closer to 1 indicating that a greater proportion of variance is accounted for by the model (NMMU, 2011).

4.2.2. Adjusted R^2

The adjusted R^2 value considers the number of independent variables present in the model. The adjusted R^2 value only increases if the addition of an extra independent variable to the model results in a significant increase in the quality of fit of the model. Similar to the coefficient of determination, adjusted R^2 values range from 0 to 1, with values closer to 1 indicating that a greater proportion of variance is accounted for by the model (NMMU, 2011).

4.2.3. Standard error

The standard error of the model is representative of the average distance of the observed data from the regression line. Higher standard errors relate to lower levels of model precision. Ideally, the standard error should be as small as possible.

4.2.4. P-values

The P-value, or calculated probability, is the probability of observing a test statistic within the observed data that is as extreme as or more extreme than the currently observed data, assuming that the null hypothesis of the study is true (NMMU, 2011). Molecular descriptors with P-values lower than 5% (0.05) are regarded as significant model parameters.

4.2.5. Confidence intervals

A confidence interval specifies the interval/range of possible values of a sample statistic that contain the true but unknown population parameter (Brown, 2011).

4.2.6. Standardised residuals

A standardised residual is the ratio of the residual of an observation to the standard deviation of the model. According to Simonoff (2016), standardised residuals should be normally distributed and observations with standardised residuals greater than ±2.5 should be investigated as potential outliers. Normal probability plots or histograms are employed to evaluate the standardised residuals for conformance to normality.

4.3. Viscosity prediction models

As discussed in Chapter 3, viscosity is defined as a liquid's resistance to flow (McMurry & Fay, 2004). The literature suggests that viscosity is governed by intermolecular forces. Intermolecular forces are, in turn, influenced by factors such as polarizability and the spatial orientation of molecules. The following molecular descriptors were therefore evaluated as candidates for use in the viscosity prediction model:

- Molecular area (Van der Waal's area);
- Molecular volume (Van der Waal's volume);
- Molecular density;
- Moments of inertia;
- Molecular shadow indices;
- Molecular dipole moments;
- Balaban index; and
- Mean polarizability.

The GFA tool of Materials Studio™ was used to create candidate models consisting of different combinations of the molecular descriptors cited above automatically. The software generated five candidate models for viscosity prediction. The molecular descriptors that occurred most frequently in these candidate models were identified and evaluated for use in the final model by application of MLR.

4.3.1. Viscosity prediction model: Four molecular descriptors

The model obtained by means of MLR was:

$$\hat{y} = b_0 + b_1(\text{Molecular area (vd Waals)}) + b_2(\text{Molecular volume (vd Waals)}) + b_3(\text{Molecular density}) + b_4(\text{Principal moment of inertia Y})$$

Where:

- $\hat{y}$: Predicted viscosity;
- b_0: Intercept;
- b_1: Coefficient for molecular area;
- b_2: Coefficient for molecular volume;
- b_3: Coefficient for molecular density; and
- b_4: Coefficient for principal moment of inertia Y.

The regression results are shown in Table 4.1. The model had a R^2 value of 0.99, therefore 99% of the variation in the viscosity data was accounted for by the model. The adjusted R^2 value of 0.99 is indicative of the fact that the correct variables were included in the model to describe the variability in viscosity. The high adjusted R^2 value also shows that the model did

not contain unnecessary descriptors (Cornell, 2002). The standard error of 0.1 cSt is indicative of the good precision of the model. In order for a molecular descriptor to have a noteworthy effect on viscosity, its P-value is required to be at or below 5%. All model descriptors conformed to the before mentioned requirement and were thus significant; none of the descriptors could therefore be excluded from the model.

Table 4.1. Statistics of viscosity prediction model: Four molecular descriptors.

Regression statistic				
R^2	0.99			
Adjusted R^2	0.99			
Standard Error	0.1			
			95% Confidence interval	
Parameter	**Coefficient**	**P-value**	**Lower 95%**	**Upper 95%**
Intercept	-2.7572	0.0717	-5.7684	0.2540
Molecular area (vdW area)	-0.0120	0.0000	-0.0168	-0.0072
Molecular volume (vdW volume)	0.0150	0.0003	0.0074	0.0225
Molecular density	4.2526	0.0489	0.0205	8.4847
Principal moment of inertia Y	0.0003	0.0000	0.0003	0.0004

Figure 4.1 serves as a visual indication of the goodness of fit of the four-descriptor model developed. The small insert on the scatter plot offers a blown-up view of the viscosities in the 1.0 cSt range. The data points were scattered close to the diagonal line at 45°, which is indicative of the very good fit of the model.

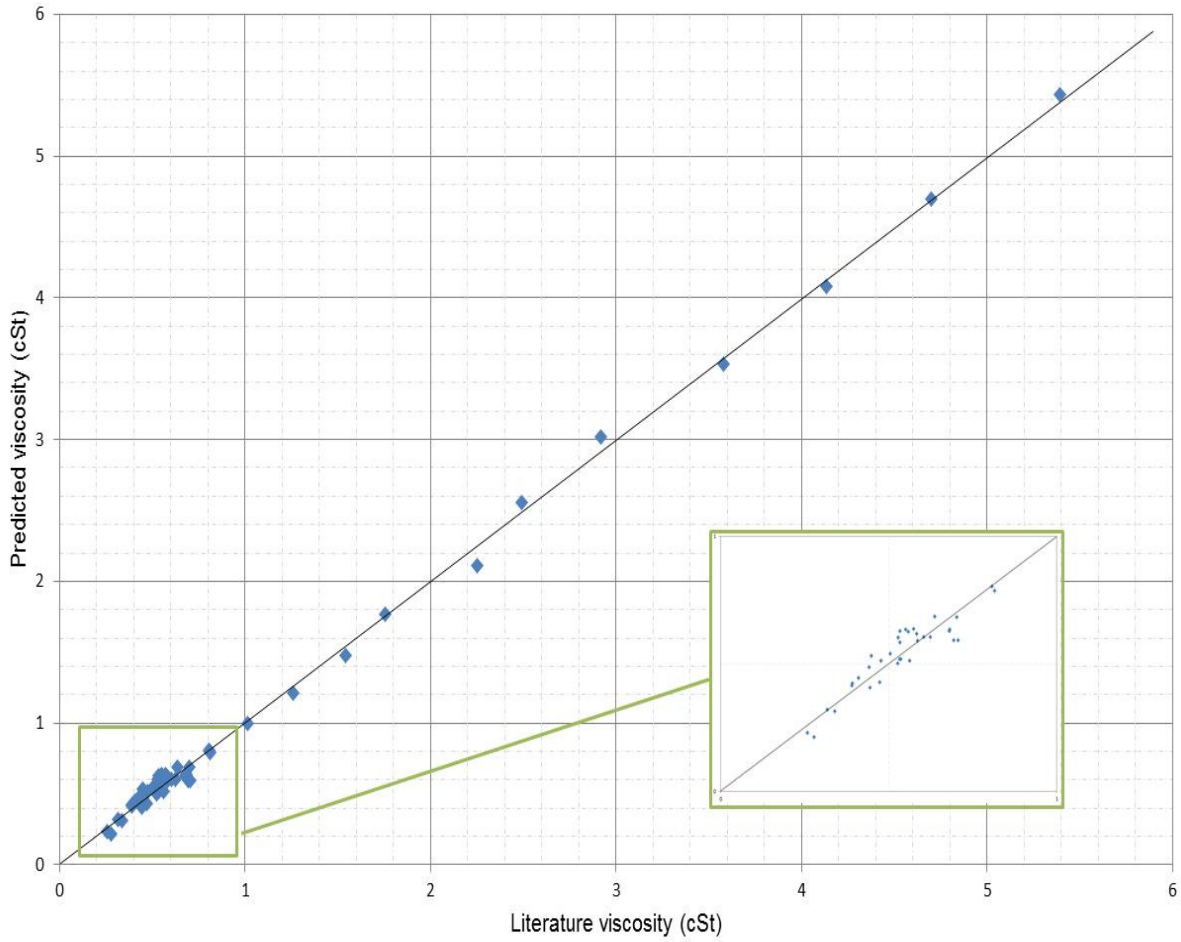

Figure 4.1. Predicted viscosity versus literature viscosity scatter plot (Four descriptors).

The tabulated regression results can be viewed in Appendix A.

4.3.2. Viscosity prediction model validation: Four molecular descriptors

Once a suitable model has been developed, it needs to be validated to determine its reliability and statistical significance. In order for QSAR models to be reliable and predictive, they should (Katrizky, et al., 2010):

- Be statistically significant and robust;
- Be validated by making use of data that were not included in the model dataset;
- Have a defined range of application.

The four-descriptor viscosity model was validated as per the procedures described in Chapter 3. These validation results are discussed below.

4.3.2.1. Standardised residuals

The graph of the standardised residuals versus the predicted viscosity is depicted in Figure 4.2. The majority of the data was clustered toward the left of the x-axis. This can be attributed to the fact that the majority of the viscosities of the molecules contained in the dataset were lower than 1.0 cSt. The graph can thus be divided into two distinct regions, namely viscosities ranging from 0.0 to 1.0 cSt and viscosities ranging from 1.1 to 5.4 cSt. No standardised residual outliers were identified for this data series.

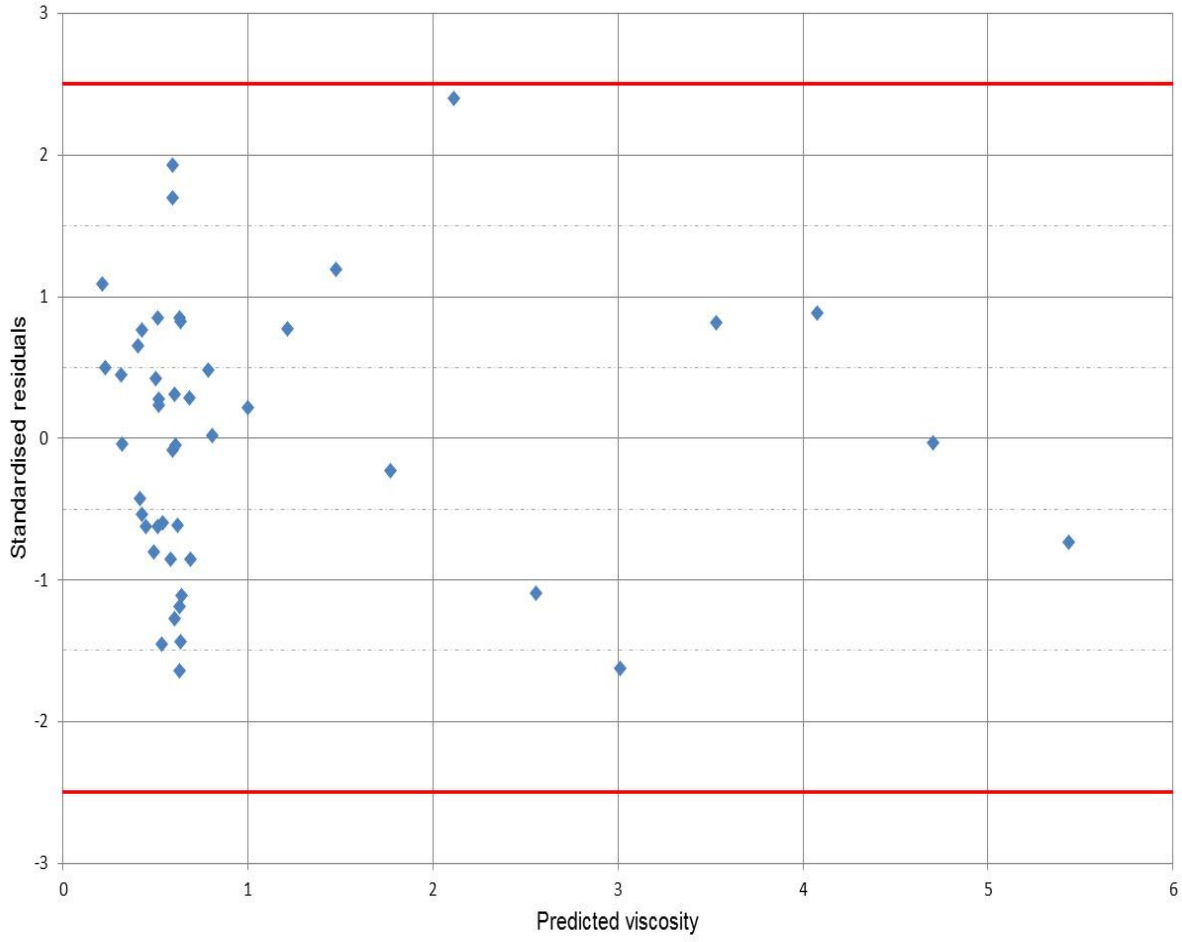

Figure 4.2. Graph of standardised residuals versus predicted viscosity (Four descriptors).

Figure 4.3 depicts the normal probability plot for the standardised residuals. The data points were scattered close to the diagonal line, which is indicative of the standard residuals conforming reasonably well to a normal distribution curve. Only two outliers were detected near the tail end of the data, which could distort the normal distribution somewhat.

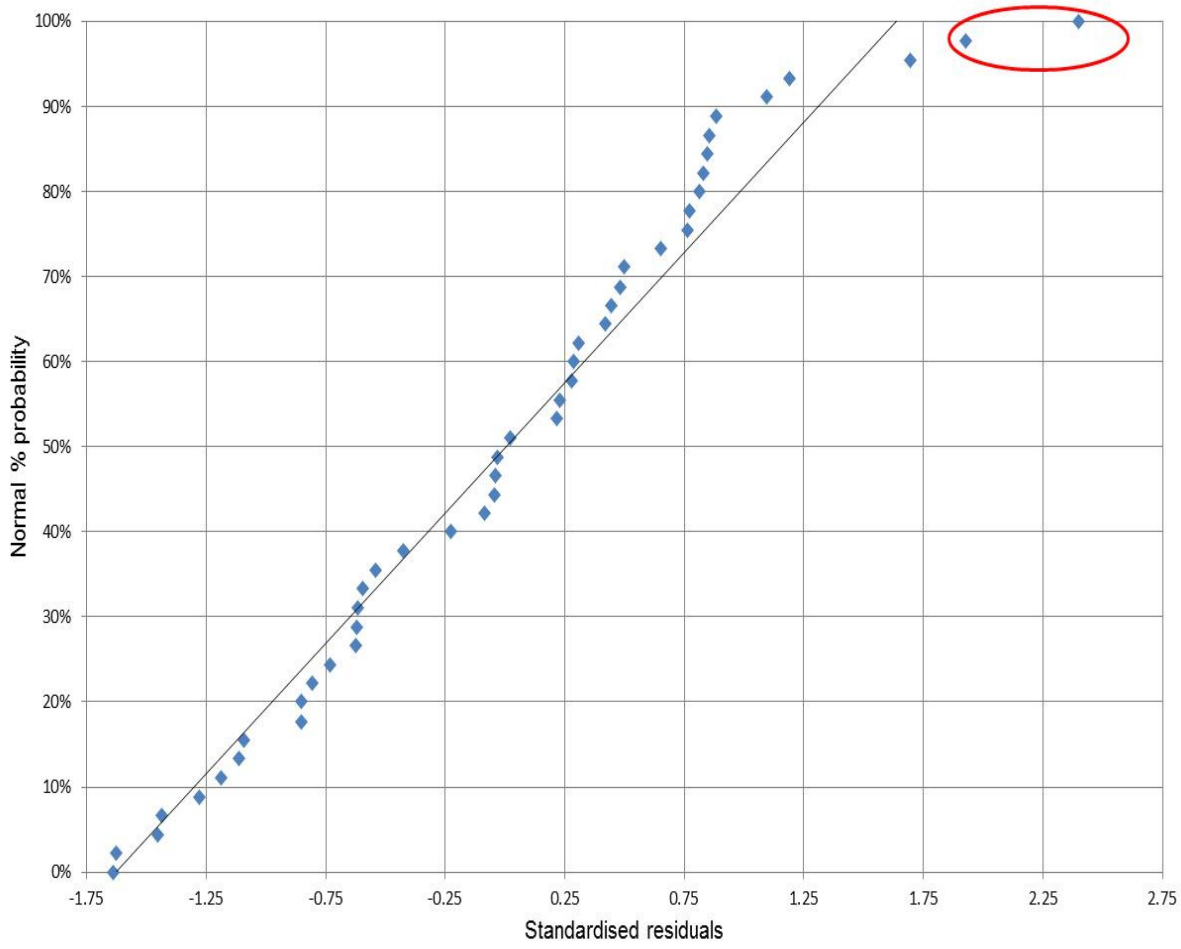

Figure 4.3. Normal probability plot of four-descriptor regression model.

4.3.2.2. LMO validation

The model obtained for dataset 1 + 2 was:

$$\hat{y}=b_0 + b_1(\text{Molecular area (vd Waals)}) + b_2(\text{Molecular volume (vd Waals)} + b_3(\text{Principal moment of inertia Y})$$

The regression results for dataset 1 + 2 are shown in Table 4.2. The validation model was able to account for 99% of the variation in the viscosity and had a sufficiently low standard error of 0.1 cSt. The P-value of the molecular density descriptor was well above the 5% significance level. The 95% confidence interval of the molecular density descriptor included a value of 0, which explains the high P-value observed for this descriptor. The molecular density descriptor was consequently removed from the model. The P-values of the remaining descriptors were significant.

Table 4.2. Statistics of viscosity prediction model (Four molecular descriptors): Dataset 1 + 2 (Predicting subset 3).

Regression statistic				
R^2	0.99			
Adjusted R^2	0.99			
Standard Error	0.1			
			95% Confidence interval	
Parameter	**Coefficient**	**P-value**	**Lower 95%**	**Upper 95%**
Intercept	-0.5591	0.7533	-4.1769	3.0587
Molecular area (vdW area)	-0.0119	0.0002	-0.0176	-0.0062
Molecular volume (vdW volume)	0.0168	0.0007	0.0078	0.0259
Molecular density	1.0668	0.6715	-4.0459	6.1796
Principal moment of inertia Y	0.0003	0.0000	0.0003	0.0004

The tabulated regression results for dataset 1 + 2 can be viewed in Appendix A.

The model obtained for dataset 2 + 3 was:

$\hat{y}=b_0 + b_1$*(Molecular area (vd Waals))* $+ b_2$*(Molecular volume (vd Waals))* $+ b_3$*(Molecular density)* $+ b_4$*(Principal moment of inertia Y)*

The regression results for dataset 2 + 3 are shown in Table 4.3. The validation model was able to account for 99% of the variation in the viscosity. The low standard error is indicative of the good precision of this model. The P-values of all descriptors were significant. The model was thus preserved in its original form.

Table 4.3. Statistics of viscosity prediction model (Four molecular descriptors): Dataset 2 + 3 (Predicting subset 1).

Regression statistic				
R^2	0.99			
Adjusted R^2	0.99			
Standard Error	0.1			
			95% Confidence interval	
Parameter	**Coefficient**	**P-value**	**Lower 95%**	**Upper 95%**
Intercept	-5.2000	0.0128	-9.1945	-1.2055
Molecular area (vdW area)	-0.0119	0.0004	-0.0179	-0.0059
Molecular volume (vdW volume)	0.0124	0.0128	0.0029	0.0219
Molecular density	7.8241	0.0080	2.2357	13.4126
Principal moment of inertia Y	0.0004	0.0000	0.0003	0.0004

The tabulated regression results for dataset 2 + 3 can be viewed in in Appendix A.

The model obtained for dataset 1 + 3 was:

$\hat{y}=b_0 + b_1$*(Molecular area (vd Waals))* $+ b_2$*(Molecular volume (vd Waals)* $+ b_3$*(Principal moment of inertia Y)*

The regression results for dataset 1 + 3 are shown in Table 4.4. The validation model was able to account for 99% of the variation in the viscosity. The low standard error of 0.1 cSt is indicative of the good precision of this model. The P-value of the molecular density descriptor was 11.6%, which is well above the 5% significance level for P-values. The 95% confidence interval of the molecular density descriptor included a value of 0, which explains the high P-value observed for this descriptor. The molecular density descriptor was consequently removed from the model. The P-values of the remaining descriptors were significant.

Table 4.4. Statistics of viscosity prediction model (Four molecular descriptors): Dataset 1 + 3 (Predicting subset 2).

Regression statistic				
R^2	0.99			
Adjusted R^2	0.99			
Standard Error	0.1			
			95% Confidence interval	
Parameter	**Coefficient**	**P-value**	**Lower 95%**	**Upper 95%**
Intercept	-2.6817	0.1476	-6.3747	1.0114
Molecular area (vdW area)	-0.0120	0.0007	-0.0184	-0.0056
Molecular volume (vdW volume)	0.0153	0.0038	0.0054	0.0252
Molecular density	4.0999	0.1161	-1.0843	9.2840
Principal moment of inertia Y	0.0003	0.0000	0.0003	0.0004

The tabulated regression results for dataset 2 + 3 can be viewed in Appendix A.

4.3.3. Viscosity prediction model: Three molecular descriptors

During the LMO validation process, the P-value of the molecular density descriptor was above the 5% significance level for two of the three datasets. This molecular descriptor was consequently removed from the initial four-descriptor model to produce an optimised model consisting of only three molecular descriptors:

$$\hat{y} = b_0 + b_1(\text{Molecular area (vd Waals)}) + b_2(\text{Molecular volume (vd Waals)}) + b_3(\text{Principal moment of inertia Y})$$

The regression results are shown in Table 4.5. The reduced three-descriptor model had a R^2 value of 0.99, which meant that 99% of the variation in the viscosity data was accounted for by the model. The adjusted R^2 value of 0.99 is moreover indicative of the fact that the correct variables were included in the model to describe the variability in viscosity. The high adjusted R^2 value also shows that the model did not contain unnecessary parameters. The low standard error of 0.1 cSt is indicative of the good precision of this model. The P-values of all descriptors were significant. The model was thus preserved in its original form.

Table 4.5. Statistics of viscosity prediction model: Three molecular descriptors.

Regression statistic				
R^2	0.99			
Adjusted R^2	0.99			
Standard Error	0.1			
			95% Confidence interval	
Parameter	**Coefficient**	**P-value**	**Lower 95%**	**Upper 95%**
Intercept	0.2661	0.0002	0.1370	0.3951
Molecular area (vdW area)	-0.0147	0.0000	-0.0188	-0.0106
Molecular volume (vdW volume)	0.0207	0.0000	0.0156	0.0258
Principal moment of inertia Y	0.0003	0.0000	0.0003	0.0003

Prediction results for the viscosity model are shown in Table 4.6. All the predicted values were within 0.1 cSt of the actual values, which is indicative of the quality of fit of the model. This is significant, considering that the model had to predict the viscosities of 46 molecules, which differed both in carbon chain length and molecular structure.

Table 4.6. Results of viscosity prediction model: Three molecular descriptors.

Molecule	Carbon number	Kinematic Viscosity (cSt)	Predicted viscosity (cSt)	Literature - Predicted viscosity (cSt)
n-Butane	n-C_4	0.26	0.28	-0.02
iso-Butane	iso-C_4	0.28	0.25	0.03
n-Pentane	n-C_5	0.34	0.31	0.03
2-Methylbutane	iso-C_5	0.32	0.33	-0.02
n-Hexane	n-C_6	0.41	0.45	-0.04
2-Methylpentane	iso-C_6	0.39	0.41	-0.02
3-Methylpentane	iso-C_6	0.39	0.43	-0.03
2,2-Dimethylbutane	iso-C_6	0.47	0.43	0.04
2,3-Dimethylbutane	iso-C_6	0.44	0.40	0.04
n-Heptane	n-C_7	0.51	0.53	-0.03
2-Methylhexane	iso-C_7	0.48	0.50	-0.02
3-Methylhexane	iso-C_7	0.45	0.53	-0.08
3-Ethylpentane	iso-C_7	0.44	0.48	-0.04
2,2-Dimethylpentane	iso-C_7	0.54	0.50	0.03
2,3-Dimethylpentane	iso-C_7	0.53	0.51	0.02
2,4-Dimethylpentane	iso-C_7	0.53	0.50	0.03
3,3-Dimethylpentane	iso-C_7	0.56	0.50	0.06
2,2,3-Trimethylbutane	iso-C_7	0.69	0.55	0.15
n-Octane	n-C_8	0.64	0.67	-0.03
2-Methylheptane	iso-C_8	0.56	0.62	-0.06
3-Methylheptane	iso-C_8	0.55	0.64	-0.09
4-Methylheptane	iso-C_8	0.53	0.63	-0.10
3-Ethylhexane	iso-C_8	0.53	0.59	-0.06
2,2-Dimethylhexane	iso-C_8	0.62	0.60	0.02
2,3-Dimethylhexane	iso-C_8	0.58	0.61	-0.03
2,4-Dimethylhexane	iso-C_8	0.71	0.59	0.11
3,3-Dimethylhexane	iso-C_8	0.59	0.60	-0.02
3,4-Dimethylhexane	iso-C_8	0.57	0.63	-0.06
2-Methyl-3-ethylpentane	iso-C_8	0.53	0.61	-0.08
2,2,3-Trimethylpentane	iso-C_8	0.68	0.64	0.04
2,2,4-Trimethylpentane	iso-C_8	0.60	0.61	-0.01
2,3,3-Trimethylpentane	iso-C_8	0.70	0.68	0.03
2,3,4-Trimethylpentane	iso-C_8	0.68	0.63	0.05
n-Nonane	n-C_9	0.81	0.78	0.03
2,2,3,3-Tertamethylpentane	iso-C_9	0.81	0.80	0.01
n-Decane	n-C_{10}	1.01	0.98	0.03
n-Undecane	n-C_{11}	1.26	1.21	0.05
n-Dodecane	n-C_{12}	1.54	1.47	0.07
n-Tridecane	n-C_{13}	1.75	1.77	-0.02
n-Tetradecane	n-C_{14}	2.25	2.12	0.13
n-Pentadecane	n-C_{15}	2.49	2.60	-0.11
n-Hexadecane	n-C_{16}	2.92	3.04	-0.12
n-Heptadecane	n-C_{17}	3.58	3.57	0.02
n-Octadecane	n-C_{18}	4.13	4.08	0.05
n-Nonadecane	n-C_{19}	4.70	4.69	0.01
n-Eicosane	n-C_{20}	5.39	5.40	-0.01

Figure 4.4 serves as visual indication of the goodness of fit of the three-descriptor model. The small insert on the scatter plot offers a blown-up view of the viscosities in the 1.0 cSt range. The data points were scattered close to the diagonal line, which is indicative of the very good fit of the model.

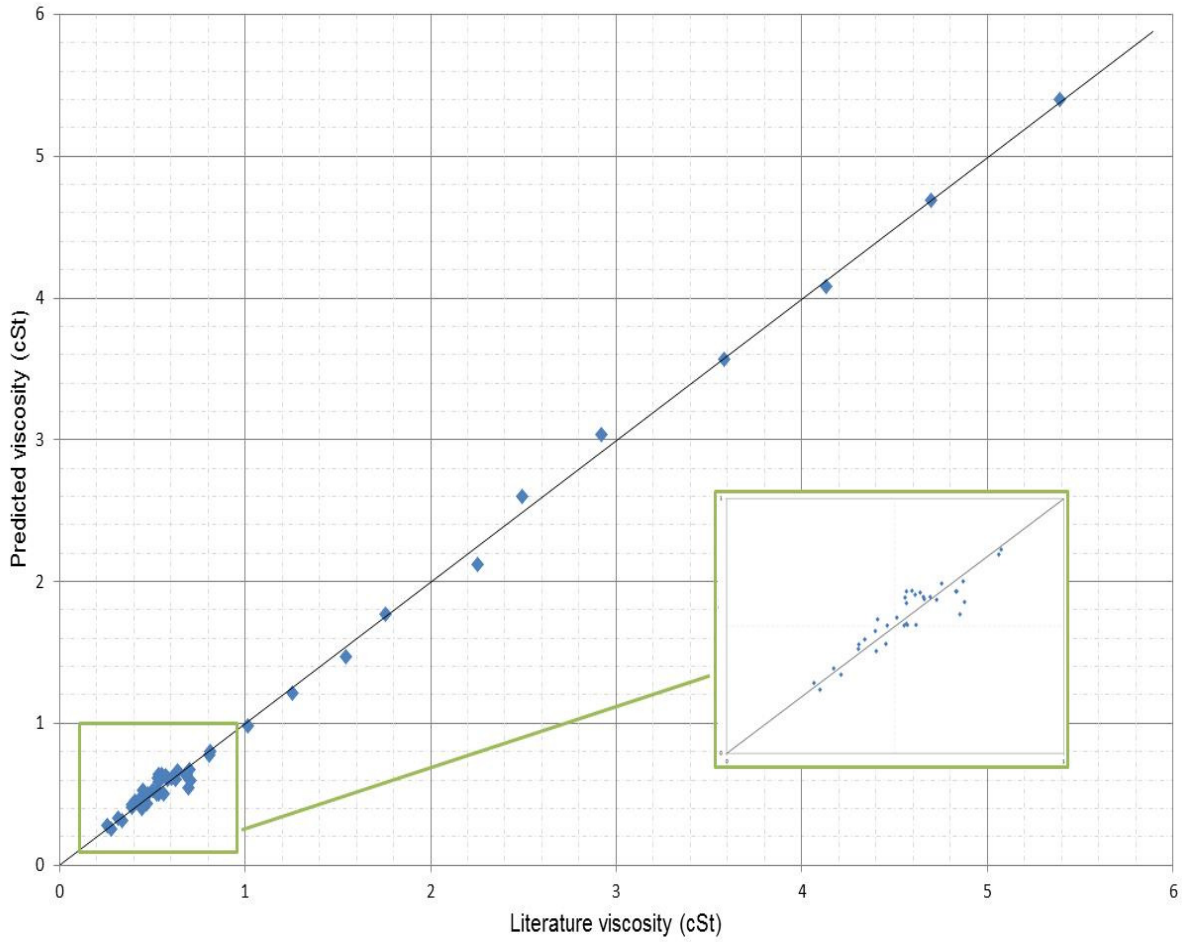

Figure 4.4. Predicted viscosity versus literature viscosity scatter plot (Three descriptors).

When considering the regression results of the four-descriptor model (Table 4.1) versus those of the three-descriptor model (Table 4.5), it can be observed that there was no noticeable change in the quality of fit of the model upon removal of the molecular density descriptor from the model. The four-descriptor model displayed an average viscosity prediction error of 7.01%, compared to a 7.00% error produced by the three-descriptor model. This serves as further confirmation that the molecular density made no notable contribution toward the quality of fit of the four-descriptor model.

4.3.4. Viscosity prediction model validation: Three molecular descriptors

The three-descriptor model discussed above was evaluated in a manner similar to the four-descriptor model. These validation results are discussed below.

4.3.4.1. Standardised residuals

The standardised residual versus predicted viscosity graph of the three-descriptor model is similar in appearance to the graph of the four-descriptor model (Figure A.1 (Appendix A) vs Figure 4.2). The majority of the data was clustered to the left side of the x-axis. As with the four-

descriptor model, this can be attributed to the majority of the dataset having viscosities lower than 1.0 cSt. The graph can thus be divided into two distinct regions, namely viscosities ranging from 0.0 to 1.0 cSt and viscosities ranging from 1.1 to 5.4 cSt. No standardised residual outliers could be detected for this data series.

Refer to Appendix A to view the standardised residuals versus predicted viscosity scatter plot of the three-descriptor model.

The normal probability plot of the three-descriptor model is similar in appearance to that of the four-descriptor model (Figure A.2 (Appendix A) vs Figure 4.3). The three-descriptor conformed reasonably well to a normal distribution. This normal probability plot also exhibited the two tail end outliers noted during discussion of the standardised residuals of the four-descriptor model.

Refer to Appendix A to view the normal probability plot of the three-descriptor model.

4.3.4.2. LMO validation

The three-descriptor model was validated similarly to the four-descriptor model described earlier. The three models obtained during the validation process all had high R^2 values, which is indicative of the goodness of fit of the models to the data. The low standard errors obtained are testament of the good precision of these models. Even though one outlier of 0.2 cSt was identified within datasets 1 + 2 and 2 + 3 respectively, the predictive accuracy of each set was still considered adequate for viscosity prediction. The P-values of all validation model descriptors were significant, hence the three-descriptor model was preserved in its current form.

The tabulated results for the LMO validation can be viewed in Appendix A.

4.3.4.3. Viscosity prediction of non-dataset molecules

Eight molecules, which did not form part of the original dataset, were used to further test the accuracy of the model. The results are tabulated in Table 4.7. The viscosities of 2,2,5-trimethylhexane and 3,3-diethylpentane were under-predicted by 46.8% and 53.8% respectively, which is notable. The viscosities of 3-methyloctane and 4-methyloctane were over-predicted by 19.7% and 14.7% respectively, which does seem notable, but this equates to an over-prediction of only 0.1 cSt.

3,3-Diethylpentane and 2,2,5-trimethylhexane were the only validation molecules with viscosities greater than 1.0 cSt. These two molecules also exhibited the highest viscosity prediction errors of all the molecules validated. Furthermore, it was noted during discussion of the standardised residuals that there are two distinct regions of viscosity ranges for the dataset

molecules, namely 0.0 to 1.0 cSt and 1.1 to 5.4 cSt. The 1.1 to 5.4 cSt viscosity region contained far fewer data points, which may affect the accuracy of predictions for non-dataset molecules in that region.

Table 4.7. Viscosity prediction of non-dataset molecules.

Molecule	Carbon number	Kinematic Viscosity (cSt)	Predicted viscosity (cSt)	Literature - Predicted viscosity (cSt)	Under-predicted (%)	Over-predicted (%)
2,2,5-Trimethylhexane	iso-C_9	1.31	0.70	0.61	46.8	
2,2,3,4-Tetramethylpentane	iso-C_9	0.81	0.79	0.02	2.5	
2-Methyloctane	iso-C_9	0.66	0.74	-0.08		12.2
2,2,4,4-Tetramethylpentane	iso-C_9	0.81	0.76	0.05	6.4	
2,5-Dimethylhexane	iso-C_8	0.58	0.60	-0.01		2.5
3-Methyloctane	iso-C_9	0.65	0.78	-0.13		19.7
4-Methyloctane	iso-C_9	0.65	0.75	-0.10		14.7
3,3-Diethylpentane	iso-C_9	1.59	0.73	0.85	53.8	

4.3.5. Final viscosity model discussion

The final viscosity prediction model for n-and iso-paraffin molecules in the $C_4 – C_{20}$ carbon number range is thus:

$\hat{y}=b_0 + b_1$(Molecular area (vd Waals)) $+ b_2$(Molecular volume (vd Waals)) $+ b_3$(Principal moment of inertia Y)

$\therefore \hat{y}= 0.2661 -0.0147$(Molecular area (vd Waals)) $+ 0.0207$(Molecular volume (vd Waals)) $+ 0.0003$(Principal moment of inertia Y)

4.3.5.1. Molecular area (Van der Waal's)

The molecular surface of a molecule refers to the surface that surrounds the nuclei of a molecule. In practice, molecules do not possess clearly defined molecular surfaces. To understand/quantify the molecular surface of a molecule better, the electron distribution of the molecule may be regarded as a three-dimensional object whose boundary is the molecular surface. The entire molecule can be found in the molecular surface (Todeshini & Consonni, 2000).

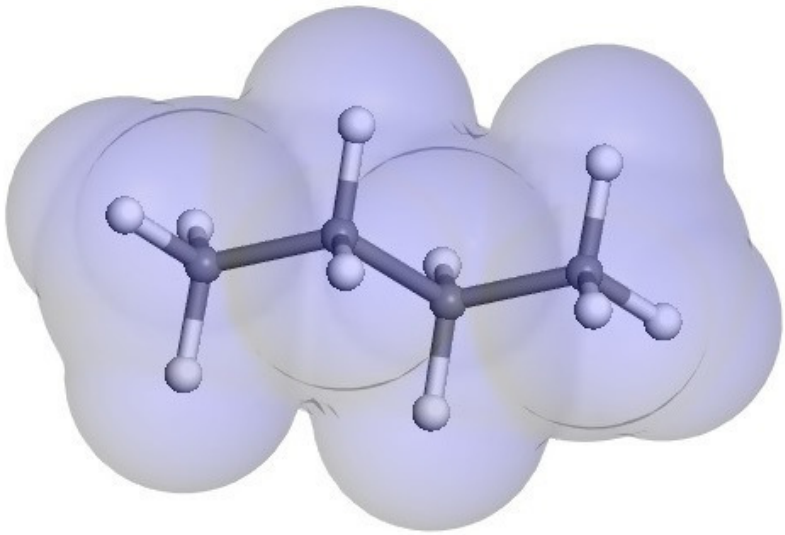

Figure 4.5. Three-dimensional view of the Van der Waal's surface of n-butane.

The van der Waal's surface of a molecule is defined as the surface that fully surrounds the spheres of the atomic nuclei of a molecule, as indicated by Figure 4.5. The van der Waal's surface area is thus the sum of the outer surfaces of all the spheres present in the molecule (Todeshini & Consonni, 2000).

The magnitude of the van der Waal's molecular area defines the extent to which a molecule is exposed to the external environment. Molecules with larger molecular surface areas are more exposed and experience higher dispersion forces than smaller molecules with smaller molecular surface areas. More spread-out shapes also allow for greater contact between molecules, whereas smaller molecules minimise molecular contact. This molecular descriptor is related to binding, transport and solubility (Dassault Systemes, 2005a).

4.3.5.2. Molecular volume (Van der Waal's)

The van der Waal's molecular volume, also known as the intrinsic molecular volume, is the volume within the van der Waal's area of a molecule. This molecular descriptor is related to binding and transport (Dassault Systemes, 2005a).

4.3.5.3. Principal moments of inertia

The moment of inertia describes the rotational motion of a molecule brought about by the distribution of the molecule's atoms in space (Cutnell & Johnson, 2004), (Molecular Networks GmbH, 2013). Linear molecules are only capable of rotating about a single axis, whereas nonlinear molecules are free to rotate about more than one axis, which is why moments of inertia are considered an important aspect of physical chemistry.

The moment of inertia about an axis can be defined by the following equation (Todeshini & Consonni, 2000):

$$\mathrm{I} = \sum_{i}^{N} m_i . {r_i}^2$$

Where:

- I: Moment of inertia
- N: Sum of all atoms;
- i: Number of the atom in the molecule (e.g. 1, 2, 3, 4…);
- m_i: Mass of the i th atom; and
- r_i: Perpendicular distance from the chosen axis of the i th atom.

For objects with moments of inertia about the X, Y and Z axes, the moments of inertia can be defined by the following equations (Todeshini & Consonni, 2000):

$$\mathrm{I}xx = \sum_{i}^{N} m_i . ({y_i}^2 + {z_i}^2)$$

$$\mathrm{I}yy = \sum_{i}^{N} m_i . ({x_i}^2 + {z_i}^2)$$

$$\mathrm{I}zz = \sum_{i}^{N} m_i . ({x_i}^2 + {y_i}^2)$$

Where x, y and z are the atom coordinates.

Since nonlinear molecules can rotate around any of the X, Y or Z axes, calculation of the moments of inertia can be complicated. Fortunately, a surface ellipsoid, which represents the whole molecule, can be obtained by determining the moments of inertia about any chosen axis. This surface ellipsoid has a unique set of axes, called the principal axes of inertia. These principal axes of inertia enable calculation of the principal moments of inertia with relative ease (Laidler, et al., 2003). The principal moments of inertia are related to the shape of a molecule and are representative of the volume occupied by the molecule in the direction of the three principal axes (Molecular Networks GmbH, 2013).

4.4. Conclusion

Validation of prediction models plays a significant role not only in verifying the statistical significance of the model obtained, but also in verifying the significance of the contribution made by each molecular descriptor to the overall model, as indicated by the removal of the molecular density property from the final model.

Some validation molecules exhibited highly inaccurate viscosity prediction results. This may have been brought about by attempting to develop a model for too wide a carbon number range. Separating the single dataset into two datasets, and developing separate models for each may increase the predictive power of the individual models, thereby enabling accurate viscosity prediction of non-dataset molecules over the entire C_4 – C_{20} carbon number range. Furthermore, it is believed that there are some other molecular descriptors, which could better account for the viscosity behaviour of these high viscosity molecules. 3,3-Diethylpentane, for example, is an almost spherical molecule, which may explain why its viscosity behaviour cannot be fully accounted for by the molecular descriptors of the final model.

The final model, as represented in this work, achieved high viscosity prediction accuracy in relation to all the molecules considered in the dataset. Even though some validation molecules exhibited inaccurate viscosity prediction results, it is concluded that QSAR techniques can successfully be employed to predict the kinematic viscosity of n- and iso-paraffins in the C_4 – C_{20} range.

Furthermore, some general observations were made in Chapter 2 in connection with the molecular properties that affect the physical properties of molecules in the jet fuel regime. When considering the descriptors identified for the prediction of viscosity, it is evident that the molecular properties that give rise to these physical properties are extraordinarily complex. Since it was possible to predict the viscosity of individual molecules in the jet fuel regime with great accuracy, it is believed that similar statistical techniques can be employed to predict the viscosity behaviour of full carbon number distribution range jet fuels.

4.5. Recommendations

The possibility of developing separate prediction models for molecules in the 0.0 to 1.0 cSt and 1.1 to 5.4 cSt viscosity ranges may be investigated.

Chapter 5 : QSAR Model for Freeze Point Prediction

5.1. Introduction

Freeze point is an important jet fuel property, which may adversely affect the optimal functioning of turbine engines. This physical property is governed by the types and quantities of hydrocarbon species present in the fuel.

Accurate freeze point prediction of structurally diverse molecules would be of significant benefit to the aviation industry. Needham et al. (1988) developed a freeze point model for 56 n- and iso-paraffins with an R^2 value of 0.57. King (1987) developed a model for 24 n-paraffins with an R^2 value of 1.0. The models developed by Needham et al. (1988) and King (1987) are illustrative of the fact that freeze point model R^2 values tend to decrease as the molecules comprising the dataset become structurally more diverse. The freeze point of jet fuel must be reported accurately to 1.0℃ (ASTM D1655-16c, 2016). Freeze point prediction models that exhibit low R^2 values are expected to predict freeze points that differ by more than the required 1.0℃.

This chapter presents the results of the QSAR methodology that has been applied to develop freeze point prediction models for n- and iso-paraffins in the C_4 – C_{20} carbon number range.

5.2. Freeze point prediction model

The procedures described in Chapter 3 were followed to create a freeze point prediction model consisting of five molecular descriptors.

The model obtained by means of MLR was:

$$\hat{y} = b_0 + b_1(\text{Zagreb index}) + b_2(\text{Molecular density}) + b_3(\text{Molecular flexibility index}) + b_4(\text{Total molecular mass}) + b_5(\text{Wiener index})$$

Where:

- $\hat{y}$: Predicted freeze point;
- b_0: Intercept;
- b_1: Coefficient for Zagreb index;
- b_2: Coefficient for molecular density;
- b_3: Coefficient for molecular flexibility index;
- b_4: Coefficient for total molecular mass; and
- b_5: Coefficient for Wiener index.

The regression results are presented in Table 5.1. The R^2 value for this model was 0.98, which indicates that the model was able to account for 98% of the variation in the freeze point data. The high adjusted R^2 value confirmed that the correct variables were included in the model to describe freeze point variability, and that the model did not contain unnecessary parameters (Cornell, 2002). Moreover, all molecular descriptors were significant, since the P-values associated with these descriptors were below the 5% threshold. However, the model exhibited a standard error of 8.1℃, which is indicative of the poor precision of the model.

When measuring the standard error against the freeze point reporting requirements of ASTM D1655 (2016), as well as the 0.8℃ reproducibility limit specified by ASTM D5972 (2016), it is clear that the accuracy of the model is below the desired value. Despite the model's deficiencies, the model was evaluated to identify possible reasons for the poor regression statistics obtained.

Table 5.1. Statistics of freeze point prediction model.

Regression statistic				
R^2	0.98			
Adjusted R^2	0.98			
Standard Error	8.1			
			95% Confidence interval	
Parameter	**Coefficient**	**P-value**	**Lower 95%**	**Upper 95%**
Intercept	-659.278	0.009	-1144.947	-173.609
Zagreb index	18.911	0.000	15.683	22.139
Molecular density	868.771	0.014	187.320	1550.222
Molecular flexibility index	44.612	0.000	38.492	50.733
Total molecular mass	-7.711	0.000	-9.139	-6.284
Wiener index	-0.058	0.014	-0.104	-0.013

The freeze point prediction results of the model are presented in Table 5.2. The model yielded results that over- and under-predicted the freeze point by an average of 8%. This may not seem notable at first glance; however, when considering the absolute residual results, which are representative of the absolute value of the difference between the literature values and the predicted values, it can be observed that the prediction error was notable.

Table 5.2. Results of freeze point prediction model.

Molecule	Carbon number	Freeze point (℃)	Predicted freeze point (℃)	Residual (℃) (Absolute)	Over/under predicted (%)
n-Butane	n-C_4	-138.4	-148.2	9.9	7.1
n-Pentane	n-C_5	-129.7	-120.7	9.0	6.9
2-Methylbutane	iso-C_5	-159.9	-161.7	1.8	1.1
n-Hexane	n-C_6	-95.3	-99.9	4.6	4.9
2-Methylpentane	iso-C_6	-153.7	-141.3	12.4	8.1
n-Heptane	n-C_7	-90.6	-82.1	8.5	9.4
2-Methylhexane	iso-C_7	-118.3	-123.7	5.5	4.6
3-Methylhexane	iso-C_7	-119.4	-123.7	4.3	3.6
3-Ethylpentane	iso-C_7	-118.6	-122.3	3.7	3.1
2,2-Dimethylpentane	iso-C_7	-123.8	-126.9	3.1	2.5
2,4-Dimethylpentane	iso-C_7	-119.2	-134.8	15.6	13.1
3,3-Dimethylpentane	iso-C_7	-134.5	-126.0	8.4	6.3
n-Octane	n-C_8	-56.8	-64.1	7.3	12.8
2-Methylheptane	iso-C_8	-109.0	-110.0	0.9	0.9
3-Methylheptane	iso-C_8	-120.5	-109.7	10.8	8.9
4-Methylheptane	iso-C_8	-121.0	-109.6	11.3	9.4
2,2,-Dimethylhexane	iso-C_8	-121.2	-121.7	0.5	0.4
3,3-Dimethylhexane	iso-C_8	-126.1	-122.8	3.3	2.6
2-Methyl-3-ethylpentane	iso-C_8	-115.0	-121.2	6.3	5.5
2,2,3-Trimethylpentane	iso-C_8	-112.3	-103.1	9.1	8.1
2,2,4-Trimethylpentane	iso-C_8	-107.4	-109.8	2.4	2.2
2,3,3-Trimethylpentane	iso-C_8	-100.9	-103.1	2.2	2.2
2,3,4-Trimethylpentane	iso-C_8	-109.2	-117.9	8.7	8.0
n-Nonane	n-C_9	-53.5	-49.0	4.5	8.4
2-Methyloctane	iso-C_9	-80.4	-95.1	14.7	18.3
3-Methyloctane	iso-C_9	-107.6	-94.4	13.2	12.3
2,2-Dimethylheptane	iso-C_9	-113.0	-116.8	3.8	3.4
2,6-Dimethylheptane	iso-C_9	-102.9	-114.0	11.1	10.7
2,2,5-Trimethylhexane	iso-C_9	-105.8	-108.4	2.6	2.5
2,3,3-Trimethylhexane	iso-C_9	-116.8	-104.2	12.6	10.8
2,3,5-Trimethylhexane	iso-C_9	-127.8	-114.8	13.0	10.2
2,4,4-Trimethylhexane	iso-C_9	-113.4	-105.2	8.1	7.2
3,3,4-Trimethylhexane	iso-C_9	-101.2	-103.6	2.4	2.4
2,2-Dimethyl-3-ethylpentane	iso-C_9	-99.5	-103.0	3.5	3.5
2,4-Dimethyl-3-ethylpentane	iso-C_9	-122.4	-115.3	7.1	5.8
2,2,4,4-Tetramethylpentane	iso-C_9	-66.5	-68.4	1.9	2.9
2,3,3,4-Tetramethylpentane	iso-C_9	-102.1	-87.2	14.9	14.6
n-Decane	n-C_{10}	-29.6	-35.3	5.7	19.2
2-Methylnonane	iso-C_{10}	-74.7	-82.2	7.6	10.2
3-Methylnonane	iso-C_{10}	-84.8	-81.7	3.1	3.7
5-Methylnonane	iso-C_{10}	-87.7	-81.0	6.7	7.6
2,2,3,3-Tetramethylhexane	iso-C_{10}	-54.0	-66.9	12.9	23.9
2,4-Dimethyl-3-isopropylpentane	iso-C_{10}	-81.7	-95.0	13.3	16.2
n-Undecane	n-C_{11}	-25.6	-24.7	0.9	3.6
n-Dodecane	n-C_{12}	-9.6	-13.0	3.5	36.1
n-Tridecane	n-C_{13}	-5.4	-3.4	2.0	37.4
n-Tetradecane	n-C_{14}	5.9	4.6	1.3	22.1
n-Pentadecane	n-C_{15}	9.9	9.5	0.4	4.5
n-Hexadecane	n-C_{16}	18.6	19.1	0.5	2.5
n-Heptadecane	n-C_{17}	22.0	22.8	0.9	3.9
n-Octadecane	n-C_{18}	28.2	29.4	1.3	4.5
n-Nonadecane	n-C_{19}	31.9	32.5	0.6	1.9
n-Eicosane	n-C_{20}	36.4	35.5	0.9	2.4

Figure 5.1 serves as a visual indication of the goodness of fit of the model. Scattering of the data points can be divided into two distinct regions, namely freeze points ranging from -160 to -50℃ and from -30 to +35℃. Data points in the -160 to -50℃ region were scattered inconsistently around the diagonal line at 45°. Except for the one outlier marked in red on the graph, data points in the -30℃ to +35℃ region were scattered close to the diagonal line, which is indicative of more accurate freeze point predictions of C_{11} – C_{20} carbon chain length n-paraffins.

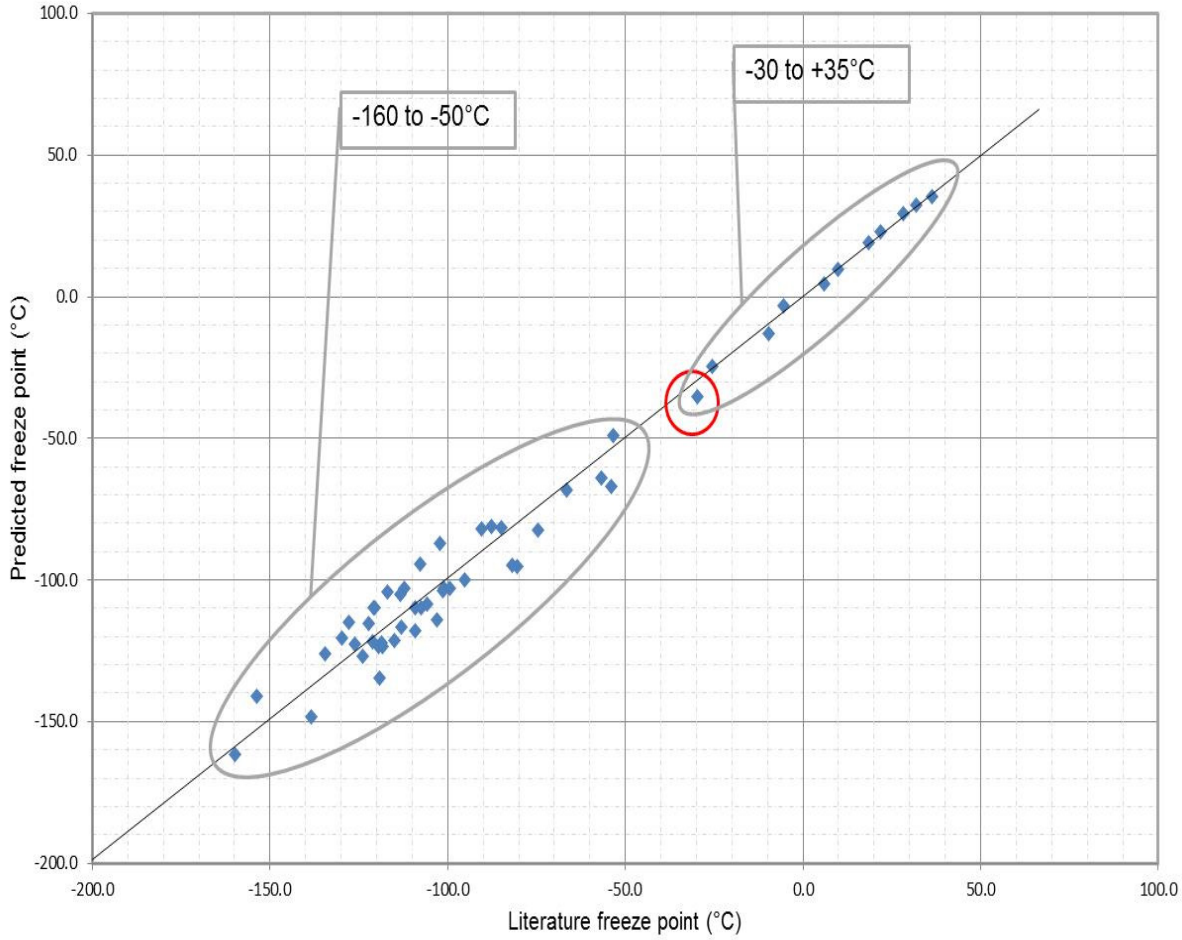

Figure 5.1. Freeze point parity plot.

5.3. Freeze point prediction model validation

The freeze point model was validated according to the procedures described in Chapter 3. The results of the various validation procedures are discussed below.

5.3.1. Standardised residuals

The graph of the standardised residuals versus the predicted freeze point is depicted in Figure 5.2. The majority of the data was clustered toward the left of the x-axis. The two distinct freeze point regions identified during discussion of the parity plot (Figure 5.1) are clearly visible here as

well. This can be attributed to the fact that the majority of the freeze points of the dataset were lower than -50.0℃. No obvious standardised residual outliers were identified for this data series.

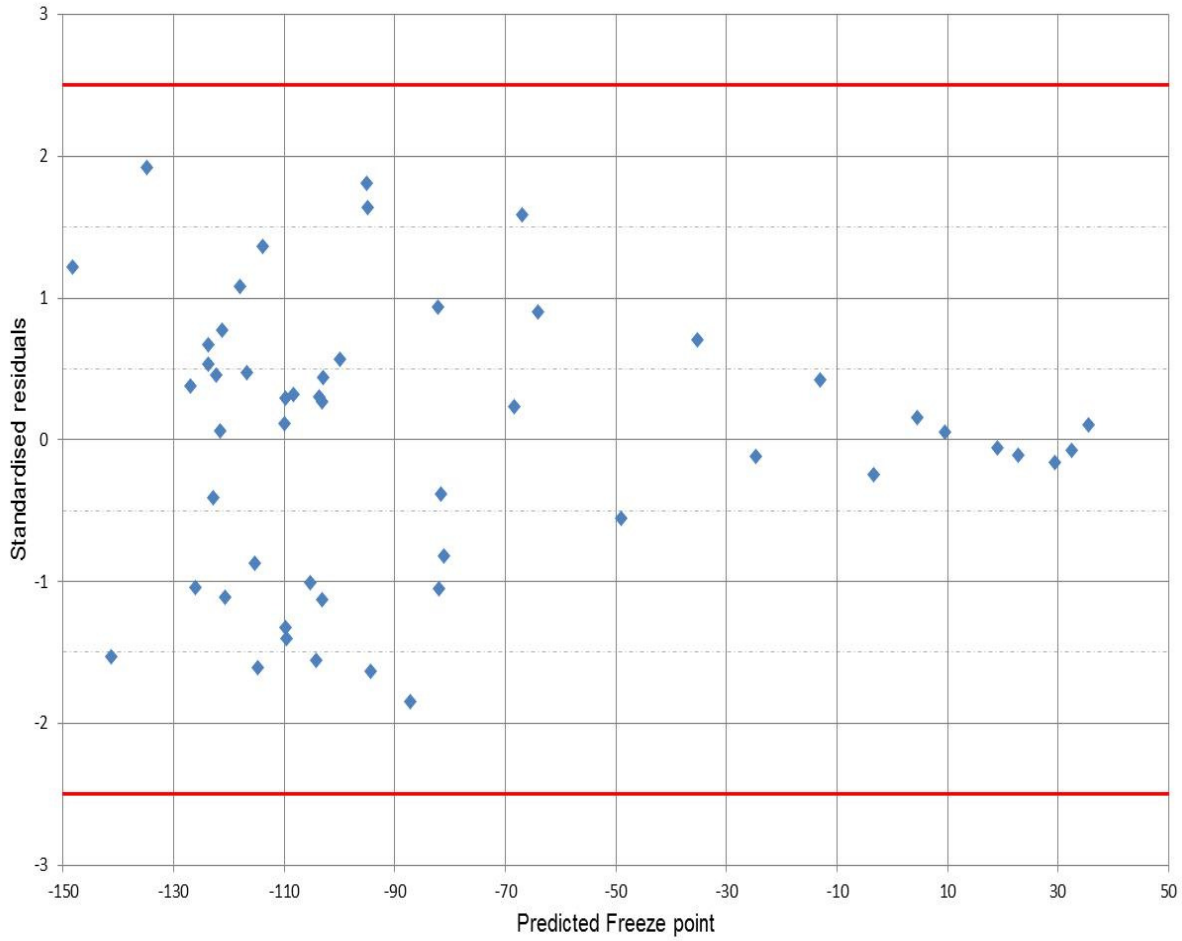

Figure 5.2. Graph of standardised residuals versus predicted freeze point.

Figure 5.3 depicts the normal probability plot for the standardised residuals. The data were scattered close to the diagonal line, which is indicative of the standard residuals conforming reasonably well to a normal distribution curve.

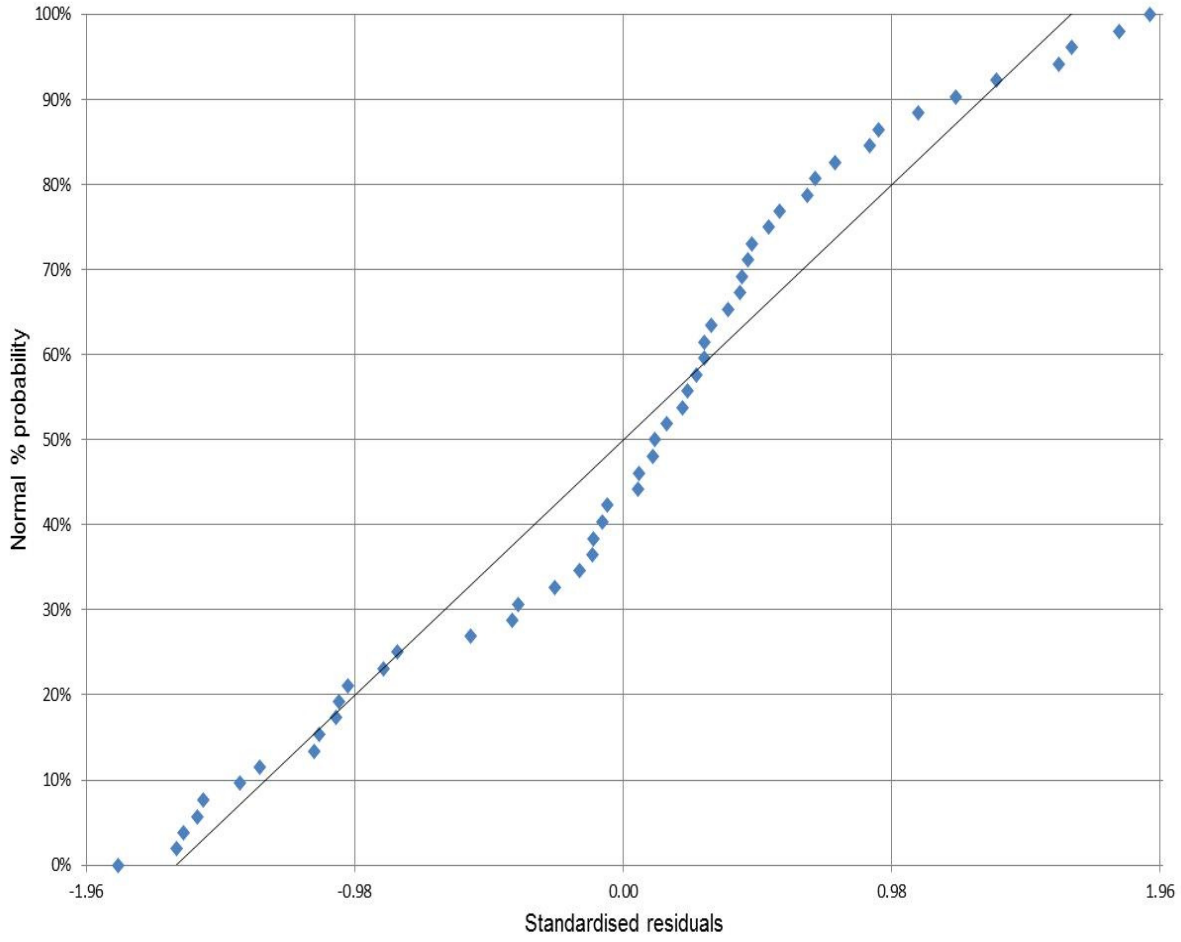

Figure 5.3. Normal probability plot of prediction model.

5.3.2. LMO validation

The model obtained for dataset 1 + 2 was:

$$\hat{y}=b_0 + b_1(\text{Zagreb index}) + b_2(\text{Molecular density}) + b_3(\text{Molecular flexibility index}) + b_4(\text{Total molecular mass})$$

The regression results for dataset 1 + 2 are presented in Table 5.3. The validation model was able to account for 97% of the variation in the freeze point and had a standard error of 8.7℃, which is comparable to the standard error of the overall model. The P-value of the Wiener index was well above the 5% significance level, whilst the P-values of the remaining descriptors were significant. The 95% confidence interval of the Wiener index included zero, which agrees with the high P-value observed for this descriptor. The Wiener index was consequently removed from the validation model.

Table 5.3. Statistics of freeze point prediction model: Dataset 1 + 2 (Predicting subset 3).

Regression statistic				
R^2	0.97			
Adjusted R^2	0.97			
Standard Error	8.7			
			95% Confidence interval	
Parameter	**Coefficient**	**P-value**	**Lower 95%**	**Upper 95%**
Intercept	-828.902	0.011	-1454.654	-203.149
Zagreb index	17.233	0.000	12.130	22.335
Molecular density	1095.301	0.016	216.916	1973.685
Molecular flexibility index	42.635	0.000	33.460	51.810
Total molecular mass	-7.264	0.000	-9.429	-5.100
Wiener index	-0.041	0.155	-0.098	0.016

The tabulated regression results for dataset 1 +2 can be viewed in Appendix B.

The model obtained for dataset 2 + 3 was:

$$\hat{y}=b_0 + b_1(Zagreb\ index) + b_2(Molecular\ density) + b_3(Molecular\ flexibility\ index) + b_4(Total\ molecular\ mass) + b_5(Wiener\ index)$$

The regression results for dataset 2 + 3 are shown in Table 5.4. The statistical data produced for this dataset correspond well to those of the first validation model. It can be observed that 98% of the variation in the freeze point was explained by the model. The standard error was similar to that of the overall model and the first validation set model. The P-value of the molecular density descriptor marginally exceeded the maximum significance level of 5%. The P-values of all other molecular descriptors were below the 5% significance level. Since the P-value of the molecular density descriptor was close to the 5% maximum P-value threshold, the validation model was preserved in its original form.

Table 5.4. Statistics of freeze point prediction model: Dataset 2 + 3 (Predicting subset 1).

Regression statistic				
R^2	0.98			
Adjusted R^2	0.98			
Standard Error	7.5			
			95% Confidence interval	
Parameter	**Coefficient**	**P-value**	**Lower 95%**	**Upper 95%**
Intercept	-657.992	0.047	-1308.168	-7.817
Zagreb index	19.442	0.000	15.603	23.281
Molecular density	859.861	0.060	-38.762	1758.484
Molecular flexibility index	45.037	0.000	37.846	52.228
Total molecular mass	-7.827	0.000	-9.493	-6.161
Wiener index	-0.065	0.018	-0.118	-0.012

The tabulated regression results for dataset 2 + 3 can be viewed in Appendix B.

The model obtained for dataset 1 + 3 was:

$$\hat{y} = b_0 + b_1(\text{Zagreb index}) + b_2(\text{Molecular density}) + b_3(\text{Molecular flexibility index}) + b_4(\text{Total molecular mass}) + b_5(\text{Wiener index})$$

The regression results for dataset 1 + 3 are presented in Table 5.5. The model was able to account for 98% of the variation in the freeze point. This model exhibited a standard error of 8.3℃, which was comparable to the standard error of the overall model. The P-values of the molecular density and Wiener index descriptors were 8.3% and 6.0% respectively, thereby exceeding the 5% significance level for P-values. All other P-values were significant. Since the P-values of the molecular density and Wiener index descriptors were close to the 5% maximum, the validation model was preserved in its original form.

Table 5.5. Statistics of freeze point prediction model: Dataset 1 + 3 (Predicting subset 2).

Regression statistic				
R^2	0.98			
Adjusted R^2	0.97			
Standard Error	8.3			
			95% Confidence interval	
Parameter	**Coefficient**	**P-value**	**Lower 95%**	**Upper 95%**
Intercept	-584.799	0.062	-1200.576	30.978
Zagreb index	18.800	0.000	14.981	22.619
Molecular density	764.808	0.083	-104.890	1634.507
Molecular flexibility index	44.319	0.000	36.870	51.769
Total molecular mass	-7.601	0.000	-9.319	-5.883
Wiener index	-0.065	0.060	-0.134	0.003

The tabulated regression results for dataset 1 + 3 can be viewed in Appendix B.

The molecular density and Wiener index descriptors had P-values just higher than 5% in two of the three validation models. To test the significance of these descriptors, they were individually omitted from the model. Removal of these descriptors from the model resulted in higher standard errors of the model; the model was therefore preserved in its original five-descriptor form.

5.3.3. Freeze point prediction of non-dataset molecules

Table 5.6 presents the freeze point prediction results of 11 non-dataset molecules. All predictions showed significant deviation from the literature values. Only 2,2,4-trimethylhexane exhibited a freeze point prediction error lower than 10%; however, even this equates to a prediction error of 11.9℃. These results indicate that the model cannot be used to predict the freeze points of molecules that did not form part of the original dataset.

Table 5.6. Freeze point prediction of non-dataset molecules.

Molecule	Carbon number	Freeze point (°C)	Predicted freeze point (°C)	Residual (°C) (Absolute)	Under-predicted (%)	Over-predicted (%)
2-Methylpropane	iso-C_4	-159.6	-182.8	23.2		14.5
3-Methylpentane	iso-C_6	-162.9	-141.7	21.2	13.0	
2,5-Dimethylhexane	iso-C_8	-91.2	-123.4	32.2		35.3
3-Methyl-3-ethylpentane	iso-C_8	-90.9	-119.1	28.2		31.0
4-Methyloctane	iso-C_9	-113.2	-93.3	19.9	17.5	
2,2,4-Trimethylhexane	iso-C_9	-120.0	-108.1	11.9	9.9	
2,2,3,3-Tetramethylpentane	iso-C_9	-9.9	-64.1	54.2		547.7
2,2,3,4-Tetramethylpentane	iso-C_9	-121.1	-86.9	34.2	28.2	
4-Methylnonane	iso-C_{10}	-98.7	-80.7	18.0	18.3	
2,2,5,5-Tetramethylhexane	iso-C_{10}	-12.6	-71.6	59.0		468.1
2,7-Dimethyloctane	iso-C_9	-54.0	-102.5	48.5		89.8

5.4. Final freeze point model discussion

The final freeze point prediction model for n- and iso-paraffins in the C_4 – C_{20} carbon number range is thus:

$$\hat{y}=b_0 + b_1(\text{Zagreb index}) + b_2(\text{Molecular density}) + b_3(\text{Molecular flexibility index}) + b_4(\text{Total molecular mass}) + b_5(\text{Wiener index})$$

$$\therefore \hat{y}=-659.278 + 18.911(\text{Zagreb index}) + 868.771(\text{Molecular density}) + 44.612(\text{Molecular flexibility index}) - 7.711(\text{Total molecular mass}) - 0.058(\text{Wiener index})$$

5.4.1. Total molecular mass

The total molecular mass of a molecule is defined as the sum of the atomic masses of all atoms in a molecule (ASTM DS 4B, 1991).

5.4.2. Molecular density

Molecular density is the ratio of molecular weight to molecular volume and is indicative of how tightly packed the atoms of a molecule are. This property is related to transport and melt behaviour (Dassault Systemes, 2005a).

5.4.3. Topological indices

Topological indices are two-dimensional molecular properties based on the concept of graph theory (Dassault Systemes, 2005d). Graph theory is a mathematical concept that can be applied to numerous other disciplines, including chemistry. In molecular graph theory, the molecule under investigation is projected onto a plane and studied as a graph that consists of vertices and edges (Johnson, 2005). The aim of molecular graph theory is to study and

distinguish molecules according to their size, shape, degree of branching and flexibility. The following molecular descriptors are classified as topological indices:

- Zagreb index;
- Wiener index; and
- Molecular flexibility index.

5.4.3.1. Zagreb indices

The Zagreb indices describe molecular size and degree of branching (Stevanovic & Zhou, 2006). In graph theory terms, the first Zagreb index, which is the Zagreb index used by Accelrys Materials Studio™, is quantified by the sum of the squares of the vertex valencies.

5.4.3.2. Wiener index

The Wiener index is used to quantify the extent of molecular branching. It is a function related to the number, length and position of branching, as well as to the number of atoms of a molecule (Todeshini & Consonni, 2000). In graph theory terms, the Wiener index can be determined by the sum of the distances between all vertice pairs.

5.4.3.3. Molecular flexibility index

This index is a measure of molecular flexibility and is modelled after an infinite chain of C(sp^3) atoms. The molecular flexibility index is based on structural properties that restrict the flexibility of molecules. Examples of such properties are (Dassault Systemes, 2005d):

- Fewer atoms;
- Branching;
- Molecules arranged in ring formation; and
- The presence of atoms with covalent radii smaller than those of C(sp^3).

This property is calculated as follows (Dassault Systemes, 2005d):

$$\Phi = \frac{\kappa_1^{\alpha} . \kappa_2^{\alpha}}{N}$$

Where:

- Φ: Molecular flexibility index;
- κ_1^{α}: Describes both the atom count and the cyclicity of molecules (Todeshini & Consonni, 2000);
- κ_2^{α}: Describes the branching of the molecule (Todeshini & Consonni, 2000);
- N: Number of vertices/Atom count.

5.5. Conclusion

Even though the freeze point prediction model had high R^2 values, the high standard error indicated low levels of model precision. ASTM D5972 (2016) stipulates that the repeatability for freeze point measurements is 0.5℃, and the reproducibility is 0.8℃. When considering the absolute residual values obtained for the dataset molecules, it can be concluded that the model made notable prediction errors that are far removed from the repeatability and reproducibility values stipulated above. The model was able to predict the freeze points of longer carbon chain length n-paraffins accurately; however, results obtained for shorter carbon chain length n- and iso-paraffins were unsatisfactory. Two distinctive freeze point regimes were observed during evaluation of the freeze point parity plot; however, it is unlikely that development of separate models for the respective regimes will result in significantly more accurate iso-paraffin freeze point predictions. Validation of the model was unsuccessful. It can consequently be concluded that the final model was not able to predict the freeze points of structurally diverse paraffinic molecules in the C_4 – C_{20} carbon number range accurately.

The poor performance of the freeze point model can be attributed to the nature of the organic molecules considered during this study. Freeze point can be defined as the temperature at which a liquid changes to a solid when cooled slowly. Molecules in the liquid state are randomly organised, but when the molecules crystallise into the solid state, they become more ordered, forming a crystal lattice (ASTM DS 4B, 1991). Freeze point is influenced by the strength of the crystal lattice (Flack & Gavezzotti, 2005). The strength of the crystal lattice in turn, is controlled by various factors, including:

- Molecular symmetry (Katrizky, et al., 2010), (Flack & Gavezzotti, 2005); and
- Intermolecular forces (Brown, et al., 2006), (Katrizky, et al., 2010).

The major flaw of this model was that it could account neither for the strength of the crystal lattice, nor for the fact that many organic molecules crystallise in different crystal structures (polymorphism). According to the literature reviewed in Chapter 2, intermolecular forces are considered a major contributor toward the freeze point behaviour of molecules; however, results obtained from the freeze point prediction investigation are indicative of the fact that freeze point behaviour remains a highly complex field of study.

Even though it was not possible to predict the freeze points of individual molecules in the jet fuel regime accurately, similar statistical techniques should be explored to attempt prediction of the freeze point behaviour of extended carbon number distribution jet fuels, due to the importance of the freeze point behaviour of these fuels.

Chapter 6 : Fractional Distillation Results

6.1. Introduction

This chapter presents the results obtained from the fractional distillation of various refinery products in order to produce n- and iso-paraffin fractions with carbon chain lengths in the C_9 – C_{18} range. These fractions served as mixture components for the subsequent statistical mixture design studies, which formed the core of this research.

6.2. n-Paraffin mixture components

6.2.1. Fractionation results

As discussed in Chapter 3, distillate fractions were collected at 2°C intervals in the 121.7 – 326.3°C temperature range as the distillation progressed. The chemical composition of each distillate was determined by means of GCxGC analysis. The GCxGC results were then used to combine the fractions in such a manner as to obtain C_9 – C_{18} mixture components, which contained the highest concentration of molecules with the desired carbon chain length. The fractionation results of the C_8 – C_{20} refinery product are presented in Table 6.1.

The final boiling point temperature of each mixture component was on average 8°C higher than the corresponding n-paraffin literature boiling point value. The final boiling point temperatures were higher than the literature boiling point values, since none of the distillates collected in the 121.7 – 324.3°C temperature range were discarded; the 2°C interval distillates were blended in a sequential manner to produce mixture components, which contained the highest concentration of molecules with the desired carbon chain length, whilst remaining representative of the complete refinery product.

The distillation had to be repeated six times in order to obtain sufficient quantities of each mixture component for the subsequent mixture design studies. Emphasis was placed on producing sufficient volumes of the C_{17} and C_{18} mixture components, since these components were present in lower concentrations in the refinery product.

Table 6.1. Results of n-paraffin fractionation.

Mixture component	Carbon number	Literature boiling point [AET] (℃)	Fractionation temperature [AET] (℃): Initial boiling point to final boiling point	Mixture component mass (g)
n-C_8	C_8H_{18}	125.7	121.7 - 133.7	0
n-C_9	C_9H_{20}	150.8	133.7 - 158.5	4332
n-C_{10}	$C_{10}H_{22}$	174.2	158.5 - 181.9	3694
n-C_{11}	$C_{11}H_{24}$	195.9	181.9 - 204.0	2462
n-C_{12}	$C_{12}H_{26}$	216.3	204.0 - 224.0	2758
n-C_{13}	$C_{13}H_{28}$	235.5	224.0 - 243.6	2767
n-C_{14}	$C_{14}H_{30}$	253.6	243.6 - 262.0	3033
n-C_{15}	$C_{15}H_{32}$	270.7	262.0 - 279.0	2762
n-C_{16}	$C_{16}H_{34}$	286.9	279.0 - 295.0	2204
n-C_{17}	$C_{17}H_{36}$	302.0	295.0 - 310.0	6096
n-C_{18}	$C_{18}H_{38}$	316.3	310.0 - 324.3	1769

6.2.2. n-Paraffin mixture component GCxGC results

The mixture components obtained through combining successive fractions, as discussed in the previous section, were analysed using GCxGC to determine the purity of the respective components.

The average carbon numbers (Figure 6.1) derived from the GCxGC analyses of the n-paraffin mixture components corresponded well with the desired carbon numbers. The average carbon number of the C_{18} mixture component was marginally higher than the desired carbon number, which is indicative of the presence of longer carbon chain length molecules within the mixture component.

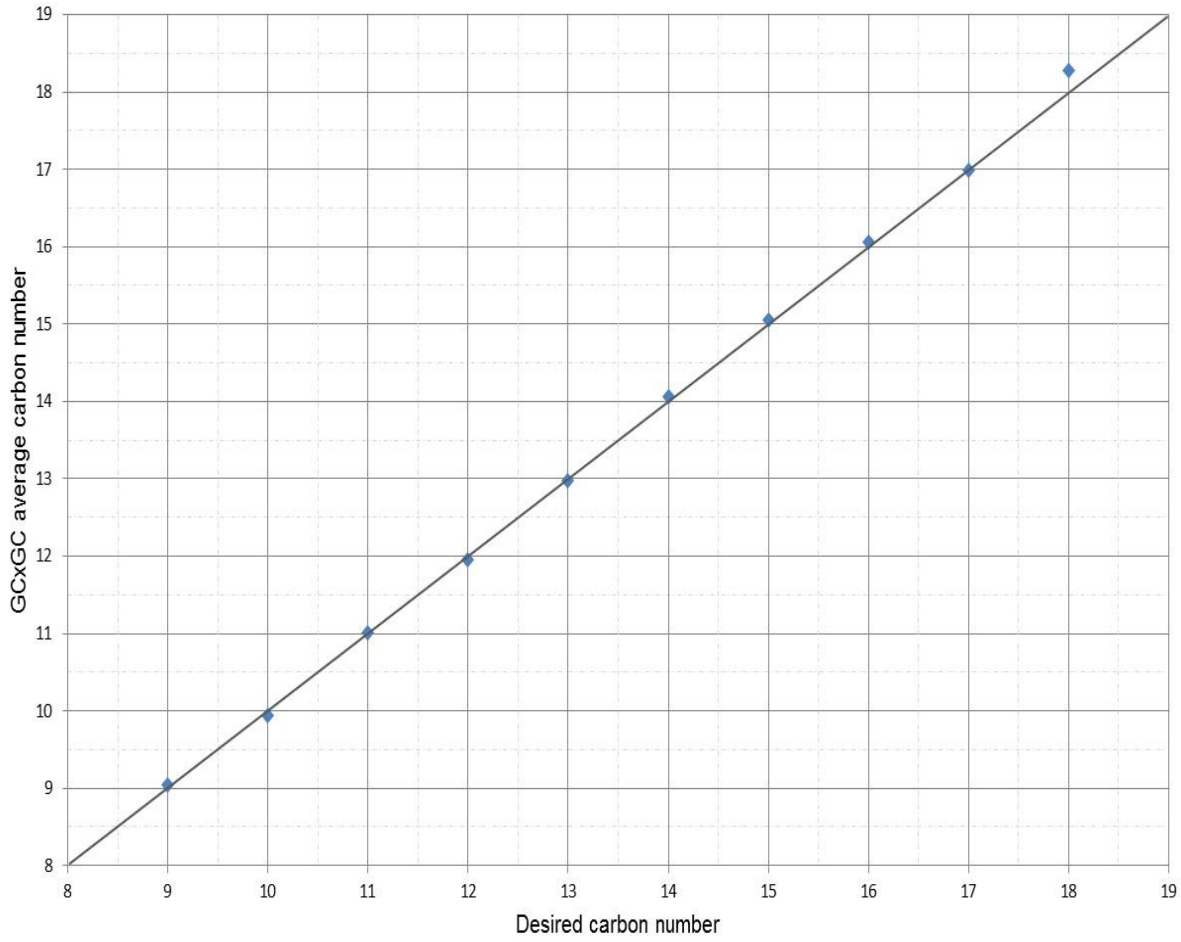

Figure 6.1. n-Paraffin average carbon number versus desired carbon number.

The compositions of the n-paraffin mixture components are depicted in Figure 6.2. The mixture components consisted predominantly of n-paraffins, as well as of smaller quantities of iso- and cyclic paraffins. Aromatic compounds were also detected in each mixture component; however, these aromatic compounds are not clearly visible on the graph, since they were only present in trace amounts within each mixture component. The relative proportions of the n- and iso-paraffins, cyclic paraffins and aromatic compounds within each mixture component were reflective of the composition of the refinery fractionated product.

Even though all C_9 – C_{18} n-paraffin mixture components contained some iso- and cyclic paraffins, these mixture components are representative of an n-paraffin rich fraction and are suitable for use in the remainder of the study.

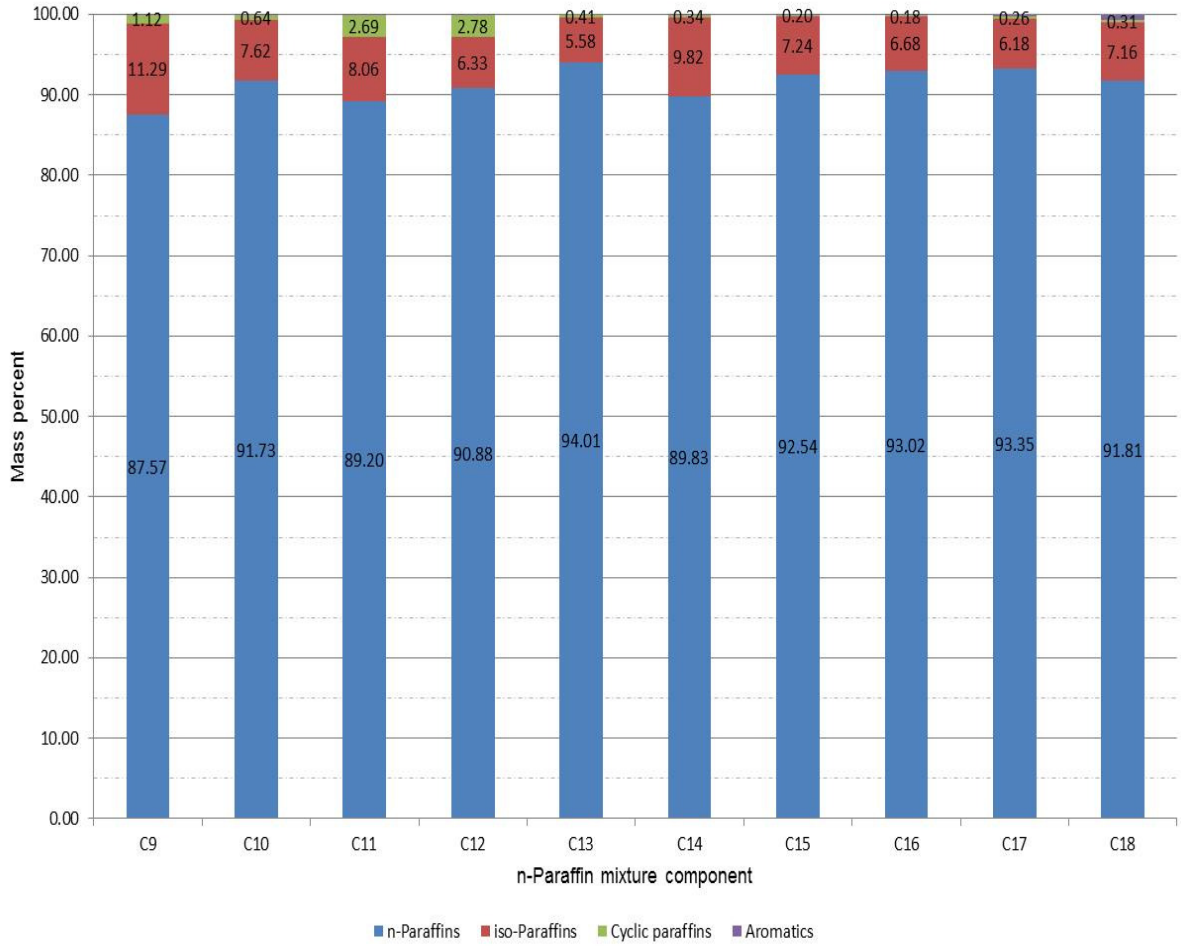

Figure 6.2. Compositional graph of n-paraffin GCxGC results.

6.2.3. n-Paraffin mixture component physical properties

After confirming the composition of the mixture components, the viscosities and freeze points of these components were measured; the results are depicted in Table 6.2. As expected, the kinematic viscosity, as well as the freeze point of the n-paraffin mixture components, increased as the carbon chain length increased.

Since the C_{17} and C_{18} mixture components were solid at 20℃, the viscosity and freeze point properties of these components could not be determined, as:

- The instrument used for determining kinematic viscosity can only operate with liquid samples; and
- The maximum freeze point measurement capability of ASTM D5972 instrumentation is 20℃, which implies that the freeze point values of these two components were in excess of 20℃ (ASTM D5972-16, 2016).

Table 6.2. Physical properties of n-paraffin mixture components.

Mixture component	Carbon number	Viscosity at 20℃ (cSt)	Freeze point (℃)
n-C_9	C_9H_{20}	1.0	-56.6
n-C_{10}	$C_{10}H_{22}$	1.2	-31.7
n-C_{11}	$C_{11}H_{24}$	1.6	-27.2
n-C_{12}	$C_{12}H_{26}$	2.0	-10.6
n-C_{13}	$C_{13}H_{28}$	2.4	-6.0
n-C_{14}	$C_{14}H_{30}$	3.0	4.1
n-C_{15}	$C_{15}H_{32}$	3.7	9.4
n-C_{16}	$C_{16}H_{34}$	4.5	16.5
n-C_{17}	$C_{17}H_{36}$	CNM*	CNM*
n-C_{18}	$C_{18}H_{38}$	CNM*	CNM*

*Could not measure.

6.3. iso-Paraffin mixture components

6.3.1. Fractionation results

Similar to the fractionation of the n-paraffin refinery product, distillates were collected at 2℃ intervals in the 116.7 – 326.3℃ temperature range as the distillation progressed. The initial fractionation temperature was lower since the boiling points of iso-paraffins tend to be lower than those of their n-paraffin counterparts. The chemical composition of each distillate fraction was also determined by means of GCxGC analysis. The GCxGC results were used to combine the fractions to obtain C_9 – C_{18} mixture components, which contained the highest concentration of the desired molecules whilst remaining representative of the complete refinery product. Fractionation results of the C_8 – C_{27} refinery product are presented in Table 6.3.

The final boiling points of the iso-paraffin mixture components ranged from 5℃ below to 7℃ above the n-paraffin literature boiling point values. The final boiling points of the mixture components systematically dropped below the n-paraffin literature boiling point values as the carbon chain length of the mixture components increased; the C_{11} and C_{16} mixture components were the only notable outliers observed during evaluation of this trend.

The distillation had to be repeated seven times in order to obtain sufficient quantities of each mixture component for the subsequent mixture design studies. Emphasis was placed on producing sufficient volumes of the C_9 mixture component, since this component was present in lower concentrations in the refinery product.

Table 6.3. Results of iso-paraffin fractionation.

Mixture component	Carbon number	n-Paraffin literature boiling point [AET] (°C)	Fractionation temperature [AET] (°C): Initial boiling point to final boiling point	Mixture component mass (g)	n-Paraffin literature boiling point – final boiling point (°C)
i-C_8	C_8H_{18}	125.7	116.7 - 133.0	389	7.3
i-C_9	C_9H_{20}	150.8	133.0 - 156.0	2044	5.2
i-C_{10}	$C_{10}H_{22}$	174.2	156.0 - 176.0	1755	1.8
i-C_{11}	$C_{11}H_{24}$	195.9	176.0 - 198.0	2789	2.1
i-C_{12}	$C_{12}H_{26}$	216.3	198.0 - 216.0	2599	-0.3
i-C_{13}	$C_{13}H_{28}$	235.5	216.0 - 234.0	2544	-1.5
i-C_{14}	$C_{14}H_{30}$	253.6	234.0 - 251.0	2403	-2.6
i-C_{15}	$C_{15}H_{32}$	270.7	251.0 - 268.0	2349	-2.7
i-C_{16}	$C_{16}H_{34}$	286.9	268.0 - 282.0	1993	-4.9
i-C_{17}	$C_{17}H_{36}$	302.0	282.0 - 299.0	2332	-3.0
i-C_{18}	$C_{18}H_{38}$	316.3	299.0 - 313.0	1836	-3.3

6.3.2. iso-Paraffin mixture component GCxGC results

The iso-paraffin mixture components discussed above were also analysed by means of a GCxGC to determine the purity of the respective components.

As illustrated in Figure 6.3, the average carbon numbers of the mixture components corresponded well to the desired carbon numbers. No notable outliers were detected for this data series.

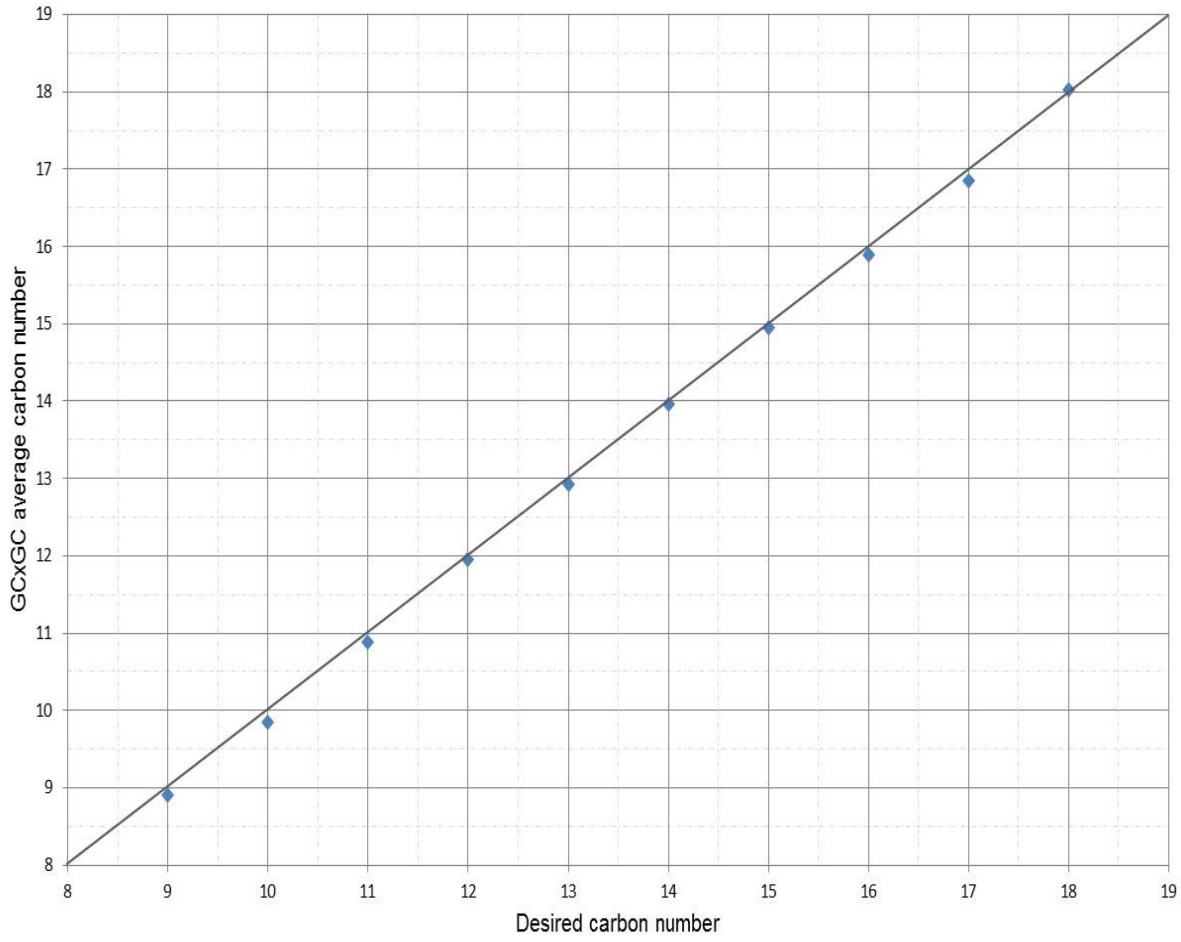

Figure 6.3. iso-Paraffin average carbon number versus desired carbon number.

The compositions of the iso-paraffin mixture components are depicted in Figure 6.4. The mixture components consisted primarily of iso-paraffins. Smaller quantities of n-paraffins and cyclic paraffins were also detected alongside trace amounts of aromatic compounds. The aromatic compounds are not visible on the graph, however, since they were only present in trace amounts within each mixture component. The relative proportions of the n- and iso-paraffins, cyclic paraffins and aromatic compounds within each mixture component were representative of the composition of the refinery product fractionated.

It was furthermore noted that the n-paraffin content of the mixture components decreased as the carbon chain length increased; the C_{13}, C_{15} and C_{17} mixture components were the only notable outliers observed during evaluation of this trend. The decrease in n-paraffin content of the mixture components corresponds to the decrease in final boiling point observed previously. The decrease in the final boiling point can thus be attributed to the lower iso-paraffin boiling points, which became more pronounced as the concentration of these iso-paraffins within the mixture components increased.

Even though the C_9 – C_{18} iso-paraffin mixture components were not pure, these mixture components are representative of iso-paraffin rich components and are suitable for use in the remainder of the study.

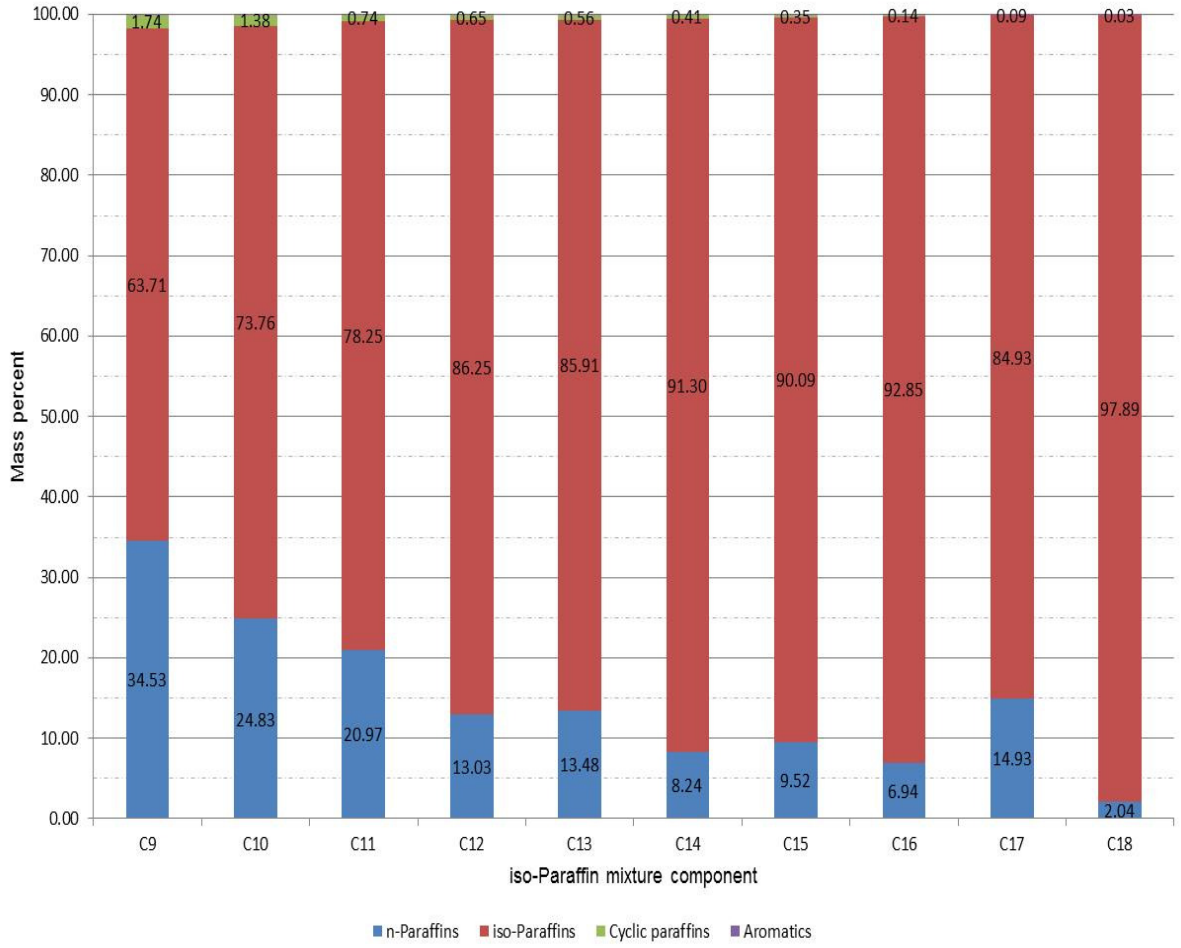

Figure 6.4. Compositional graph of iso-paraffin GCxGC results.

6.3.3. iso-Paraffin mixture component physical properties

After confirming the composition of the iso-paraffin mixture components, the viscosities and freeze points of these components were measured. The results are depicted in Table 6.4. The freeze point of the C_9 mixture component could not be measured since the minimum freeze point measurement capability of ASTM D5972 instrumentation is -80℃, which implies that the freeze point value of this component was below -80℃ (ASTM D5972-16, 2016). Furthermore, the freeze point values did not follow the general trend associated with an increase in carbon chain length. The i-C_{11} component exhibited a lower freeze point than the i-C_{10} component; the same trends were observed for the i-C_{13} and i-C_{12} components, as well as for the i-C_{15} and i-C_{14} components.

After the aforementioned anomalous freeze point behaviour was observed, the densities of the mixture components at 20℃ were also measured. Similar to the viscosity, the density increased, as the carbon chain length increased, offering no apparent explanation for the freeze point behaviour observed. Closer examination of the GCxGC results also did not offer any obvious explanation for this freeze point behaviour.

Table 6.4. Physical properties of the iso-paraffin mixture components.

Mixture component	**Carbon number**	**Viscosity at 20℃ (cSt)**	**Freeze point (℃)**	**Density at 20℃ (g/cm^3)**
i-C_9	C_9H_{20}	0.9	CNM*	0.7186
i-C_{10}	$C_{10}H_{22}$	1.1	-59.8	0.7307
i-C_{11}	$C_{11}H_{24}$	1.4	-66.9	0.7418
i-C_{12}	$C_{12}H_{26}$	1.8	-47.0	0.7513
i-C_{13}	$C_{13}H_{28}$	2.3	-51.6	0.7593
i-C_{14}	$C_{14}H_{30}$	2.8	-39.9	0.7663
i-C_{15}	$C_{15}H_{32}$	3.5	-41.2	0.7724
i-C_{16}	$C_{16}H_{34}$	4.3	-36.0	0.7774
i-C_{17}	$C_{17}H_{36}$	5.4	-30.9	0.7825
i-C_{18}	$C_{18}H_{38}$	6.6	-28.0	0.7865

*Could not measure.

6.4. n-Paraffin/iso-paraffin viscosity and freeze point comparison

In order to investigate the differences in physical properties due to the differences in molecular structure of the n- and iso-paraffin mixture components produced, the viscosities and freeze points of the respective components were compared graphically.

The viscosities of the n- and iso-paraffin mixture components at 20℃ are depicted in Figure 6.5. The iso-paraffin components exhibited marginally lower viscosities than their n-paraffin counterparts. None of the unexpected viscosity behaviour discussed in the literature review (Chapter 2, Figure 2.6) was observed, however, since these mixture components contained a multitude of paraffinic compounds, which masked the viscosity behaviour of individual molecules. When studying the effect of varying carbon number distributions and i:n mass ratios on the viscosity of jet fuel, it is thus anticipated that the carbon chain length will dominate the selection of mixture components, rather than the i:n mass ratio.

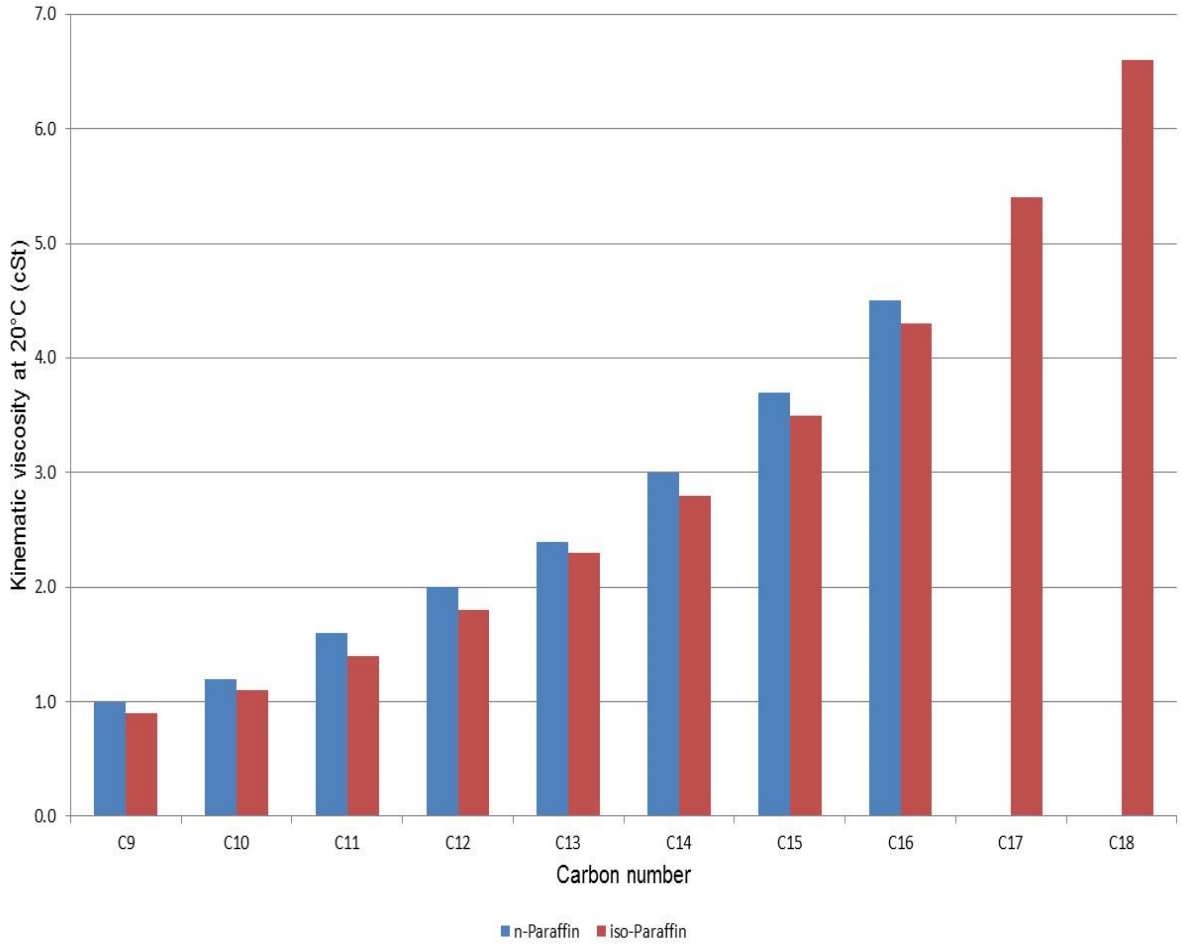

Figure 6.5. n-Paraffin versus iso-paraffin viscosity graph.

Figure 6.6 depicts the freeze point comparison of the various n- and iso-paraffin mixture components produced. The n-paraffin mixture components possessed significantly higher freeze points than their iso-paraffin counterparts, which is why iso-paraffins, rather than n-paraffins, have historically always been preferred when producing jet fuel. As discussed previously, the freeze points of the C_{17} – C_{18} n-paraffin mixture components could not be measured by using the analytical instrumentation available. The aforementioned indicates that longer carbon chain length n-paraffin mixture components are detrimental to the freeze point of jet fuel mixtures.

The presence of n-paraffins in jet fuel can be manipulated to some extent by refinery processes such as isomerisation; however, it is unlikely that all n-paraffins will be removed from the fuel during production. This means that, if a refinery product earmarked for jet fuel production contained n- and iso-paraffins, both of these paraffins would be present in the fuel after completion of the refining process. The effect of n-paraffins on the freeze point of jet fuel can thus not be excluded from the study. It is therefore anticipated that both i:n mass ratio and carbon number distribution will affect the freeze point behaviour of jet fuel mixtures in the subsequent mixture design studies.

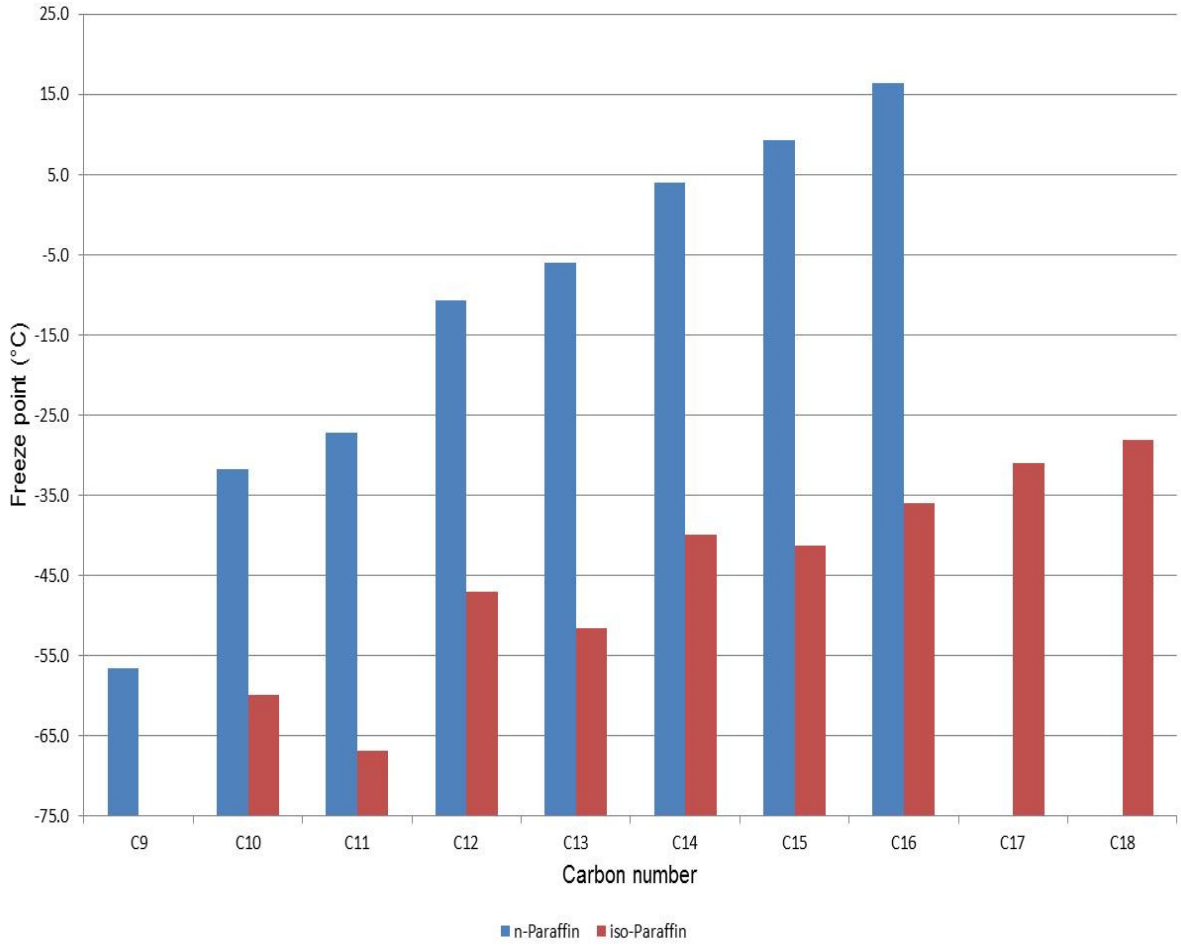

Figure 6.6. n-Paraffin versus iso-paraffin freeze point graph.

6.5. Conclusion

Fractionation of the n-paraffin mixture components was fairly simple, whereas fractionation of the iso-paraffin components was more complicated, since no constant fractionation temperature trend could be established for these mixture components. The final boiling point trend observed for the iso-paraffin mixture components could be attributed to the increase in iso-paraffin content, as the carbon chain length of the mixtures increased. The presence of undesired molecules within the various n- and iso-paraffin mixture components was primarily due to the composition of the refinery products, which were fractionated in a sequential manner.

The viscosity trends observed were as expected, since the viscosity increased with an increase in carbon number for both the n- and iso-paraffin components. Marginal differences in the viscosities between the n- and iso-paraffin mixture components were observed per carbon number. It is therefore anticipated that the i:n mass ratio will have a low influence on the selection of the mixture components, when studying the effect of variation in i:n mass ratio and carbon number distribution on the viscosity of jet fuel mixtures. In contrast, it is expected that

carbon number distribution will have a significant impact on the selection of mixture components.

The freeze points of the n- and iso-paraffin mixture components increased with an increase in the carbon chain length. The iso-paraffin mixture components exhibited inconsistent freeze point behavioural trends; the cause of this behaviour could not be explained by the analytical data available. The freeze points of the iso-paraffin mixture components were significantly lower than their n-paraffin carbon number equivalents. Even though it was acknowledged that the n-paraffin content of jet fuel could be manipulated during the refining process, it was noted that the presence of these molecules in the fuel might be unavoidable; the n-paraffin mixture components should thus not be excluded from the subsequent mixture design study. It is therefore expected that both carbon number distribution and i:n mass ratio will affect the selection of the mixture components when studying the effect of variation in i:n mass ratio and carbon number distribution on the freeze point of jet fuel mixtures.

Although it was not possible to produce pure n- and iso-paraffin mixture components, these mixture components are still suitable for use during construction of extended carbon number distribution jet fuels by application of statistical mixture design techniques.

6.6. Recommendations

It is recommended that ^{1}H and ^{13}C Nuclear Magnetic Resonance (NMR) spectroscopy analyses be conducted on the iso-paraffin mixture components to determine whether the molecular structure of these components can account for the freeze point phenomenon observed.

Chapter 7 : Mixture Design Results

7.1. Introduction

Statistical mixture design techniques are useful tools when studying the effects of mixture components on response variables. These techniques are beneficial when determining the most important mixture components, as well as when formulating mixtures with specific response variable characteristics. Mixture design techniques also enable the mixture components to be reduced by removing insignificant components (Bondari, 2005). In the study of fuels and fuel components, the terminology of mixture design is often replaced by “blend design”, as these fuel component mixtures are more commonly referred to as blends. However, in the context of this study, the terminology of mixture design and mixture models will be retained. This chapter presents the predictive models that were developed as part of this research to study the viscosity and freeze point behaviour of synthetic jet fuel, by varying the i:n mass ratio and the carbon number distribution.

7.2. Definition of statistical terms

Since the statistics associated with mixture models are of vital importance, the statistical terms used in this chapter, which had not been discussed previously in Chapter 4, are discussed below.

7.2.1. Cross-validated R^2

The Design-Expert® software applied the Leave One Out (LOO) validation procedure to produce the cross-validated R^2 value for each model. In the LOO procedure, a single mixture is removed from the original dataset, after which the model is recalculated for the remainder of the dataset. The newly computed model is then used to predict the viscosity and freeze point of the excluded mixture. This procedure is repeated for all the mixtures in order to produce a single regression statistic, which is known as the cross-validated R^2. Cross-validated R^2 values range from 0 to 1; values closer to 1 indicate that the model accounts for a greater proportion of variance.

7.2.2. Significance level

Model parameters with significance levels at or below 10% are regarded as significant contributors toward proper functioning of the model.

7.3. Mixture design

After entering all the required parameters (Chapter 3) into the Design-Expert® software, the software yielded a mixture design consisting of 50 mixtures, which had to be prepared and analysed for viscosity and freeze point. The mixtures were prepared using the n- and iso-paraffin mixture components produced by means of fractional distillation, as discussed previously in Chapter 3 and Chapter 6. The results are depicted in Table 7.1. The freeze point of mixture number 30 was below the minimum operating temperature of the freeze point analyser and could thus not be measured; this observation was consequently excluded from the design. Furthermore, 29 of the mixtures exhibited freeze points that were in the -20℃ to 14℃ temperature range and therefore the kinematic viscosity of these mixtures could not be measured at -20℃ or -47℃.

Table 7.1. Mixture design for variation of i:n mass ratio and carbon number distribution.

	Mixture components (Mass %)		Numeric factors (Mass %)										Blend properties (Responses)	
Run	iso-Paraffin	n-Paraffin	C_9	C_{10}	C_{11}	C_{12}	C_{13}	C_{14}	C_{15}	C_{16}	C_{17}	C_{18}	Freeze point (℃)	Viscosity at 20℃ (cSt)
1	50	50	10.0	10.0	10.0	10.0	10.0	10.0	10.0	10.0	10.0	10.0	-10.3	2.4
2	100	0	0.0	0.0	0.0	0.0	20.0	0.0	0.0	40.0	40.0	0.0	-37.9	4.0
3	50	50	40.0	20.0	0.0	0.0	40.0	0.0	0.0	0.0	0.0	0.0	-33.8	1.4
4	0	100	0.0	0.0	40.0	0.0	0.0	0.0	0.0	20.0	40.0	0.0	8.1	3.0
5	50	50	0.0	0.0	40.0	0.0	20.0	0.0	0.0	0.0	40.0	0.0	-2.9	2.6
6	0	100	0.0	0.0	0.0	0.0	0.0	40.0	0.0	20.0	0.0	40.0	14.4	4.5
7	50	50	40.0	0.0	0.0	0.0	0.0	0.0	20.0	0.0	40.0	0.0	-5.1	2.2
8	100	0	0.0	40.0	0.0	20.0	0.0	0.0	0.0	0.0	40.0	0.0	-43.0	2.1
9	50	50	20.0	0.0	40.0	40.0	0.0	0.0	0.0	0.0	0.0	0.0	-34.2	1.5
10	50	50	0.0	0.0	0.0	40.0	20.0	0.0	0.0	40.0	0.0	0.0	-4.2	2.7
11	50	50	0.0	0.0	0.0	0.0	40.0	20.0	40.0	0.0	0.0	0.0	-12.7	2.9
12	100	0	0.0	0.0	0.0	40.0	0.0	0.0	0.0	0.0	20.0	40.0	-37.3	3.5
13	100	0	0.0	0.0	20.0	40.0	0.0	0.0	40.0	0.0	0.0	0.0	-56.6	2.2
14	0	100	0.0	20.0	0.0	0.0	0.0	0.0	40.0	0.0	0.0	40.0	11.8	3.5
15	50	50	0.0	0.0	0.0	40.0	0.0	20.0	0.0	0.0	40.0	0.0	-2.6	3.0
16	100	0	0.0	0.0	0.0	40.0	20.0	0.0	0.0	40.0	0.0	0.0	-52.3	2.6
17	75	25	0.0	40.0	20.0	0.0	40.0	0.0	0.0	0.0	0.0	0.0	-42.5	1.6
18	0	100	40.0	0.0	0.0	0.0	0.0	40.0	20.0	0.0	0.0	0.0	-9.7	1.9
19	50	50	20.0	0.0	0.0	0.0	0.0	40.0	0.0	40.0	0.0	0.0	-9.9	2.5
20	100	0	40.0	0.0	0.0	0.0	0.0	0.0	0.0	40.0	0.0	20.0	-44.0	2.1
21	50	50	0.0	20.0	0.0	40.0	0.0	0.0	0.0	0.0	0.0	40.0	0.5	2.6
22	100	0	20.0	0.0	0.0	0.0	0.0	0.0	40.0	0.0	40.0	0.0	-42.6	2.8
23	50	50	0.0	40.0	20.0	0.0	0.0	40.0	0.0	0.0	0.0	0.0	-19.6	1.7
24	0	100	40.0	0.0	20.0	0.0	0.0	0.0	0.0	0.0	0.0	40.0	6.6	2.1
25	50	50	0.0	40.0	0.0	0.0	0.0	0.0	40.0	20.0	0.0	0.0	-12.4	2.2
26	50	50	20.0	0.0	40.0	0.0	0.0	0.0	40.0	0.0	0.0	0.0	-19.0	1.8
27	50	50	0.0	0.0	0.0	0.0	20.0	40.0	0.0	0.0	0.0	40.0	2.3	3.8
28	100	0	20.0	0.0	0.0	0.0	40.0	40.0	0.0	0.0	0.0	0.0	-53.6	2.0
29	0	100	0.0	0.0	0.0	40.0	0.0	0.0	40.0	20.0	0.0	0.0	0.4	2.9
30	100	0	40.0	20.0	0.0	40.0	0.0	0.0	0.0	0.0	0.0	0.0	BDL	1.2
31	50	50	0.0	0.0	20.0	0.0	0.0	0.0	0.0	40.0	0.0	40.0	4.1	4.0
32	0	100	0.0	40.0	0.0	40.0	0.0	0.0	0.0	0.0	20.0	0.0	-5.1	1.9
33	0	100	0.0	40.0	0.0	40.0	0.0	0.0	0.0	0.0	20.0	0.0	-5.2	1.9
34	50	50	10.0	10.0	10.0	10.0	10.0	10.0	10.0	10.0	10.0	10.0	-10.4	2.4
35	50	50	10.0	10.0	10.0	10.0	10.0	10.0	10.0	10.0	10.0	10.0	-10.4	2.4
36	50	50	0.0	0.0	0.0	0.0	40.0	20.0	40.0	0.0	0.0	0.0	-12.6	2.9
37	50	50	40.0	0.0	0.0	0.0	0.0	0.0	20.0	0.0	40.0	0.0	-5.3	2.2
38	0	100	0.0	40.0	0.0	0.0	20.0	0.0	0.0	40.0	0.0	0.0	2.7	2.2
39	0	100	0.0	40.0	0.0	0.0	20.0	0.0	0.0	40.0	0.0	0.0	2.4	2.2
40	50	50	0.0	0.0	40.0	0.0	20.0	0.0	0.0	0.0	40.0	0.0	-3.7	2.6
41	0	100	20.0	0.0	0.0	40.0	40.0	0.0	0.0	0.0	0.0	0.0	-17.5	1.8
42	100	0	20.0	0.0	0.0	0.0	0.0	40.0	0.0	0.0	40.0	0.0	-45.2	2.6
43	100	0	0.0	0.0	40.0	0.0	40.0	0.0	0.0	20.0	0.0	0.0	-62.5	2.1
44	0	100	0.0	0.0	40.0	0.0	40.0	20.0	0.0	0.0	0.0	0.0	-14.7	2.1
45	50	50	0.0	0.0	20.0	0.0	0.0	0.0	0.0	40.0	0.0	40.0	4.2	4.0
46	100	0	0.0	0.0	40.0	0.0	0.0	40.0	0.0	20.0	0.0	0.0	-55.6	2.2
47	100	0	0.0	0.0	0.0	0.0	20.0	0.0	40.0	40.0	0.0	0.0	-43.5	3.5
48	50	50	40.0	20.0	0.0	0.0	40.0	0.0	0.0	0.0	0.0	0.0	-34.6	1.4
49	100	0	0.0	40.0	0.0	0.0	0.0	0.0	20.0	0.0	0.0	40.0	-40.4	2.5
50	0	100	0.0	0.0	0.0	0.0	40.0	0.0	0.0	0.0	40.0	20.0	13.9	4.0

*BDL: Below Detection Limit.

The inability to measure the viscosities of these mixtures at -20℃ or -47℃ rendered the mixture design unworkable; without a proper functioning model the investigation could not progress. In order to proceed with the investigation, ASTM D341 (2009) was applied to predict a proposed viscosity limit at 20℃, by making use of the proposed viscosity limits of 12.0 cSt at -47℃ and 4.5 cSt at -20℃, as discussed in Chapter 1:

$$\log(v + 0.7) = A - B \log T$$

Where:

- v: Viscosity (cSt);
- T: Temperature (K);
- A: Coefficient A, calculated from known 12.0 cSt viscosity at -47℃;
- B: Coefficient B, calculated from known 4.5 cSt viscosity at -20℃;

The above mentioned equation was solved by means of Microsoft Excel. The Solver function was used to optimise coefficients A and B. A proposed viscosity limit of 1.8 cSt at 20℃ was obtained, and the viscosities of all mixtures were consequently measured at 20℃.

7.4. Mixture models

The procedures described in Chapter 3 were followed to produce models for studying the effect of i:n mass ratio and carbon number distribution on the viscosity and freeze point of jet fuel mixtures. As discussed in Chapter 3, the design space was too constrained and a feasible candidate set could not be obtained for mixtures in the C_9 – C_{18} carbon number range. The design was consequently simplified by omitting the C_{18} mixture component from construction of the design. However, to ensure inclusion of the C_{18} mixture component in the design, the sum of the C_9 – C_{17} mixture components was restricted in the Design-Expert® software to allow for the presence of 0 – 40 mass percent of the C_{18} components. It is therefore important to note that, even though the viscosity and freeze point models do not reflect the presence of the C_{18} mixture components, they were nonetheless included in the design.

7.4.1. Model for viscosity

The final viscosity model obtained from the Design-Expert® software was:

$\hat{y}_1$ = 5.39(n-paraffin) + 4.39(iso-paraffin) + 0.13(n-paraffin x iso-paraffin) -5.69(n-paraffin x C_9) -4.95(n-paraffin x C_{10}) -4.62(n-paraffin x C_{11})
-3.44(n-paraffin x C_{12}) -2.68(n-paraffin x C_{13}) -1.81(n-paraffin x C_{14}) -2.21(n-paraffin x C_{15}) -1.51(n-paraffin x C_{16}) -0.71(n-paraffin x C_{17})
-4.16(iso-paraffin x C_9) -3.98(iso-paraffin x C_{10}) -3.30(iso-paraffin x C_{11}) -2.47(iso-paraffin x C_{12})-1.69(iso-paraffin x C_{13}) -2.12(iso-paraffin x C_{14})
-1.35(iso-paraffin x C_{15})-0.70(iso-paraffin x C_{16}) -0.09(iso-paraffin x C_{17}) +2.34(n-paraffin x iso-paraffin x C_{11}) -3.29(n-paraffin x iso-paraffin x C_{17})

The model had a R^2 value of 0.96, therefore 96% of the variation in the viscosity data was accounted for by the model. The adjusted R^2 value of 0.94 is indicative that the correct variables were included in the model to describe the variability in viscosity. The high adjusted R^2 value also shows that the model did not contain unnecessary parameters (Cornell, 2002). The cross-validated R^2 value indicates that the model was able to accurately predict the viscosity of 84% of mixtures, which were excluded from the model during the LOO validation procedure. All model parameters were at or below the 10% significance level; none of the parameters could thus be excluded from the model.

The kinematic viscosity of jet fuel needs to be reported accurately to ± 0.1 cSt (ASTM D1655-16c, 2016). The standard error of the model was 0.2 cSt, which is wider than the 0.1 cSt reporting value stipulated by ASTM D1655 (2016); however, when considering the complexity of the mixture design, a 0.1 cSt difference between the standard error and the ASTM D1655 reporting value is acceptable. The model was thus considered fit for use.

Figure 7.1 depicts the scatter plot obtained from Design-Expert® with regard to the comparison of the predicted and measured viscosities. The majority of the observations were scattered close to the diagonal line at 45°, which serves as proof that the model can be used to good effect to predict viscosity as a function of the i:n mass ratio and carbon number distribution.

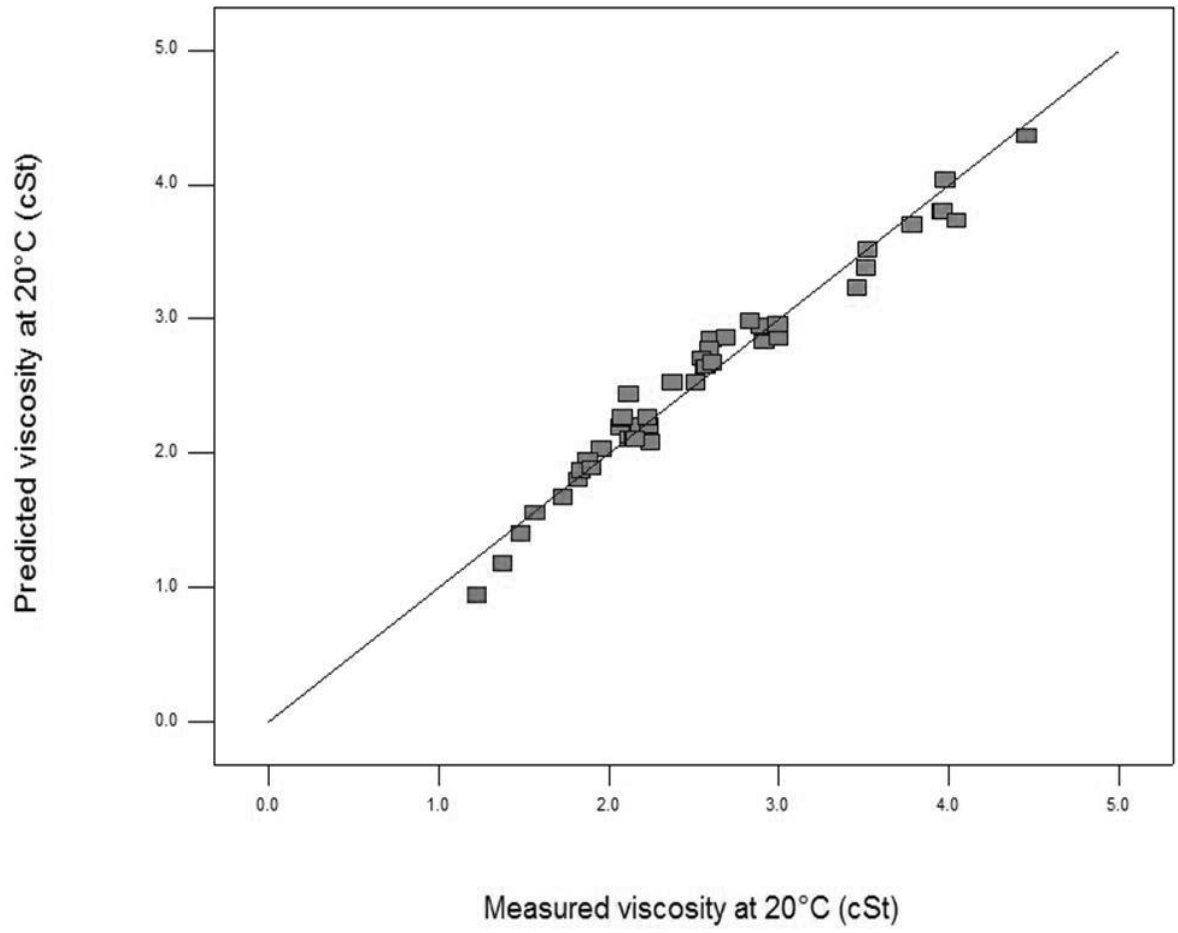

Figure 7.1. Predicted viscosity versus measured viscosity scatter plot.

Predicted contour graphs can be used to interpret the effects of mixture components on model responses, and were generated using the Design-Expert® software. The effect of the i:n mass ratio and carbon number distribution on the viscosity was consequently studied by generating predicted contours as a function of changes in the mixture components. The contour plots of all the mixture components yielded similar results, therefore only the C_{11} and C_{12} mixture components will be discussed. Figure 7.2 and Figure 7.3 depict the predicted contours of viscosity for different compositions of the i:n mass ratio. Figure 7.2 depicts the predicted contours as a function of changing C_{11} and C_{12} components for mixtures with an i:n mass ratio of 84:16. It can be observed that the viscosity increased, as the amounts of C_{11} and C_{12} components in the mixture decreased. Figure 7.3 depicts the predicted contours as a function of changing C_{11} and C_{12} components for mixtures with an i:n mass ratio of 5:95. The viscosity also increased, as the amounts of C_{11} and C_{12} components decreased. When comparing Figure 7.2 and Figure 7.3, it can be observed that mixtures that contained higher concentrations of n-paraffins, exhibited marginally higher viscosities. The graphs are similar in appearance, since the viscosity differences between the n- and iso-paraffin mixture components are marginal in the C_9 – C_{16} carbon number range. Since the C_{17} and C_{18} n-paraffin mixture components were solid at 20℃, their viscosities could not be measured (Chapter 6); however, it is expected that

larger quantities of these components would have a negative impact on the viscosity of jet fuel. The aforementioned indicates that carbon number distribution has a much more significant effect on the viscosity of jet fuel mixtures than does the i:n mass ratio, which corresponds with the observations made and reported in Chapter 6.

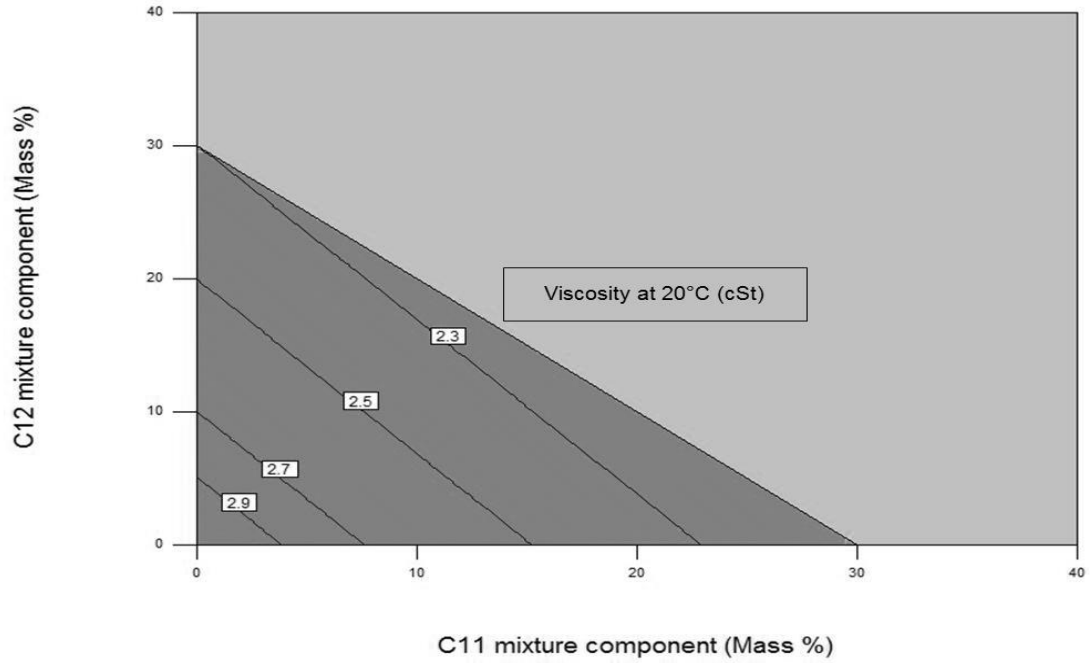

Figure 7.2. Predicted contours as a function of changing C_{11} and C_{12} components with an i:n mass ratio of 84:16.

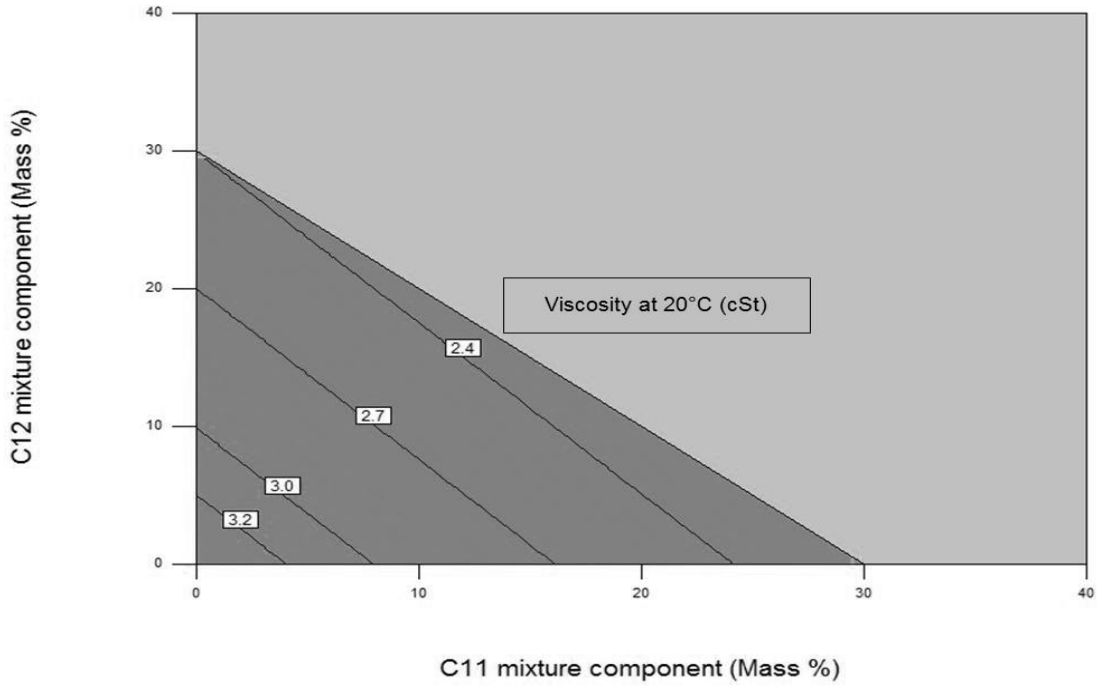

Figure 7.3. Predicted contours as a function of changing C_{11} and C_{12} components with an i:n mass ratio of 5:95.

7.4.2. Model for freeze point

The final freeze point model obtained from Design-Expert® was:

$\hat{y}_2$ = 35.90(n-paraffin) -21.77(iso-paraffin) +66.43(n-paraffin x iso-paraffin) -49.87(n-paraffin x C_9) -45.87(n-paraffin x C_{10}) -53.71(n-paraffin x C_{11})- 53.17(n-paraffin xC_{12}) -51.16(n-paraffin x C_{13}) -46.67(n-paraffin x C_{14}) -32.17(n-paraffin x C_{15}) -13.19(n-paraffin x C_{16}) -6.64(n-paraffin x C_{17}) -42.56(iso-paraffin x C_9) -32.23(iso-paraffin x C_{10}) -55.83(iso-paraffin x C_{11}) -36.71(iso-paraffin x C_{12}) -38.87(iso-paraffin x C_{13}) -23.04(iso-paraffin x C_{14}) -21.43(iso-paraffin x C_{15}) -15.30(iso-paraffin x C_{16}) -7.70(iso-paraffin x C_{17}) -96.40(n-paraffin x iso-paraffin x C_9) -50.69(n-paraffin x iso-paraffin x C_{10}) + 59.44(n-paraffin x iso-paraffin x C_{17})

The model exhibited a R^2 value of 0.99, therefore 99% of the variation in the freeze point data was accounted for by the model. The adjusted R^2 value was 0.98. The adjusted R^2 penalizes the normal R^2 if non-significant parameters are included in the model, which in this case shows that the correct variables were included in the model to explain the variability in freeze point, and that the model did not contain unnecessary parameters. The cross-validated R^2 value moreover indicates that the model accurately predicted 96% of the freeze points for mixtures that were excluded from the model during the LOO validation procedure. All model parameters were at or below the 10% significance level; none of the parameters could thus be excluded from the model.

The freeze point of jet fuel must be reported accurately to ±1.0℃ (ASTM D1655-16c, 2016). The standard error of the model was 2.7℃, which is 1.7℃ wider than the 1.0℃ reporting value stipulated by ASTM D1655 (2016). When considering the complexity of the mixture design, this difference is deemed sufficiently small and the model was thus still considered fit for use.

Figure 7.4 depicts the scatter plot obtained from Design-Expert® for comparison of the predicted and measured freeze points. The majority of the observations were scattered close to the diagonal line. This suggests that the model can therefore be used to predict freeze point as a function of the i:n mass ratio and carbon number distribution.

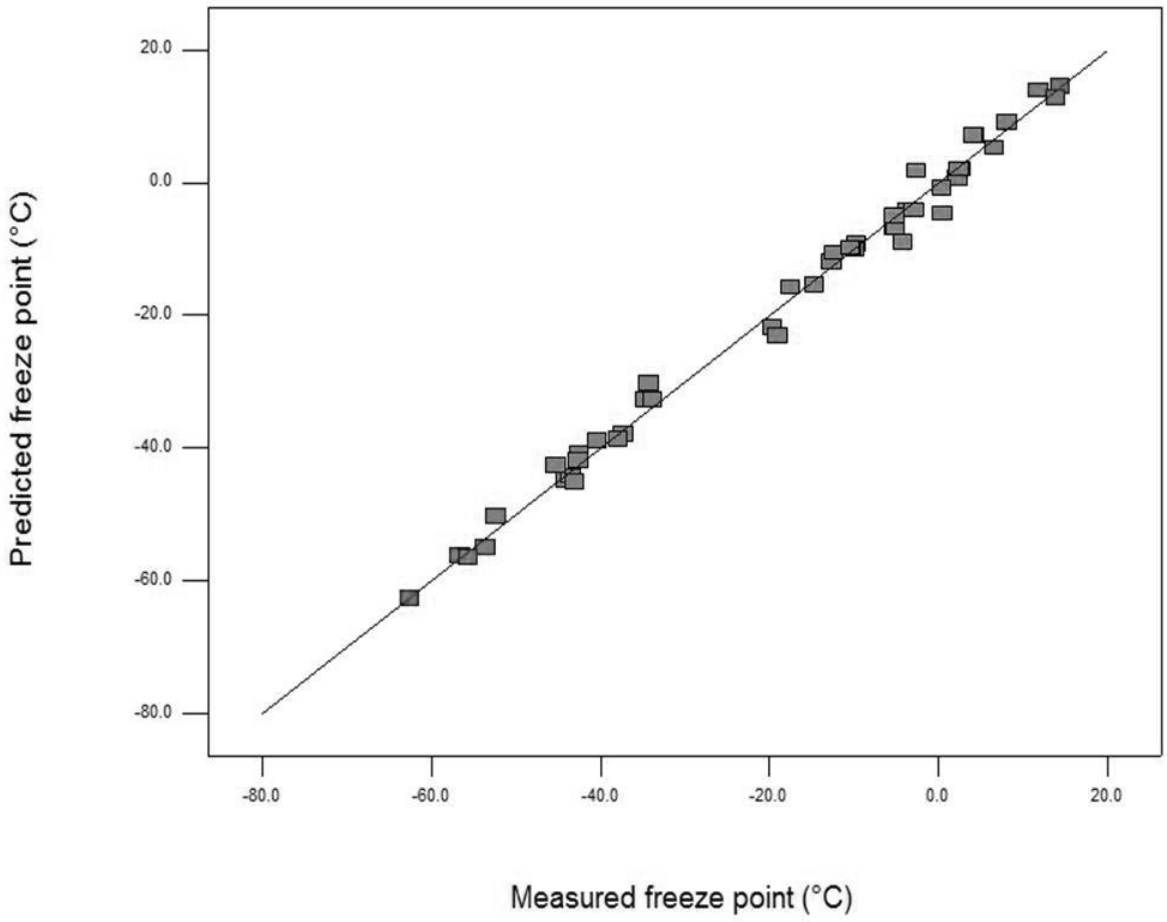

Figure 7.4. Predicted freeze point versus measured freeze point scatter plot.

The effect of the i:n mass ratio and carbon number distribution on freeze point was studied by generating predicted contours as a function of changes in the mixture components. The predicted contour plots of all the mixture components produced similar results, consequently only the C_9 and C_{10} mixture components will be discussed. Figure 7.5 and Figure 7.6 depicts the predicted contours of freeze point for different compositions of the i:n mass ratio. Figure 7.5 depicts the predicted contours as a function of changing C_9 and C_{10} components for mixtures with an i:n mass ratio of 84:16. It can be observed that the freeze point increased significantly

as the amounts of C_9 and C_{10} components in the mixture decreased. Figure 7.6 depicts the predicted contours as a function of changing C_9 and C_{10} components for mixtures with an i:n mass ratio of 5:95. The freeze point also increased significantly as the amounts of C_9 and C_{10} components decreased. Affens et al. (1984) studied the effect of composition on the freeze point of model hydrocarbon fuels. The authors found that, when a high freeze point hydrocarbon was dissolved in a suitable low freeze point solute, and an ideal solution was formed, this ideal solution would possess a freeze point that was equivalent to that of the solute (Affens, et al., 1984). In the context of this study, it is believed that the C_9 and C_{10} mixture components serve as solvents for the longer carbon chain length mixture components, thereby decreasing the freeze point of the mixture, as the relative proportions of the C_9 and C_{10} components increase within the mixture.

When comparing Figure 7.5 and Figure 7.6, it can be observed that mixtures which contained higher concentrations of n-paraffins, exhibited higher freeze points. Therefore, the i:n mass ratio in the jet fuel mixture has a significant effect on the freeze point of the blend. Furthermore, the effect of the carbon number distribution on the freeze point is dependent on the i:n mass ratio of the jet fuel blend. The aforementioned corresponds with the observations made and reported in Chapter 6.

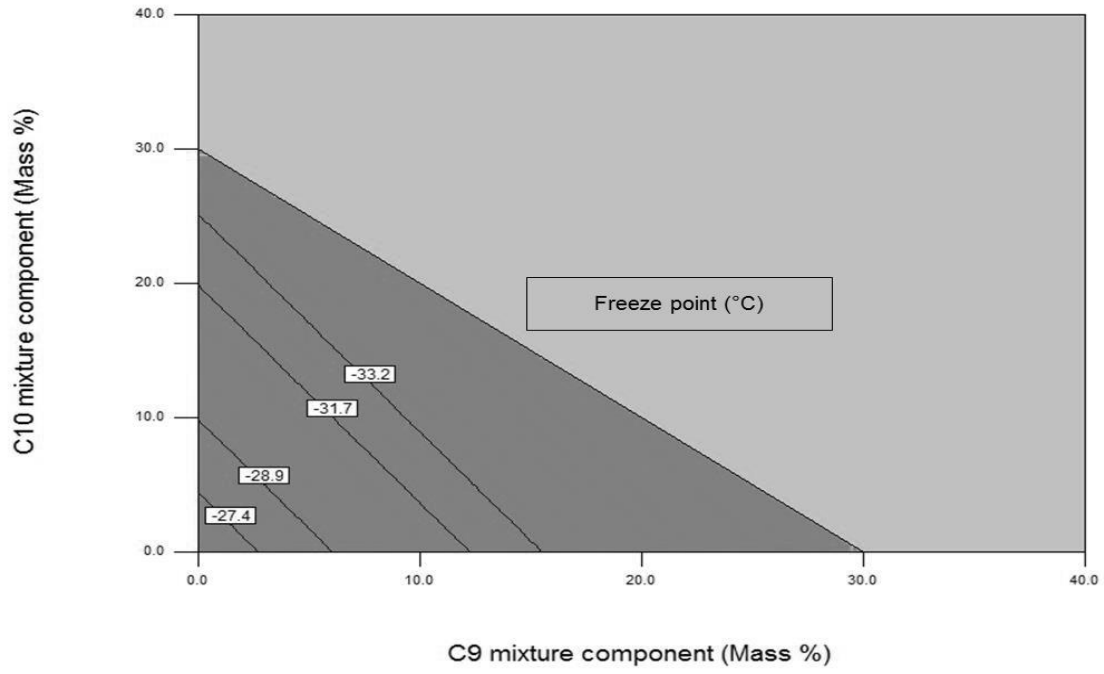

Figure 7.5. Predicted contours as a function of changing C_9 and C_{10} components with an i:n mass ratio of 84:16.

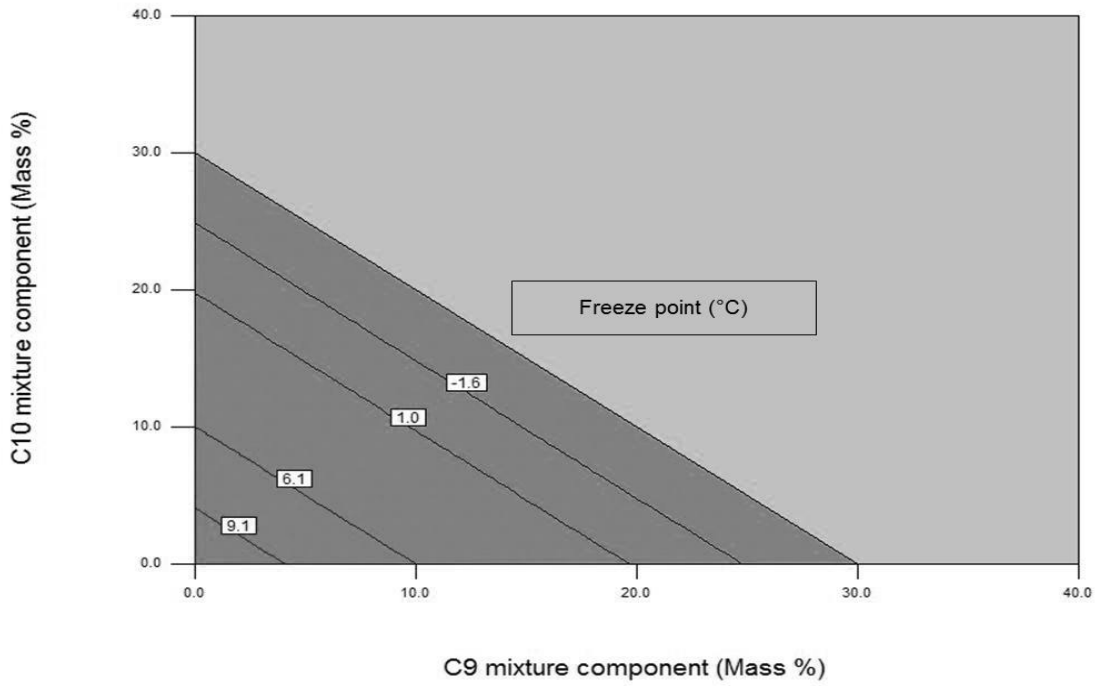

Figure 7.6. Predicted contours as a function of changing C_9 and C_{10} components with an i:n mass ratio of 5:95.

7.5. Model validation

After suitable models have been developed, they need to be validated in order to determine their accuracy. The viscosity and freeze point models were validated according to the procedures described in Chapter 3. The validation results are discussed below.

The freeze point and viscosity results for nine validation mixtures attained from the numerical optimisation function of the Design-Expert® software are shown in Table 7.2. The differences between the predicted and measured viscosities at 20℃ for all mixtures were negligible. The differences between the predicted and measured freeze point results varied significantly. Certain freeze point predictions were fairly accurate, whereas others were decidedly inaccurate, as indicated by the freeze point results of mixtures two and nine. The accuracy of the freeze point prediction results also appeared to decrease significantly when the n-paraffin concentration increased above approximately 5 mass percent.

Table 7.2. Validation results.

Mixture	**1**	**2**	**3**	**4**	**5**	**6**	**7**	**8**	**9**
n-Paraffin mixture component (Mass %)	0	2	2	4	5	5	7	10	11
iso-Paraffin mixture component (Mass %)	100	98	98	96	95	95	93	90	89
C_9 (Mass %)	13.6	20.8	4.5	3.8	4.3	28.6	15.3	6.4	13.2
C_{10} (Mass %)	33.3	20.5	25.0	3.6	20.3	24.4	17.0	4.2	1.4
C_{11} (Mass %)	9.2	6.3	1.2	39.4	5.0	0.7	22.5	27.1	34.0
C_{12} (Mass %)	4.2	2.9	13.1	4.0	35.1	18.2	13.3	2.8	35.4
C_{13} (Mass %)	3.5	7.4	12.3	3.3	6.6	0.0	4.3	39.4	1.0
C_{14} (Mass %)	4.7	12.4	26.3	39.4	8.0	13.0	7.9	2.8	1.0
C_{15} (Mass %)	3.7	16.5	17.7	2.8	20.7	2.3	4.9	3.7	1.4
C_{16} (Mass %)	10.7	2.5	0.0	1.1	0.0	6.1	4.1	9.9	1.2
C_{17} (Mass %)	1.9	2.9	0.0	1.0	0.0	4.9	5.4	1.5	0.9
C_{18} (Mass %)	15.1	7.8	0.0	1.6	0.0	1.7	5.5	2.1	10.4
Measured freeze point (°C)	-52.2	-50.0	-51.9	-51.6	-49.0	-46.3	-36.9	-42.7	-29.7
Measured viscosity at 20°C (cSt)	1.8	1.8	1.9	1.9	1.9	1.5	1.7	2.0	1.7
Desired/predicted freeze point (°C)	-50.0	-50.0	-50.0	-55.0	-50.0	-50.0	-50.0	-50.0	-50.0
Desired/predicted viscosity at 20°C (cSt)	1.8	1.8	1.8	1.8	1.8	1.4	1.7	2.2	1.8

Figure 7.7 depicts the accuracy of the final viscosity model when predicting the viscosities of mixtures that did not form part of the model development process. At first glance it appears as if some of the observations were scattered far from the diagonal line at 45°. However, the scale of the x- and y-axes should be taken into consideration; both axes are scaled from 1.2 to 2.4 cSt, which is quite narrow and might adversely affect deductions made when studying the graph without taking note of this. The observations were in fact scattered close to the diagonal line and all mixtures yielded validation errors that were within the model error of 0.2 cSt. The viscosity model can thus be used with some confidence to predict viscosity as a function of the i:n mass ratio and carbon number distribution.

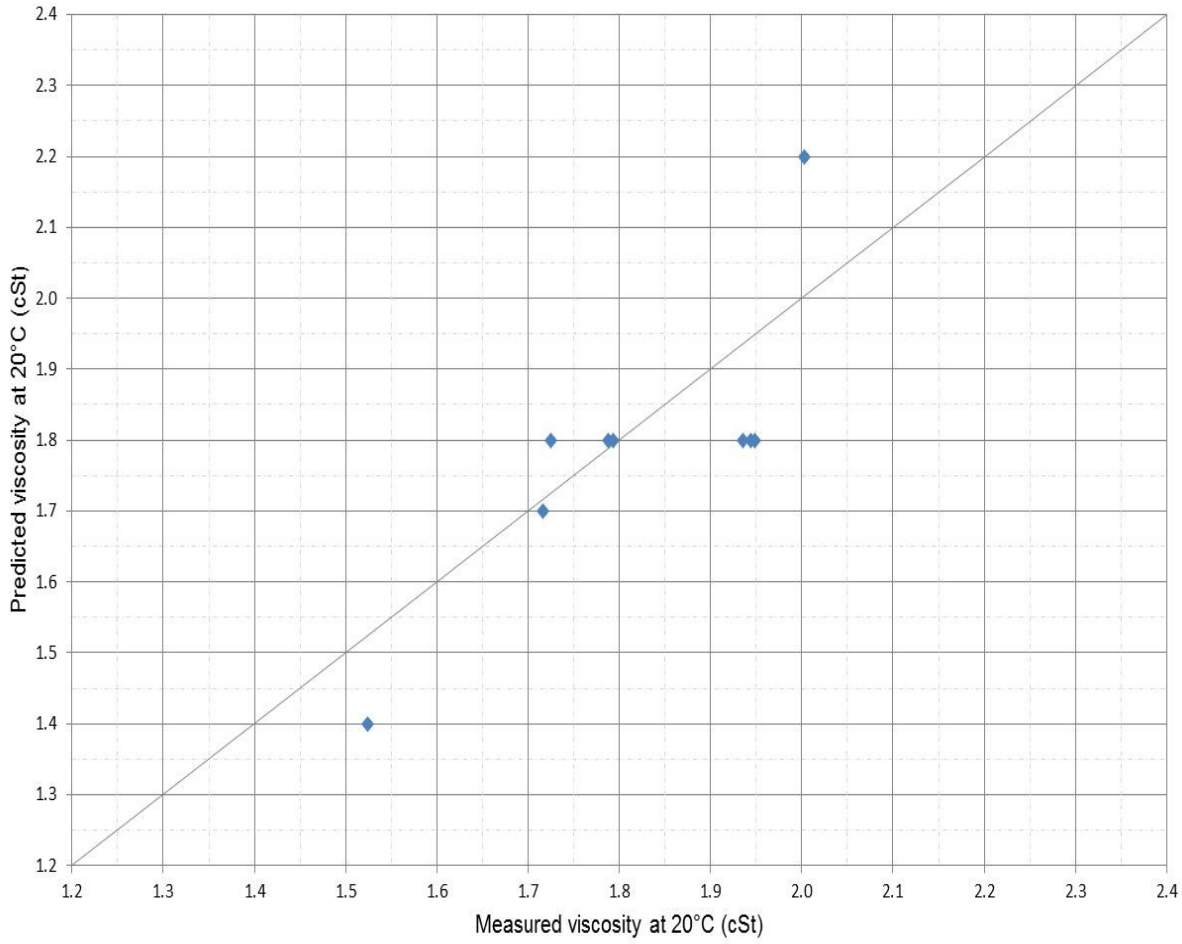

Figure 7.7. Predicted viscosity versus measured viscosity scatter plot for validation mixtures.

Figure 7.8 depicts the accuracy of the freeze point model when predicting the freeze points of mixtures that did not form part of the model development process. The three observations to the right of the x-axis yielded severe validation errors. The most notable outlier was validation mixture nine, which exhibited a measured freeze point of -29.7℃, compared to a predicted freeze point of -50.0℃. Only four validation mixtures yielded validation errors that were within the model error of 2.7℃. The freeze point model thus lacks the accuracy required for freeze point prediction of jet fuels that did not form part of the development process. The model should thus be used with caution.

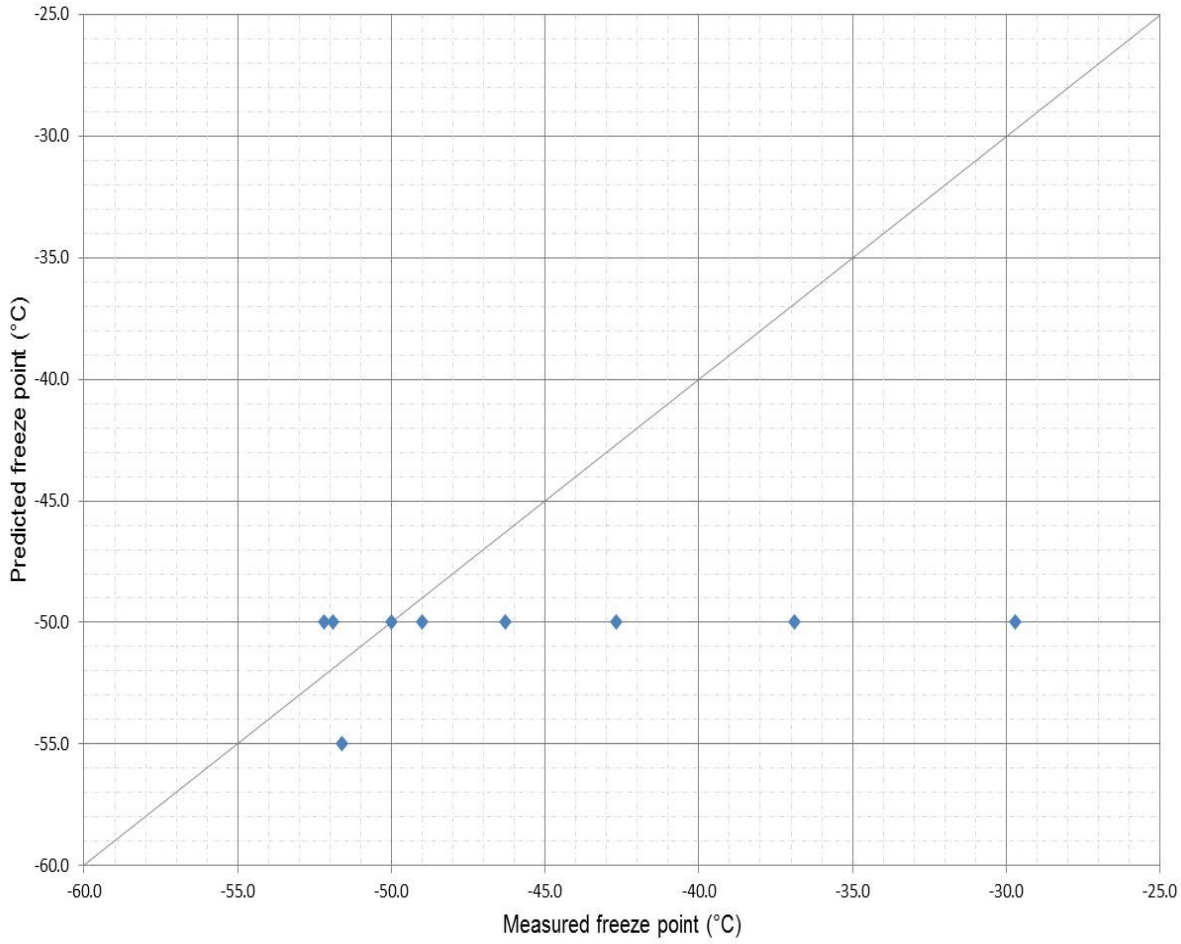

Figure 7.8. Predicted freeze point versus measured freeze point scatter plot for validation mixtures.

Figure 7.9 depicts the graphical comparison of the measured viscosities at 20℃ and -20℃. The validation mixtures only exceeded the proposed ASTM 4.5 cSt viscosity limit at -20℃, once the deduced 1.8 cSt limit at 20℃ was exceeded, thus serving as confirmation that the ASTM D341 conversion was successful.

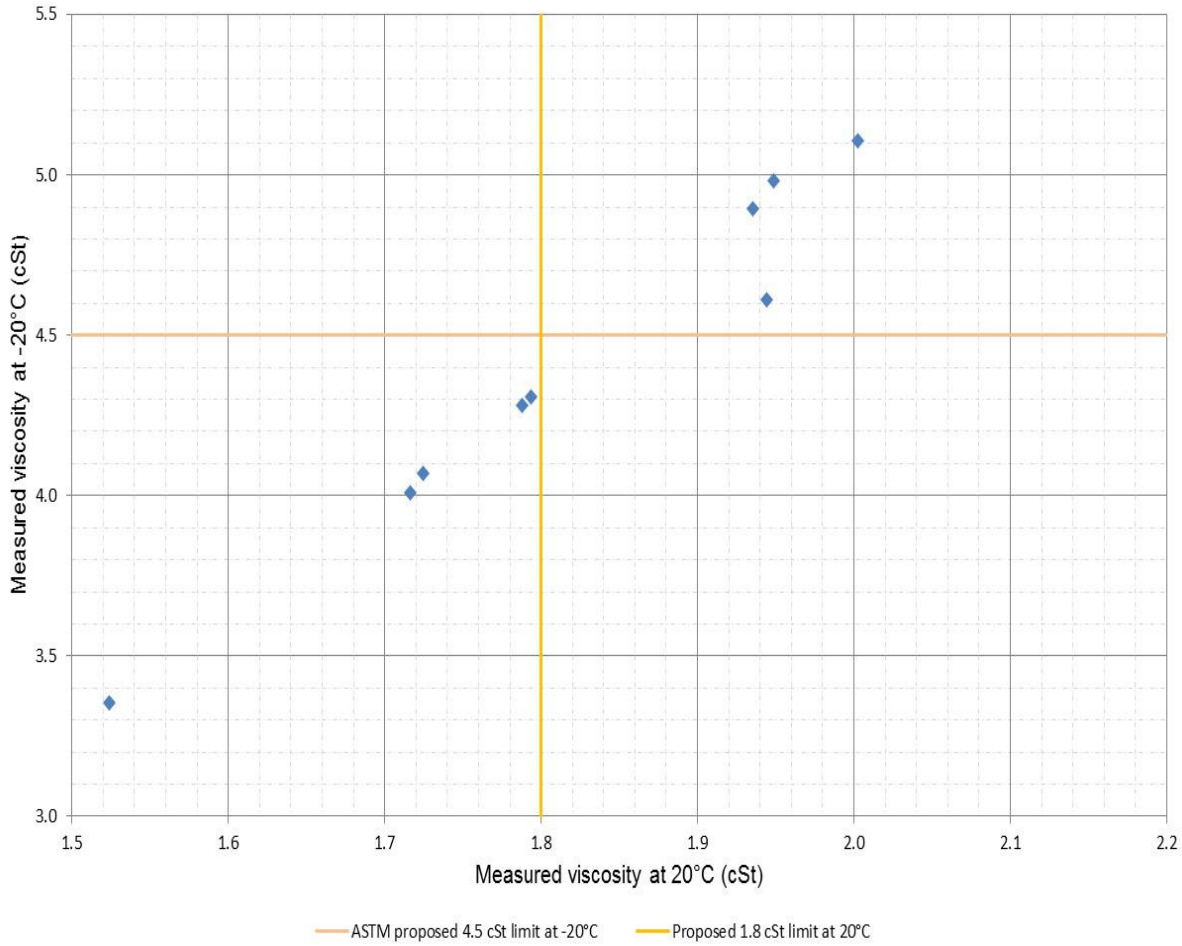

Figure 7.9. Measured viscosity at 20℃ versus viscosity at -20℃ scatter plot for the validation mixtures.

7.6. Ideal jet fuel mixtures

Optimization studies can be conducted to determine optimum jet fuel mixtures that satisfy specific freeze point and viscosity targets of the blend. This is important for recommendations of suitable jet fuel mixtures that adhere to or perform better than the requirements specified by OEMs and governing bodies, such as the ASTM International.

It was acknowledged that the freeze point model is unreliable; however, due to the complexity of the mixture design, development of alternative models was not pursued. The freeze point model was thus used in its current form to conduct optimisation studies. Results of the optimisation studies described in Chapter 3 are discussed below.

7.6.1. Ideal ASTM jet fuel mixture

As a result of the concerns raised by aviation industry OEMs, ASTM International is currently investigating the need for jet fuels to possess viscosities not exceeding 12 cSt as the fuel

approaches the maximum freeze point limit (ASTM D1655-16c, 2016). Annexure X1.6.2 of ASTM D1655-16c (2016) states that jet fuel can exceed the 12 cSt viscosity maximum specified by OEMs, as the fuel approaches the freeze point specification limit (-40℃ for Jet A or -47℃ for Jet A-1), when the viscosity at -20℃ exceeds 5.5 cSt for Jet A or 4.5 cSt for Jet A-1.

As mentioned previously, the validation mixtures presented in Table 7.2 were obtained by means of the numerical optimisation function of the Design-Expert® software. These mixtures can consequently also be used for optimisation studies. The nine mixtures were used to determine a single ideal i:n mass ratio and carbon number distribution for Jet A-1 fuels that would possess viscosities lower than 4.5 cSt at -20℃ and freeze points below -50℃ by calculating the average i:n ratio and carbon number distribution of the nine mixtures. The results of the subsequent mixture that was prepared and analysed are depicted in Table 7.3. The maximum allowable quantity of n-paraffins in the mixture was 5 mass percent. The C_9 – C_{15} mixture components constituted approximately 90 mass percent of the mixture, whilst the C_{16} – C_{18} components were limited to approximately 10 mass percent. Whilst the maximum allowable quantities of C_{16} – C_{18} mixture components may seem insignificant, the presence of these components will make a significant contribution toward increasing jet fuel production volumes. The measured viscosity of the ideal mixture adhered to the deduced maximum viscosity limit of 1.8 cSt at 20℃, as well as to the ASTM proposed maximum of 4.5 cSt at -20℃. The measured freeze point of the mixture did not meet the specified -50℃ target; however, it still adhered to the maximum ASTM freeze point limit of -47℃ maximum.

Table 7.3. Ideal ASTM jet fuel mixture results.

n-Paraffin mixture component (Mass %)	5
iso-Paraffin mixture component (Mass %)	95
C_9 (Mass %)	12.3
C_{10} (Mass %)	16.6
C_{11} (Mass %)	16.1
C_{12} (Mass %)	14.3
C_{13} (Mass %)	8.7
C_{14} (Mass %)	12.8
C_{15} (Mass %)	8.2
C_{16} (Mass %)	3.9
C_{17} (Mass %)	2.1
C_{18} (Mass %)	4.9
Measured freeze point (℃)	-47.1
Measured viscosity at 20℃ (cSt)	1.8
Measured viscosity at -20℃ (cSt)	4.3

7.6.2. Ideal jet fuel mixture for minimum viscosity and freeze point

This research was conducted to prove or disprove the following hypothesis:

> *There exists an ideal i:n ratio and an ideal carbon number distribution that enables the production of jet fuel, which possesses the best low temperature fluidity properties attainable.*

Since the hypothesis of the study had to be proved or disproved, the numerical optimisation function of Design-Expert® was used to produce 10 theoretical blends that minimised both freeze point and viscosity, as predicted by their respective models. The freeze point and viscosity results for the 10 optimised mixtures acquired from the software are presented in Table 7.4. All mixtures specified a freeze point below -62°C and viscosity lower than 1.2 cSt at 20°C. The i:n mass ratio of the mixtures was maximized, whilst the C_9 and C_{11} mixture components ranged between 22 and 32 and between 27 and 40 mass percent respectively.

Table 7.4. Optimum blends for minimised freeze point and viscosity.

Mixture	**1**	**2**	**3**	**4**	**5**	**6**	**7**	**8**	**9**	**10**
n-Paraffin mixture component (Mass %)	0	0	0	0	0	0	0	0	0	0
iso-Paraffin mixture component (Mass %)	100	100	100	100	100	100	100	100	100	100
C_9 (Mass %)	30.0	22.0	22.0	30.0	24.0	5.0	32.0	31.0	30.0	32.0
C_{10} (Mass %)	2.0	20.0	15.0	4.0	24.0	33.0	10.0	6.0	16.0	12.0
C_{11} (Mass %)	32.0	34.0	30.0	32.0	30.0	40.0	35.0	27.0	27.0	33.0
C_{12} (Mass %)	33.0	10.0	9.0	21.0	2.0	2.0	2.0	26.0	0.0	3.0
C_{13} (Mass %)	1.0	5.0	6.0	2.0	10.0	5.0	1.0	1.0	13.0	9.0
C_{14} (Mass %)	0.0	2.0	9.0	4.0	0.0	7.0	1.0	1.0	0.0	0.0
C_{15} (Mass %)	1.0	2.0	8.0	0.0	2.0	2.0	13.0	5.0	13.0	1.0
C_{16} (Mass %)	1.0	2.0	0.0	2.0	6.0	2.0	6.0	3.0	1.0	7.0
C_{17} (Mass %)	0.0	1.0	0.0	4.0	0.0	3.0	0.0	1.0	0.0	1.0
C_{18} (Mass %)	0.0	2.0	1.0	1.0	2.0	1.0	0.0	-1.0	0.0	2.0
Predicted freeze point (°C)	-65.9	-63.9	-62.5	-64.1	-62.8	-62.6	-63.0	-62.8	-62.6	-63.5
Predicted viscosity at 20°C (cSt)	1.1	1.1	1.2	1.2	1.1	1.2	1.2	1.2	1.2	1.2

The 10 mixtures in Table 7.4 were used to determine a single ideal i:n mass ratio and carbon number distribution for jet fuels that possess viscosities lower than 1.2 cSt at 20°C and freeze points below -62°C by calculating the average i:n mass ratio and carbon number distribution of the 10 mixtures. The results of the subsequent mixture as prepared and analysed can be viewed in Table 7.5. The mixture contained only iso-paraffin mixture components in order to adhere to the minimum viscosity and freeze point requirements. The $C_9 – C_{15}$ mixture components constituted 95 mass percent of the mixture, whilst the $C_{16} – C_{18}$ components were limited to 5 mass percent. The measured viscosity was within the standard error of the viscosity model; however, the measured freeze point was 15.7°C lower than the average of the predicted freeze point values of the 10 theoretical mixtures. It is believed that the extremely low freeze point of -79.1°C can be attributed to the large quantities of C_9 and C_{11} components present in

the mixture, since the freeze point of the iso-C_9 component was so low that it could not be measured with the available analytical equipment, and that of the iso-C_{11} component was -66.9℃.

Table 7.5. Ideal i:n jet fuel mixture for minimising freeze point and viscosity.

n-Paraffin mixture component (Mass %)	0
iso-Paraffin mixture component (Mass %)	100
C_9 (Mass %)	25.8
C_{10} (Mass %)	14.2
C_{11} (Mass %)	32.0
C_{12} (Mass %)	10.8
C_{13} (Mass %)	5.3
C_{14} (Mass %)	2.4
C_{15} (Mass %)	4.7
C_{16} (Mass %)	3.0
C_{17} (Mass %)	1.0
C_{18} (Mass %)	0.8
Measured freeze point (℃)	-79.1
Measured viscosity at 20℃ (cSt)	1.3
Measured viscosity at -20℃ (cSt)	2.9

Figure 7.10 serves as graphical comparison of the compositions for the ideal jet fuel mixtures discussed in Sections 7.6.1 and 7.6.2. The ideal jet fuel mixture for minimising freeze point and viscosity (the red line on the graph) contained larger quantities of C_9 and C_{11} mixture components than the ideal ASTM jet fuel mixture (the blue line on the graph). The ideal jet fuel mixture for minimising freeze point and viscosity thus contained reduced amounts of the C_{10} and C_{12} – C_{18} mixture components than the ideal ASTM jet fuel mixture. Both mixtures contained larger quantities of shorter carbon chain length components in order to meet the freeze point requirements of the respective blends. The ideal ASTM jet fuel mixture was able to accommodate larger quantities of longer carbon chain length components due to the less stringent viscosity and freeze points requirements of the mixture. The i:n mass ratio of the ideal jet fuel mixture for minimising freeze point and viscosity was 100:0 and that of the ideal ASTM jet fuel mixture was 95:5.

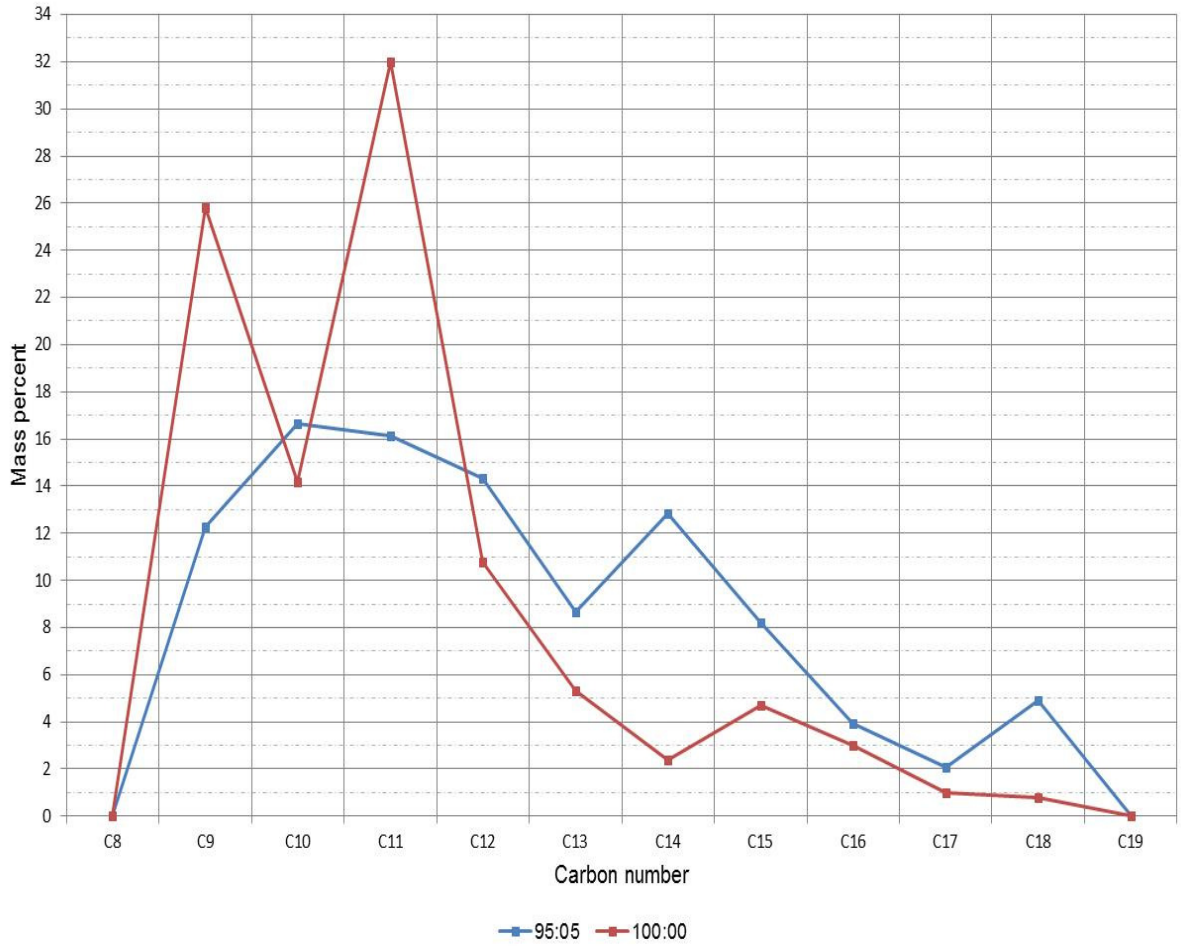

Figure 7.10. Compositional comparison of ideal jet fuels.

7.6.3. Ideal jet fuel mixture for best low temperature fluidity properties attainable

Jet fuel mixtures that possess the best low temperature fluidity properties attainable should thus be a combination of the ideal ASTM and the ideal minimum viscosity and freeze point jet fuel mixtures presented in Table 7.3 and Table 7.5. There is consequently no single ideal i:n mass ratio and carbon number distribution, but rather a range for each of the aforementioned characteristics. The ideal i:n mass ratio and carbon number distribution ranges are depicted in Table 7.6. Selection of the most suitable i:n mass ratio and carbon number distribution for jet fuel production would thus be dictated by the desired freeze point and viscosity properties of the mixture. Mixtures possessing higher viscosities and freeze points will contain larger quantities of n-paraffins and C_{12} – C_{18} mixture components, along with lower quantities of C_9 – C_{11} components. Mixtures possessing lower viscosities and freeze points will contain lesser amounts of n-paraffins and C_{12} – C_{18} mixture components, along with larger quantities of C_9 – C_{11} components. Due to factors such as production constraints and increased capital expenditure, it is unlikely that petroleum refiners will produce jet fuels that possess viscosities and freeze points that are significantly lower than the maximum limits prescribed by governing bodies.

Table 7.6. Ideal i:n mass ratio and carbon number distribution for optimum jet fuel blends.

n-Paraffin mixture component (Mass %)	0 - 5
iso-Paraffin mixture component (Mass %)	95 - 100
C_9 (Mass %)	12 - 26
C_{10} (Mass %)	14 -17
C_{11} (Mass %)	16 - 32
C_{12} (Mass %)	11 - 14
C_{13} (Mass %)	5 - 9
C_{14} (Mass %)	2 - 13
C_{15} (Mass %)	5 - 8
C_{16} (Mass %)	3 - 4
C_{17} (Mass %)	1 - 2
C_{18} (Mass %)	0 - 5
Freeze point (°C)	-79.1 to -47.1
Viscosity at 20°C (cSt)	1.3 – 1.8
Viscosity at -20°C (cSt)	2.9 – 4.3

7.7. Conclusion

The regression statistics and validation results of the viscosity model were very good. The model was able to predict the viscosities of jet fuels in the C_9 - C_{18} carbon number range with high accuracy. The model can thus be used in practice to predict viscosity as a function of the i:n mass ratio and carbon number distribution for jet fuels in the C_9 – C_{18} carbon number range. Furthermore, it was found that carbon number distribution has a much more significant effect on the viscosity of jet fuel mixtures than did variation in the i:n mass ratio. Even though the model was constructed by using viscosity measurements at 20°C, it was possible to produce jet fuels adhering to the proposed ASTM International viscosity limit of 4.5 cSt at -20°C, thereby demonstrating that the ASTM D341 conversion performed during construction of the model was successful.

The regression statistics for the freeze point model were good when considering the complexity of the mixture design. It was found that carbon number distribution and i:n mass ratio have a significant effect on the freeze points of jet fuel mixtures. However, validation of the model produced unsatisfactory results. Maddox (2012) found that as little as 0.5 – 1.0% of precipitated wax might be sufficient to cause gelation of fuel, which leads to the conclusion that freeze point cannot be fully be described by only the bulk properties of the fuel. Freeze point is intrinsically a crystallisation phenomenon, in which the random presence of trace amounts of molecules and "seeding" nuclei may play an important role. It is thus concluded that the model could not fully account for the effect of the crystal formation characteristics of mixture components on the accuracy of freeze point predictions. The inability of the model to account for crystal formation tendencies agrees with the conclusions drawn in Chapter 5. It is further concluded that the freeze point model is unreliable and should be used with caution.

This research was conducted to prove or disprove the following hypothesis:

> *There exists an ideal i:n ratio and an ideal carbon number distribution that enables the production of jet fuel, which possesses the best low temperature fluidity properties attainable.*

Although the freeze point model could not fully account for the crystal formation of mixture components, it was possible to determine ideal i:n mass ratio and carbon number distribution ranges that would enable the production of jet fuel, which possesses the best low temperature fluidity properties attainable. Therefore it is proposed that the results that have been generated and discussed in this study have indeed provided proof that the hypothesis is true.

However, it must be noted that, if the freeze point model had been able to account fully for the crystal formation characteristics of mixture components, the ideal i:n mass ratio and carbon number distribution ranges might have differed from those currently prescribed. Furthermore, i:n mass ratio and carbon number distribution cannot be treated as two separate entities. Altering either of these compositional parameters would affect the remaining parameter. In order to adhere to the freeze point specification maximum, the carbon number distribution of jet fuel mixtures would have to be decreased, and the relative proportions C_9 – C_{11} components increased, as the n-paraffin content of the mixtures increased.

This study considered only the low temperature fluidity properties of jet fuel and disregarded other physical properties, which are also critical for the correct functioning of turbine engines. If physical properties, such as flash point, density and D86 boiling point distribution had been considered, the ideal i:n mass ratio and carbon number distribution ranges specified might also have differed from the ones currently prescribed. Furthermore, ASTM D7566 (2015) stipulates that jet fuels containing synthesised hydrocarbons must contain at least 8% aromatic compounds; if this minimum specification was taken into consideration, the i:n mass ratio and carbon number distribution ranges specified might also have differed from the ones currently recommended.

Development of accurate freeze point prediction models will remain perplexing until molecular descriptors adequately describing crystal formation of the molecules present in jet fuel can be established.

Chapter 8 : Conclusions and Recommendations

8.1. Introduction

The purpose of this study was to vary both the i:n mass ratio and the carbon number distribution of synthetic jet fuel components in the C_9 - C_{18} carbon number range in such a manner as to obtain a fuel that would meet the freeze point requirements of Jet A-1, whilst maintaining a viscosity profile that was not readily susceptible to changes in temperature, as discussed in ASTM D1655-16c.

The research was conducted to prove or disprove the following hypothesis:

> *There exists an ideal i:n ratio and an ideal carbon number distribution that enables the production of jet fuel, which possesses the best low temperature fluidity properties attainable.*

This chapter serves to conclude the dissertation and thus summarises the conclusions drawn from the study. Furthermore, recommendations for future studies are also included.

8.2. QSAR models for viscosity and freeze point prediction

QSAR models for kinematic viscosity and freeze point prediction of n- and iso-paraffins in the C_4 – C_{20} carbon number range were developed, using literature values as references.

8.2.1. Viscosity prediction model

The final three-descriptor viscosity prediction model obtained was:

> $\hat{y}$*= 0.2661 -0.0147(Molecular area (vd Waals)) + 0.0207(Molecular volume (vd Waals)) + 0.0003(Principal moment of inertia Y)*

Validation plays a significant role during model development, since it allows for verification of the validity of the molecular descriptors included in the model. Validation procedures also highlight flaws that may have not been apparent during the development phase of the model.

The final viscosity model achieved the highest viscosity prediction accuracy for all the molecules considered in the dataset. Nonetheless, even though the viscosity model produced good regression statistics, it was deduced that there might be alternative molecular descriptors that more accurately describe the viscosity behaviour. The aforementioned indicates that a multitude of viscosity prediction models could exist due to the wide variety of molecular descriptors available for use during model development.

Even though some validation irregularities were discovered, it was concluded that QSAR techniques could successfully be employed to predict the kinematic viscosity of n- and iso-paraffins in the C_4 – C_{20} carbon number range.

8.2.2. Freeze point prediction model

The final five-descriptor model obtained for freeze point prediction was:

$$\hat{y} = -659.278 + 18.911(\text{Zagreb index}) + 868.771(\text{Molecular density}) + 44.612(\text{Molecular flexibility index}) - 7.711(\text{Total molecular mass}) - 0.058(\text{Wiener index})$$

The final model yielded high R^2 values, however, the standard error associated with the model was also high, which is indicative of the model's low precision. The model accurately predicted the freeze points of longer carbon chain n-paraffins, which formed part of the dataset used for development of the model. However, freeze point prediction of shorter carbon chain n- and iso-paraffins proved unsuccessful. Validation of the model also failed, since the freeze point predictions for molecules with unknown freeze point values were inaccurate. The final freeze point model was thus unable to accurately predict the freeze points of structurally diverse paraffinic molecules in the C_4 – C_{20} carbon number range. The inadequate performance of the freeze point model was attributed to the inability of the model to account for the crystal formation characteristics of the target molecules, especially in terms of the strength of the crystal lattice and polymorphism.

The information gathered during the QSAR studies indicate that the molecular properties that give rise to the viscosity and freeze point behaviour of n- and iso-paraffins are exceptionally complex. When considering the results obtained from the freeze point prediction model, it is evident that much more work needs to be done to understand these relationships fully.

8.3. Fractional distillation

Before the mixture design study could commence, n- and iso-paraffin mixture components in the C_9 – C_{18} carbon number range had to be produced by means of fractional distillation.

The final boiling points of the mixture components were dominated by the boiling points of the n-paraffins present in the mixtures. However, as the concentration of the iso-paraffins within the mixtures increased, the final boiling points of the mixture components decreased. The aforementioned corresponds with the boiling point trends observed during the literature study, and indicates that molecular structure plays an important role in determining the boiling points of organic molecules. Furthermore, the various n- and iso-paraffin mixture components contained

undesired molecules; however, these undesired molecules were unavoidable due to the composition of the refinery products fractionated.

The viscosities of the n- and iso-paraffin mixture components increased with an increase in carbon chain length, as expected. The viscosities of the n-paraffin mixture components were only marginally higher than those of the iso-paraffin mixture components per carbon number. The marginal viscosity differences observed during comparison of the n- and iso-paraffin mixture components indicate that carbon chain length has a more significant effect on the viscosities of jet fuel mixtures than i:n mass ratio.

As expected, the freeze points of the n- and iso-paraffin mixture components increased with an increase in carbon chain length; however, the freeze point results of the iso-paraffin components did not follow a smooth trend. The analytical data available could not account for the irregularities observed. It was further found that the freeze points of the iso-paraffin mixture components were significantly lower than those of their n-paraffin counterparts. The aforementioned shows that both carbon chain length and i:n mass ratio have a significant effect on the freeze points of jet fuel mixtures. It can thus be deduced that molecular structure plays an important role in determining the freeze point characteristics of organic molecules.

Even though it was acknowledged that the respective n- and iso-paraffin mixture components were not pure, it was concluded that these components were nonetheless suitable for use during construction of extended carbon number distribution jet fuels by application of statistical mixture design techniques.

8.4. n-Paraffin and iso-paraffin mixture design

Following the successful production of n- and iso-paraffin mixture components in the $C_9 – C_{18}$ carbon number range, the Design-Expert® software was used to develop predictive models to study the effects of variation in i:n mass ratio and carbon number distribution on the viscosity and freeze point properties of synthetic jet fuel.

8.4.1. Viscosity model

The final model obtained for viscosity was:

$\hat{y}_1$ = 5.39(n-paraffin) + 4.39(iso-paraffin) + 0.13(n-paraffin x iso-paraffin) -5.69(n-paraffin x C_9) -4.95(n-paraffin x C_{10}) -4.62(n-paraffin x C_{11})
-3.44(n-paraffin x C_{12}) -2.68(n-paraffin x C_{13}) -1.81(n-paraffin x C_{14}) -2.21(n-paraffin x C_{15}) -1.51(n-paraffin x C_{16}) -0.71(n-paraffin x C_{17})
-4.16(iso-paraffin x C_9) -3.98(iso-paraffin x C_{10}) -3.30(iso-paraffin x C_{11}) -2.47(iso-paraffin

x C_{12})-1.69(iso-paraffin x C_{13}) -2.12(iso-paraffin x C_{14})
-1.35(iso-paraffin x C_{15})-0.70(iso-paraffin x C_{16}) -0.09(iso-paraffin x C_{17}) +2.34(n-paraffin x iso-paraffin x C_{11}) -3.29(n-paraffin x iso-paraffin x C_{17})

The final viscosity model exhibited high R^2, adjusted R^2 and cross-validated R^2 values. The standard error of the model was wider than the accuracy reporting value of the ASTM International (ASTM D1655-16c, 2016); however, due to the complexity of the mixture design, this viscosity difference was acceptable. Even though the standard error was wider than the ASTM reporting value, the model was able to predict the viscosities of jet fuel mixtures in the C_9 - C_{18} carbon number range with good accuracy. It was consequently concluded that the model could be used to predict viscosity as a function of the i:n mass ratio and carbon number distribution for jet fuels in the C_9 – C_{18} carbon number range. Furthermore, it was determined that the viscosities of jet fuel mixtures are primarily influenced by carbon number distribution, which confirms the conclusions drawn during the discussion of the fractionation results. The aforementioned indicates that carbon number distribution is a critical aspect to consider during jet fuel production.

8.4.2. Freeze point model

The final model obtained for freeze point was:

$\hat{y}_2$ = 35.90(n-paraffin) -21.77(iso-paraffin) +66.43(n-paraffin x iso-paraffin) -49.87(n-paraffin x C_9) -45.87(n-paraffin x C_{10}) -53.71(n-paraffin x C_{11})- 53.17(n-paraffin xC_{12}) -51.16(n-paraffin x C_{13}) -46.67(n-paraffin x C_{14}) -32.17(n-paraffin x C_{15}) -13.19(n-paraffin x C_{16}) -6.64(n-paraffin x C_{17}) -42.56(iso-paraffin x C_9) -32.23(iso-paraffin x C_{10}) -55.83(iso-paraffin x C_{11}) -36.71(iso-paraffin x C_{12}) -38.87(iso-paraffin x C_{13}) -23.04(iso-paraffin x C_{14}) -21.43(iso-paraffin x C_{15}) -15.30(iso-paraffin x C_{16}) -7.70(iso-paraffin x C_{17}) -96.40(n-paraffin x iso-paraffin x C_9) -50.69(n-paraffin x iso-paraffin x C_{10}) + 59.44(n-paraffin x iso-paraffin x C_{17})

The final freeze point model also exhibited high R^2, adjusted R^2 and cross-validated R^2 values. Despite the good regression statistics obtained, validation of the model produced unsatisfactory results. According to Maddox (2012), minute quantities of precipitated wax can cause gelation of fuel. Freeze point is thus a function of the crystallisation characteristics of individual molecules, rather than the bulk properties of the fuel. The presence of trace amounts of molecules and “seeding” nuclei may therefore play an important role in the freeze point behaviour of jet fuel mixtures. It was further determined that the model could not fully account for the crystal formation characteristics of individual n- and iso-paraffin mixture components,

thereby producing inaccurate freeze point predictions. The aforementioned corresponds with the findings made concerning the QSAR freeze point prediction model.

Furthermore, carbon number distribution and i:n mass ratio have a significant effect on the freeze points of jet fuel mixtures and are closely related. In order to adhere to the freeze point specification maximum, the carbon number distribution of jet fuel mixtures would have to be decreased and the relative proportions of shorter carbon chain length components increased, as the iso-paraffin content within the mixtures decreased.

8.4.3. Optimisation studies

Even though the freeze point model was unreliable, it was possible to determine ideal i:n mass ratio and carbon number distribution ranges that would enable the production of jet fuel, which possesses the best low temperature fluidity properties attainable. It was consequently concluded that the hypothesis was true. However, if the freeze point model had been able to account fully for the crystal formation characteristics of mixture components, alternative ideal i:n mass ratio and carbon number distribution ranges might have been established. Furthermore, if other critical jet fuel properties had been taken into consideration, this study might also have produced alternative ideal i:n mass ratio and carbon number distribution ranges.

Development of accurate freeze point prediction models will remain challenging until molecular descriptors adequately describing crystal formation tendencies of the molecules present in jet fuel can be established.

When considering the information gathered during the course of this study, the words of James Ashenhurst come to mind; he boldly stated "*…further proof, as if more was needed, that predicting melting/boiling points from chemical structures can be a fool's errand.*" (Ashenhurst, 2010).

8.5. Recommendations for future studies

8.5.1. QSAR models for viscosity prediction

Based on the outcome of the efforts to construct a viscosity model using QSAR, it was recommended to investigate the possibility of developing separate viscosity prediction models for molecules in the 0.0 to 1.0 cSt and 1.1 to 5.4 cSt viscosity ranges. It is envisaged that this could lead to better accuracy of prediction.

8.5.2. Fractional distillation results: iso-Paraffin freeze points

It was recommended that ^{1}H and ^{13}C NMR spectroscopy analyses should be conducted on the iso-paraffin mixture components in order to determine whether the molecular structure (specifically the branching attributes) of these components could account for the freeze point phenomenon observed.

Bibliography

Affens, W. A., Hall, J. M., Holt, S. & Hazlett, R. N., 1984. Effect of composition on freezing points of model hydrocarbon fuels. *Elsevier,* 63(4), pp. 543-547.

Agee, M. A., n.d. *Economic conversion of natural gas to synthetic petroleum liquids.* [Online] Available at: https://web.anl.gov/PCS/acsfuel/preprint%20archive/Files/42_2_SAN%20FRANCISCO_04-97_0672.pdf
[Accessed 10 February 2016].

Andrews, A. & Logan, J., 2008. *Fischer-Tropsch fuels from coal, natural gas and biomass: Background and policy,* Washington: Congressional Research Service.

Ashenhurst, J., 2010. *Molecular Tetris.* [Online]
Available at: http://www.masterorganicchemistry.com/2010/07/09/chemical-tetris/
[Accessed 10th August 2017].

ASTM D1655-16c, 2016. *Standard specification for aviation turbine fuels,* Pennsylvania: ASTM.

ASTM D341-09, 2009. *Standard practice for viscosity-temperature charts for liquid petroleum products.* Pennsylvania: ASTM.

ASTM D5972-16, 2016. *Standard Test Method for freezing point of aviation fuels (Automatic phase transition method),* Pennsylvania: ASTM.

ASTM D7042-14, 2014. *Standard test method for dynamic viscosity and density of liquids by Stabinger viscometer (and the calculation of kinematic viscosity).* Pennsylvania: ASTM.

ASTM D7566-15c, 2015. *Standard specification for aviation turbine fuel containing synthesised hydrocarbons.* Pennsylvania: ASTM.

ASTM DS 4B, 1991. *Physical constants of hydrocarbons and non-hydrocarbon compounds.* Pennsylvania: ASTM.

Blakey, S., Wilson, C. W., Midgley, R. & Farmery, M., 2011. Fuel effects on range versus payload for modern jet aircraft. *The Aeronautical journal,* 115(1171), p. 3622.

Boeing, 2017. *History: DC-3 Commercial transport.* [Online]
Available at: http://www.boeing.com/history/products/dc-3.page
[Accessed 21st August 2017].

Bondari, K., 2005. *Mixture Experiments and Their applications in Agricultural Research.* Philadelphia, SAS Institute Inc..

Born, M. & Wolf, E., 1999. *Principles of Optics: Electromagnetic Theory of Propagation, Interference and Diffraction of Light.* 7th ed. Cambridge: Cambridge University Press.

Brittz, R., 2012. *Impact of refinery processing configurations on acheiving the required cold flow properties for jet fuels.* Potchefstroom: NWU (Dissertation).

Brown, J. D., 2011. Confidence intervals, limits, and levels. *SIG Newsletter,* 15(2), pp. 23-27.

Brown, T. L., LeMay, E. & Bursten, B. E., 2006. *Chemistry, the central science.* 10th ed. New Jersey: Pearson Education, Inc.

Burch, K. J. & Whitehead, E. G., 2004. Melting-Point Models of Alkanes. *Journal of Chemical and Engineering Data,* Volume 49, pp. 858-863.

Carhart, H. W., Pinkel, I. & Warren, J. H., 1976. Aircraft kerosine vs. wide-cut fuel: Safety considerations. *SAE [Technical Papers],* Volume 760527, p. 17.

Charton, M. & Charton, B., 1994. Quantitative description of structural effects on melting points of substituted alkanes. *Journal of Physical Organic Chemistry,* 7(4), pp. 196-206.

Chevron Corporation, 2006a. *Aviation fuels technical review.* San Ramon: Chevron Corporation.

Chevron Corporation, 2006b. *Alternative jet fuels.* San Ramon: Chevron Corporation.

Chevron Corporation, 2007. *Diesel fuels technical review.* San Ramon: Chevron Corporation.

Coetzer, R. L. J., Rossouw, R. F. & Lin, D. K. J., 2008. Dual response surface optimisation with hard-to-control variables for sustainable gasifier performance.. *Journal of the Royal Statistical Society-Series C Applied Statistics,* 57(5), pp. 587-657.

Colwell, R. F., 2009. *Oil Refinery Processes: A Brief Overview.* Oak Ridge, TN: Process Engineering Associates, LLC.

Coordinating Research Council, 2010. *Develop an aviation fuel cold flow flowability test to replace freezing point measurement,* Alpharetta: CRC.

Cornell, J. A., 2002. *Experiments with Mixtures: Designs, Models, and the Analysis of Mixture Data.* s.l.:Wiley.

Corporan, E. et al., 2005. *Impacts of synthetic jet fuel on the emissions of a turbine engine combustor.* Sitges, International Association for Stability, Handling and Use of Liquid Fuels, Inc., pp. 3-16.

Cutnell, J. D. & Johnson, K. W., 2004. *Physics.* 6th ed. Hoboken: Wiley & Sons, Inc.

Dassault Systemes, 2005a. *Materials Studio online help: Descriptor models: Spatial descriptors,* Vélizy-Villacoublay: Dassault Systemes.

Dassault Systemes, 2005b. *Materials Studio online help: Geometry optimisation,* Vélizy-Villacoublay: Dassault Systemes.

Dassault Systemes, 2005c. *Materials Studio online help: Vamp tutorial: Geometry optimisation and transition state calculation with VAMP,* Vélizy-Villacoublay: Dassault Systemes.

Dassault Systemes, 2005d. *Materials Studio online help:Topological descriptors,* Vélizy-Villacoublay: s.n.

Dassault Systemes, 2014. *BIOVA Matrials Studio VAMP datasheet.* [Online]
Available at: http://www. accelrys.com/products/datasheets/vamp.pdf
[Accessed 24 May 2016].

De Klerk, A., 2008. *Fischer-Tropsch refining.* Pretoria: UP (Thesis-PhD).

Demirbas, A. & Bamufleh, H. S., 2017. Optimization of crude oil refining products to valuable fuel blends. *Petroleum Science and Technology,* 35(4), pp. 406-412.

Derringer, G. & Suich, R., 1980. Simultaneous optimisation of several response variables. *Journal of Quality Technology,* Volume 12, pp. 214-219.

Espinosa, G. et al., 2001. A Fuzzy ARTMAP-Based Quantitative Structure-Property Relationship (QSPR) for Predicting Physical Properties of Organic Compounds. *Industrial & Engineering Chemistry Research,* Volume 40, pp. 2757-2766.

Flack, H. & Gavezzotti, A., 2005. *Crystal packing,* Chester: International union of crystallography.

Fortier, R., 2004. *The balloon era,* Ottawa: Canada Aviation Museum.

Honeywell Aerospace, 2016. *Auxiliary power units.* [Online]
Available at: https://aerospace.honeywell.com/product-listing/auxiliary-power-units
[Accessed 14 March 2016].

Johnson, C., 2005. *Molecular graph theory.* Massachusetts: WPI (Thesis-MSc).

Katrizky, A. R. et al., 1999. *Prediction of liquid viscosity for organic compounds by a quantitative structure-property relationship,* Flordia: University of Florida.

Katrizky, A. R. et al., 2010. Quantitative correlation of physical and chemical properties with chemical structure: Utility of prediction. *Chemical reviews,* 110(10), pp. 5714-5789.

King, R. K., 1987. *A graph theoretical and topological approach to chemical structure, reactivity and dynamics,* Athens, Georgia: U.S. office of Naval Research.

Laidler, K. J., Meiser, J. H. & Sanctuary, B. C., 2003. *Physical chemistry.* 4th ed. Boston: Houghton Mifflin Company.

Lawicki, D., 2002. *Jet fuel characteristics.* s.l., s.n.

Maddox, J., 2012. *Cold flow additives,* Milton Hill: Infineum.

Maier, S., 2005. Targeting the city: Debates and silences about aerial bombing of World War II. *International review of the Red Cross,* 87(859), pp. 429-444.

Marano, J. J. & Ciferno, J. P., 2001. *Life-cycle greenhouse-gas emissions inventory for Fischer-Tropsch fuels,* Washington, D.C.: U.S. Department of Energy.

McMurry, J. & Fay, R. C., 2004. *Chemistry.* 4th ed. New Jersey: Pearson education, Inc.

Molecular Networks GmbH, 2013. *Algorithms for the encoding of molecular structures,* Erlangen: Molecular networks GmbH.

Moses, C. A., Roets, P. N. J., Viljoen, C. L. & Wilson, G. R., 2009. *Effect of chemistry and boiling-point distribution on the properties and characteristics of synthesized paraffinic kerosene and blends with Jet A.* Prague, International Association for Stability, Handling and Use of Liquid Fuels, Inc., pp. 1-28.

NASA, 2002. *Celebrating a century of flight,* Washington, D.C.: NASA,

NASA, 2003. *Learning to fly: The Wright bothers' adventure,* Washington, D.C.: NASA.

Needham, D. E., Wei, I. C. & Seybold, P. G., 1988. Molecular modeling of the physical properties of alkanes. *Journal of the American Chemical Society,* 110(13), pp. 4186-94.

NMMU, 2011. *Innoventon: Bivariate regression for analysts, scientists and engineers.* Port Elizabeth: NMMU.

Novillo, E., Pardo, M. & Garcia-Luis, A., 2010. *Novel approaches for the integration of high temperature PEM fuel cells into aircrafts.* Brooklyn, NY, American Society of Mechanical Engineers, pp. 479-487.

Olsen, T., 2014. An oil refinery walk-through. *Chemical engineering progress,* May.pp. 33-40.

Parmaliana, A., Sanfilippo, D., Vaccari, A. & Arena, F., 1998. *Natural gas conversion.* 1st ed. Philadelphia: Elsevier Science.

Pilodist GmbH, n.d. *Pilodist GmbH website: Pilodist 104.* [Online]
Available at: www.pilodist.de/wp-content/uploads/2015/10/PILODIST-104.pdf
[Accessed 31 October 2016].

Ramanathan, R. & Turaga, U. T., 2003. Catalytic reforming: Revisiting its importance in the modern refinery. *Journal of scientific & industrial research,* Volume 62, pp. 963-978.

Rawat, S. & Sati, O. P., 2014. Melting point models of alkanes by using physico-chemical properties. *International Journal of Pharmacy and Life Sciences,* 5(1), pp. 3241-3245.

Riazi, M. R. & Al-Roomi, Y. A., 2000. *Minimum laboratory data for physical properties of hydrocarbon mixtures and petroleum products..* Washington, D.C., American Chemical Society, pp. PETR-039.

Robson, W. J. et al., 2017. Class Type Separation of the Polar and Apolar Components of Petroleum. *Analytical Chemistry,* 89(5), pp. 2919-2927.

SAPIA, 2008. *Petrol and diesel in South Africa and the impact on air quality.* Sandton: SAPIA.

Shimadzu Corporation, 2012. *Fundamental principles of comprehensive 2D GC.* Kyoto: Shimadzu Corporation.

Shi, Z. & Tao, Z., 2013. *The content of the iso-paraffins in jet fuel and its influence on properties.* Rhodes, International Association for Stability, Handling and Use of Liquid Fuels, Inc., pp. 1-4.

Simonoff, J. S., 2016. *Regression diagnostics.* [Online]
Available at: www.stern.nyu.edu/~jsimonof/classes/2301/pdf/diagnost.pdf
[Accessed 24 June 2016].

Stat-Ease, Inc., 2014. *Design-Expert Help:Mixture designs,* Minneapolos: Stat-Ease, Inc..

Stevanovic, D. & Zhou, B., 2006. *A note on Zagreb indices.* [Online]
Available at: https://draganstevanovic.files.wordpress.com/2012/09/z_s_102.pdf
[Accessed 24 October 2006].

Stranges, A. N., 2001. Germany's synthetic fuel industry. *ECAER Energeia,* 12(5), pp. 1-6.

Todeshini, R. & Consonni, V., 2000. *Handbook of molecular descriptors.* Winheim: Wiley-VCH Verlag GmbH.

Van der Laan, G. P., 1999. *Kinetics, selectivity and scale up of the Fischer-Tropsch Synthesis.* Groningen: University of Groningen (Thesis-PhD).

Van der Westhuizen, K. E., 2016. *GCxGC info [Correspondence].* Sasolburg: Sasol.

Viljoen, C. L., 2015. *High iso/-n- ratios are bad for low T viscosity [Correspondence],* Sasolburg: Sasol.

Wansbrough, H., n.d. *Refining crude oil.* [Online]
Available at: http://nzic.org.nz/ChemProcesses/energy/7A.pdf
[Accessed 28 October 2016].

Wood, D. A., Nwaoha, C. & Towler, B. F., 2012. Gas-to-Liquids (GTL): A review of an industry offering several routes for monetizing natural gas. *Journal of natural gas and engineering,* Volume 9, pp. 196-208.

Zhuze, T. P., 1951. The mechanism of action of the additions causing a lowering of the freezing temperature of paraffinic petroleum products. *Kolloidnyi Zhurnal,* Volume 13, pp. 27-37.

Appendix A

Table A.1. Results of the viscosity prediction model: Four molecular descriptors.

Molecule	Carbon number	Kinematic Viscosity (cSt)	Predicted viscosity (cSt)	Literature - Predicted viscosity (cSt)
n-Butane	n-C_4	0.26	0.23	0.03
iso-Butane	iso-C_4	0.28	0.21	0.06
n-Pentane	n-C_5	0.34	0.31	0.03
2-Methylbutane	iso-C_5	0.32	0.32	0.00
n-Hexane	n-C_6	0.41	0.45	-0.04
2-Methylpentane	iso-C_6	0.39	0.42	-0.02
3-Methylpentane	iso-C_6	0.39	0.42	-0.03
2,2-Dimethylbutane	iso-C_6	0.47	0.43	0.04
2,3-Dimethylbutane	iso-C_6	0.44	0.41	0.04
n-Heptane	n-C_7	0.51	0.54	-0.03
2-Methylhexane	iso-C_7	0.48	0.51	-0.04
3-Methylhexane	iso-C_7	0.45	0.53	-0.08
3-Ethylpentane	iso-C_7	0.44	0.49	-0.05
2,2-Dimethylpentane	iso-C_7	0.54	0.52	0.02
2,3-Dimethylpentane	iso-C_7	0.53	0.52	0.01
2,4-Dimethylpentane	iso-C_7	0.53	0.50	0.02
3,3-Dimethylpentane	iso-C_7	0.56	0.51	0.05
2,2,3-Trimethylbutane	iso-C_7	0.69	0.59	0.10
n-Octane	n-C_8	0.64	0.69	-0.05
2-Methylheptane	iso-C_8	0.56	0.63	-0.07
3-Methylheptane	iso-C_8	0.55	0.63	-0.08
4-Methylheptane	iso-C_8	0.53	0.63	-0.10
3-Ethylhexane	iso-C_8	0.53	0.58	-0.05
2,2-Dimethylhexane	iso-C_8	0.62	0.61	0.02
2,3-Dimethylhexane	iso-C_8	0.58	0.62	-0.04
2,4-Dimethylhexane	iso-C_8	0.71	0.59	0.11
3,3-Dimethylhexane	iso-C_8	0.59	0.59	-0.01
3,4-Dimethylhexane	iso-C_8	0.57	0.64	-0.07
2-Methyl-3-ethylpentane	iso-C_8	0.53	0.60	-0.07
2,2,3-Trimethylpentane	iso-C_8	0.68	0.63	0.05
2,2,4-Trimethylpentane	iso-C_8	0.60	0.61	0.00
2,3,3-Trimethylpentane	iso-C_8	0.70	0.69	0.02
2,3,4-Trimethylpentane	iso-C_8	0.68	0.63	0.05
n-Nonane	n-C_9	0.81	0.81	0.00
2,2,3,3-Tertamethylpentane	iso-C_9	0.81	0.79	0.03
n-Decane	n-C_{10}	1.01	1.00	0.01
n-Undecane	n-C_{11}	1.26	1.21	0.05
n-Dodecane	n-C_{12}	1.54	1.47	0.07
n-Tridecane	n-C_{13}	1.75	1.77	-0.01
n-Tetradecane	n-C_{14}	2.25	2.11	0.14
n-Pentadecane	n-C_{15}	2.49	2.56	-0.06
n-Hexadecane	n-C_{16}	2.92	3.01	-0.10
n-Heptadecane	n-C_{17}	3.58	3.53	0.05
n-Octadecane	n-C_{18}	4.13	4.08	0.05
n-Nonadecane	n-C_{19}	4.70	4.70	0.00
n-Eicosane	n-C_{20}	5.39	5.44	-0.04

Table A.2. Results of the viscosity prediction model (Four molecular descriptors): Dataset 1 + 2 (Predicting subset 3).

Molecule	Carbon number	Kinematic Viscosity (cSt)	Predicted viscosity (cSt)	Literature - Predicted viscosity (cSt)
n-Butane	n-C_4	0.26	0.23	0.03
2-Methylbutane	iso-C_5	0.32	0.32	0.00
3-Methylpentane	iso-C_6	0.39	0.42	-0.03
n-Heptane	n-C_7	0.51	0.54	-0.03
3-Ethylpentane	iso-C_7	0.44	0.49	-0.05
2,4-Dimethylpentane	iso-C_7	0.53	0.50	0.02
n-Octane	n-C_8	0.64	0.69	-0.05
4-Methylheptane	iso-C_8	0.53	0.63	-0.10
2,3-Dimethylhexane	iso-C_8	0.58	0.62	-0.04
3,4-Dimethylhexane	iso-C_8	0.57	0.64	-0.07
2,2,4-Trimethylpentane	iso-C_8	0.60	0.61	0.00
n-Nonane	n-C_9	0.81	0.81	0.00
n-Undecane	n-C_{11}	1.26	1.21	0.05
n-Tetradecane	n-C_{14}	2.25	2.11	0.14
n-Heptadecane	n-C_{17}	3.58	3.53	0.05
n-Eicosane	n-C_{20}	5.39	5.44	-0.04
iso-Butane	iso-C_4	0.28	0.21	0.06
n-Hexane	n-C_6	0.41	0.45	-0.04
2,2-Dimethylbutane	iso-C_6	0.47	0.43	0.04
2-Methylhexane	iso-C_7	0.48	0.51	-0.04
2,2-Dimethylpentane	iso-C_7	0.54	0.52	0.02
3,3-Dimethylpentane	iso-C_7	0.56	0.51	0.05
2-Methylheptane	iso-C_8	0.56	0.63	-0.07
3-Ethylhexane	iso-C_8	0.53	0.58	-0.05
2,4-Dimethylhexane	iso-C_8	0.71	0.59	0.11
2-Methyl-3-ethylpentane	iso-C_8	0.53	0.60	-0.07
2,3,3-Trimethylpentane	iso-C_8	0.70	0.69	0.02
2,2,3,3-Tertamethylpentane	iso-C_9	0.81	0.79	0.03
n-Dodecane	n-C_{12}	1.54	1.47	0.07
n-Pentadecane	n-C_{15}	2.49	2.56	-0.06
n-Octadecane	n-C_{18}	4.13	4.08	0.05
n-Pentane	n-C_5	0.34	0.31	0.03
2-Methylpentane	iso-C_6	0.39	0.42	-0.02
2,3-Dimethylbutane	iso-C_6	0.44	0.41	0.04
3-Methylhexane	iso-C_7	0.45	0.53	-0.08
2,3-Dimethylpentane	iso-C_7	0.53	0.52	0.01
2,2,3-Trimethylbutane	iso-C_7	0.69	0.59	0.10
3-Methylheptane	iso-C_8	0.55	0.63	-0.08
2,2-Dimethylhexane	iso-C_8	0.62	0.61	0.02
3,3-Dimethylhexane	iso-C_8	0.59	0.59	-0.01
2,2,3-Trimethylpentane	iso-C_8	0.68	0.63	0.05
2,3,4-Trimethylpentane	iso-C_8	0.68	0.63	0.05
n-Decane	n-C_{10}	1.01	1.00	0.01
n-Tridecane	n-C_{13}	1.75	1.77	-0.01
n-Hexadecane	n-C_{16}	2.92	3.01	-0.10
n-Nonadecane	n-C_{19}	4.70	4.70	0.00

Table A.3. Results of the viscosity prediction model (Four molecular descriptors): Dataset 2 + 3 (Predicting subset 1).

Molecule	Carbon number	Kinematic Viscosity (cSt)	Predicted viscosity (cSt)	Literature - Predicted viscosity (cSt)
iso-Butane	iso-C_4	0.28	0.21	0.06
n-Hexane	n-C_6	0.41	0.45	-0.04
2,2-Dimethylbutane	iso-C_6	0.47	0.43	0.04
2-Methylhexane	iso-C_7	0.48	0.51	-0.04
2,2-Dimethylpentane	iso-C_7	0.54	0.52	0.02
3,3-Dimethylpentane	iso-C_7	0.56	0.51	0.05
2-Methylheptane	iso-C_8	0.56	0.63	-0.07
3-Ethylhexane	iso-C_8	0.53	0.58	-0.05
2,4-Dimethylhexane	iso-C_8	0.71	0.59	0.11
2-Methyl-3-ethylpentane	iso-C_8	0.53	0.60	-0.07
2,3,3-Trimethylpentane	iso-C_8	0.70	0.69	0.02
2,2,3,3-Tertamethylpentane	iso-C_9	0.81	0.79	0.03
n-Dodecane	n-C_{12}	1.54	1.47	0.07
n-Pentadecane	n-C_{15}	2.49	2.56	-0.06
n-Octadecane	n-C_{18}	4.13	4.08	0.05
n-Pentane	n-C_5	0.34	0.31	0.03
2-Methylpentane	iso-C_6	0.39	0.42	-0.02
2,3-Dimethylbutane	iso-C_6	0.44	0.41	0.04
3-Methylhexane	iso-C_7	0.45	0.53	-0.08
2,3-Dimethylpentane	iso-C_7	0.53	0.52	0.01
2,2,3-Trimethylbutane	iso-C_7	0.69	0.59	0.10
3-Methylheptane	iso-C_8	0.55	0.63	-0.08
2,2-Dimethylhexane	iso-C_8	0.62	0.61	0.02
3,3-Dimethylhexane	iso-C_8	0.59	0.59	-0.01
2,2,3-Trimethylpentane	iso-C_8	0.68	0.63	0.05
2,3,4-Trimethylpentane	iso-C_8	0.68	0.63	0.05
n-Decane	n-C_{10}	1.01	1.00	0.01
n-Tridecane	n-C_{13}	1.75	1.77	-0.01
n-Hexadecane	n-C_{16}	2.92	3.01	-0.10
n-Nonadecane	n-C_{19}	4.70	4.70	0.00
n-Butane	n-C_4	0.26	0.23	0.03
2-Methylbutane	iso-C_5	0.32	0.32	0.00
3-Methylpentane	iso-C_6	0.39	0.42	-0.03
n-Heptane	n-C_7	0.51	0.54	-0.03
3-Ethylpentane	iso-C_7	0.44	0.49	-0.05
2,4-Dimethylpentane	iso-C_7	0.53	0.50	0.02
n-Octane	n-C_8	0.64	0.69	-0.05
4-Methylheptane	iso-C_8	0.53	0.63	-0.10
2,3-Dimethylhexane	iso-C_8	0.58	0.62	-0.04
3,4-Dimethylhexane	iso-C_8	0.57	0.64	-0.07
2,2,4-Trimethylpentane	iso-C_8	0.60	0.61	0.00
n-Nonane	n-C_9	0.81	0.81	0.00
n-Undecane	n-C_{11}	1.26	1.21	0.05
n-Tetradecane	n-C_{14}	2.25	2.11	0.14
n-Heptadecane	n-C_{17}	3.58	3.53	0.05
n-Eicosane	n-C_{20}	5.39	5.44	-0.04

Table A.4. Results of the viscosity prediction model (Four molecular descriptors): Dataset 1 + 3 (Predicting subset 2).

Molecule	Carbon number	Kinematic Viscosity (cSt)	Predicted viscosity (cSt)	Literature - Predicted viscosity (cSt)
n-Butane	n-C_4	0.26	0.23	0.03
2-Methylbutane	iso-C_5	0.32	0.32	0.00
3-Methylpentane	iso-C_6	0.39	0.42	-0.03
n-Heptane	n-C_7	0.51	0.54	-0.03
3-Ethylpentane	iso-C_7	0.44	0.49	-0.05
2,4-Dimethylpentane	iso-C_7	0.53	0.50	0.02
n-Octane	n-C_8	0.64	0.69	-0.05
4-Methylheptane	iso-C_8	0.53	0.63	-0.10
2,3-Dimethylhexane	iso-C_8	0.58	0.62	-0.04
3,4-Dimethylhexane	iso-C_8	0.57	0.64	-0.07
2,2,4-Trimethylpentane	iso-C_8	0.60	0.61	0.00
n-Nonane	n-C_9	0.81	0.81	0.00
n-Undecane	n-C_{11}	1.26	1.21	0.05
n-Tetradecane	n-C_{14}	2.25	2.11	0.14
n-Heptadecane	n-C_{17}	3.58	3.53	0.05
n-Eicosane	n-C_{20}	5.39	5.44	-0.04
n-Pentane	n-C_5	0.34	0.31	0.03
2-Methylpentane	iso-C_6	0.39	0.42	-0.02
2,3-Dimethylbutane	iso-C_6	0.44	0.41	0.04
3-Methylhexane	iso-C_7	0.45	0.53	-0.08
2,3-Dimethylpentane	iso-C_7	0.53	0.52	0.01
2,2,3-Trimethylbutane	iso-C_7	0.69	0.59	0.10
3-Methylheptane	iso-C_8	0.55	0.63	-0.08
2,2-Dimethylhexane	iso-C_8	0.62	0.61	0.02
3,3-Dimethylhexane	iso-C_8	0.59	0.59	-0.01
2,2,3-Trimethylpentane	iso-C_8	0.68	0.63	0.05
2,3,4-Trimethylpentane	iso-C_8	0.68	0.63	0.05
n-Decane	n-C_{10}	1.01	1.00	0.01
n-Tridecane	n-C_{13}	1.75	1.77	-0.01
n-Hexadecane	n-C_{16}	2.92	3.01	-0.10
n-Nonadecane	n-C_{19}	4.70	4.70	0.00
iso-Butane	iso-C_4	0.28	0.21	0.06
n-Hexane	n-C_6	0.41	0.45	-0.04
2,2-Dimethylbutane	iso-C_6	0.47	0.43	0.04
2-Methylhexane	iso-C_7	0.48	0.51	-0.04
2,2-Dimethylpentane	iso-C_7	0.54	0.52	0.02
3,3-Dimethylpentane	iso-C_7	0.56	0.51	0.05
2-Methylheptane	iso-C_8	0.56	0.63	-0.07
3-Ethylhexane	iso-C_8	0.53	0.58	-0.05
2,4-Dimethylhexane	iso-C_8	0.71	0.59	0.11
2-Methyl-3-ethylpentane	iso-C_8	0.53	0.60	-0.07
2,3,3-Trimethylpentane	iso-C_8	0.70	0.69	0.02
2,2,3,3-Tertamethylpentane	iso-C_9	0.81	0.79	0.03
n-Dodecane	n-C_{12}	1.54	1.47	0.07
n-Pentadecane	n-C_{15}	2.49	2.56	-0.06
n-Octadecane	n-C_{18}	4.13	4.08	0.05

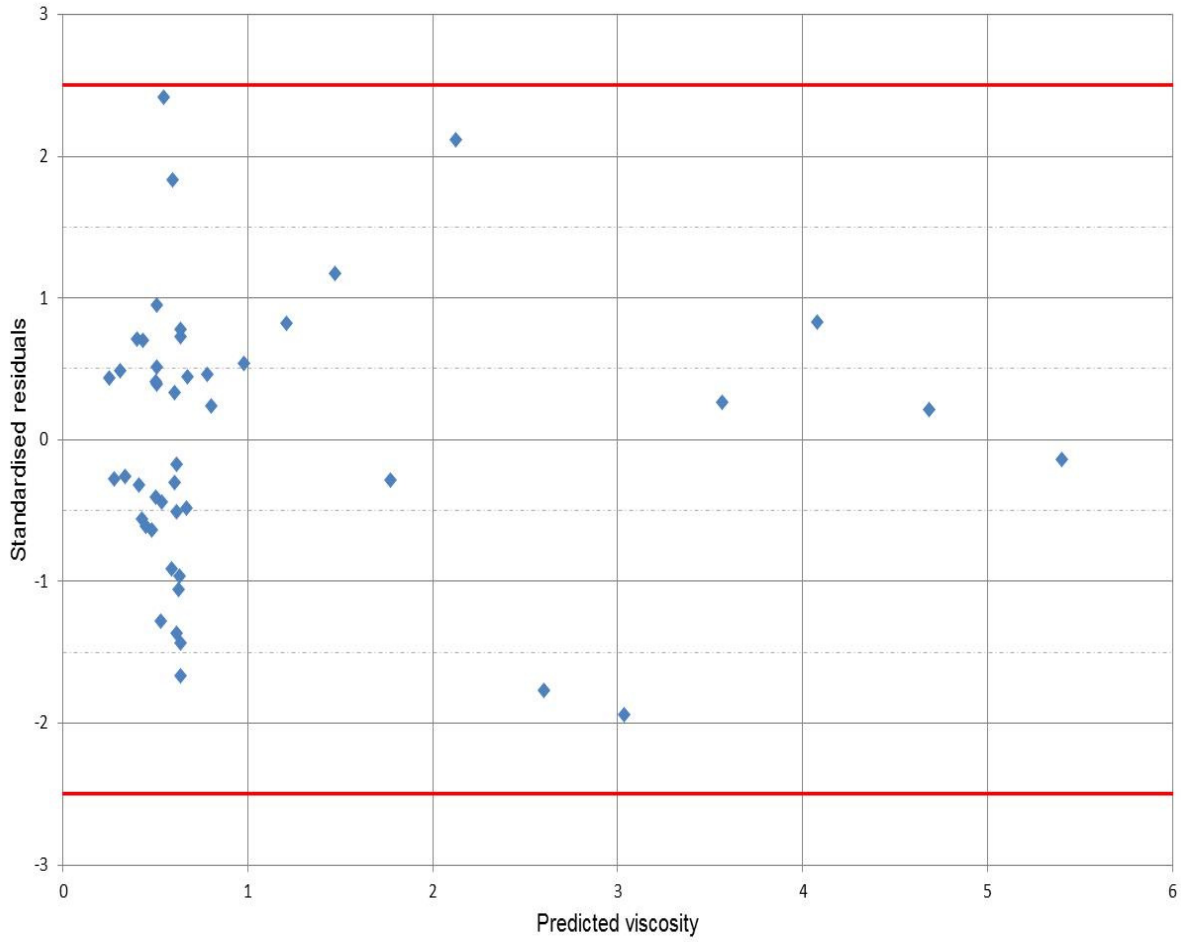

Figure A.1. Graph of standardised residuals versus predicted viscosity (Three descriptors).

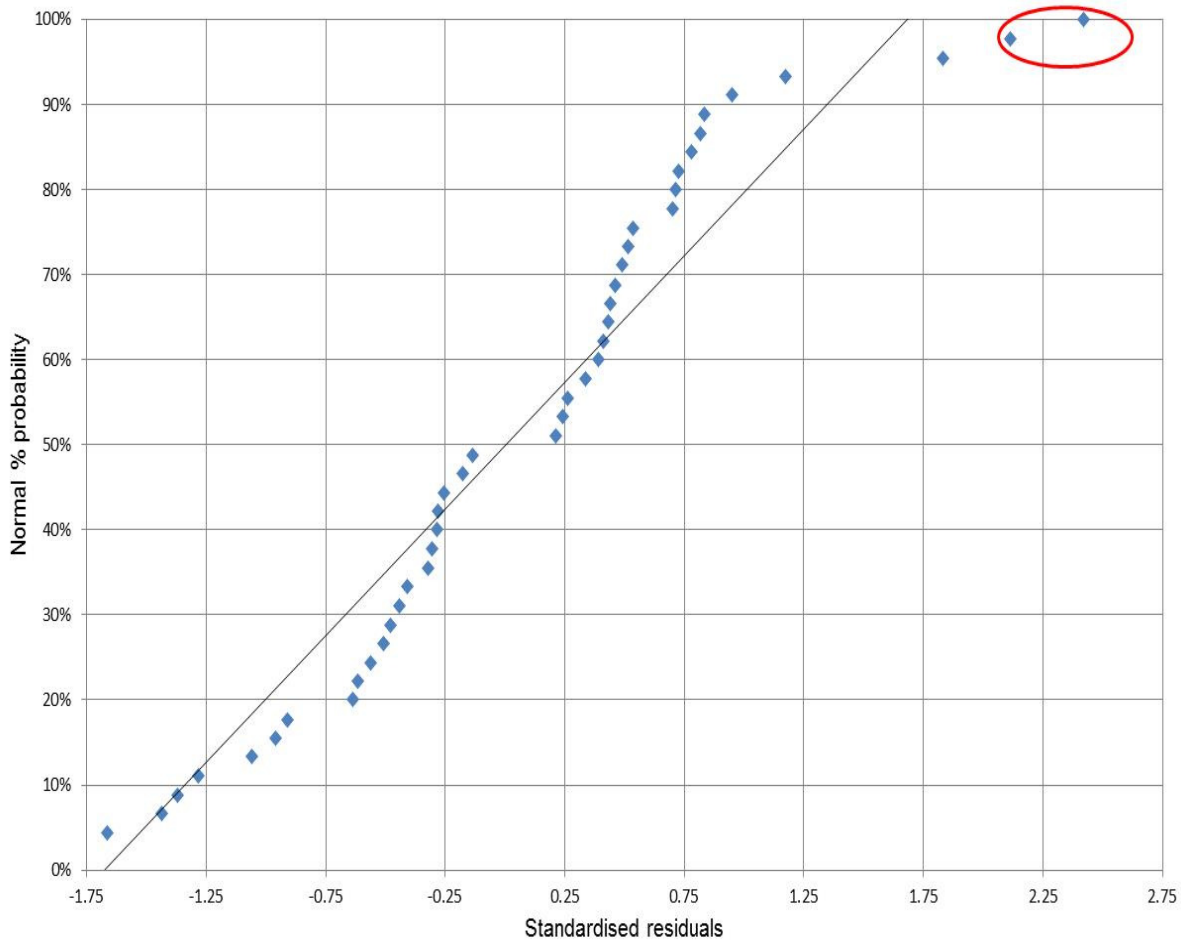

Figure A.2. Prediction model normal probability plot (Three molecular descriptors).

Table A.5. Statistics of the viscosity prediction model (Three molecular descriptors): Dataset 1 + 2 (Predicting subset 3).

Regression statistic				
R^2	0.99			
Adjusted R^2	0.99			
Standard Error	0.1			
			95% Confidence interval	
Parameter	**Coefficient**	**P-value**	**Lower 95%**	**Upper 95%**
Intercept	0.1952	0.0102	0.0502	0.3402
Molecular area (vd Waals)	-0.0125	0.0000	-0.0172	-0.0078
Molecular volume (vd Waals)	0.0182	0.0000	0.0124	0.0241
Principal moment of inertia Y	0.0003	0.0000	0.0003	0.0003

Table A.6. Statistics of the viscosity prediction model (Three molecular descriptors): Dataset 2 + 3 (Predicting subset 1).

Regression statistic				
R^2	0.99			
Adjusted R^2	0.99			
Standard Error	0.1			
			95% Confidence interval	
Parameter	**Coefficient**	**P-value**	**Lower 95%**	**Upper 95%**
Intercept	0.3876	0.0003	0.1972	0.5780
Molecular area (vd Waals	-0.0170	0.0000	-0.0224	-0.0116
Molecular volume (vd Waals)	0.0229	0.0000	0.0163	0.0294
Principal moment of inertia Y	0.0003	0.0000	0.0003	0.0004

Table A.7. Statistics of the viscosity prediction model (Three molecular descriptors): Dataset 1 + 3 (Predicting subset 2).

Regression statistic				
R^2	0.99			
Adjusted R^2	0.99			
Standard Error	0.1			
			95% Confidence interval	
Parameter	**Coefficient**	**P-value**	**Lower**	**Upper 95%**
Intercept	0.2366	0.0041	0.0817	0.3915
Molecular area (vd Waals)	-0.0147	0.0000	-0.0202	-0.0091
Molecular volume (vd Waals)	0.0209	0.0000	0.0138	0.0280
Principal moment of inertia Y	0.0003	0.0000	0.0003	0.0003

Table A.8. Results of the viscosity prediction model (Three molecular descriptors): Dataset 1 + 2 (Predicting subset 3).

Molecule	Carbon number	Kinematic Viscosity (cSt)	Predicted viscosity (cSt)	Literature - Predicted viscosity (cSt)
n-Butane	n-C_4	0.26	0.26	0.00
2-Methylbutane	iso-C_5	0.32	0.32	0.00
3-Methylpentane	iso-C_6	0.39	0.42	-0.02
n-Heptane	n-C_7	0.51	0.53	-0.03
3-Ethylpentane	iso-C_7	0.44	0.47	-0.03
2,4-Dimethylpentane	iso-C_7	0.53	0.49	0.03
n-Octane	n-C_8	0.64	0.67	-0.04
4-Methylheptane	iso-C_8	0.53	0.63	-0.10
2,3-Dimethylhexane	iso-C_8	0.58	0.61	-0.02
3,4-Dimethylhexane	iso-C_8	0.57	0.62	-0.05
2,2,4-Trimethylpentane	iso-C_8	0.60	0.60	0.00
n-Nonane	n-C_9	0.81	0.80	0.01
n-Undecane	n-C_{11}	1.26	1.23	0.03
n-Tetradecane	n-C_{14}	2.25	2.15	0.10
n-Heptadecane	n-C_{17}	3.58	3.58	0.00
n-Eicosane	n-C_{20}	5.39	5.41	-0.02
iso-Butane	iso-C_4	0.28	0.24	0.04
n-Hexane	n-C_6	0.41	0.44	-0.03
2,2-Dimethylbutane	iso-C_6	0.47	0.42	0.06
2-Methylhexane	iso-C_7	0.48	0.50	-0.02
2,2-Dimethylpentane	iso-C_7	0.54	0.50	0.04
3,3-Dimethylpentane	iso-C_7	0.56	0.49	0.07
2-Methylheptane	iso-C_8	0.56	0.63	-0.07
3-Ethylhexane	iso-C_8	0.53	0.59	-0.05
2,4-Dimethylhexane	iso-C_8	0.71	0.59	0.11
2-Methyl-3-ethylpentane	iso-C_8	0.53	0.60	-0.07
2,3,3-Trimethylpentane	iso-C_8	0.70	0.65	0.05
2,2,3,3-Tertamethylpentane	iso-C_9	0.81	0.77	0.04
n-Dodecane	n-C_{12}	1.54	1.50	0.05
n-Pentadecane	n-C_{15}	2.49	2.62	-0.12
n-Octadecane	n-C_{18}	4.13	4.10	0.03
n-Pentane	n-C_5	0.34	0.31	0.03
2-Methylpentane	iso-C_6	0.39	0.40	-0.01
2,3-Dimethylbutane	iso-C_6	0.44	0.39	0.05
3-Methylhexane	iso-C_7	0.45	0.52	-0.07
2,3-Dimethylpentane	iso-C_7	0.53	0.50	0.03
2,2,3-Trimethylbutane	iso-C_7	0.69	0.53	0.17
3-Methylheptane	iso-C_8	0.55	0.64	-0.09
2,2-Dimethylhexane	iso-C_8	0.62	0.60	0.02
3,3-Dimethylhexane	iso-C_8	0.59	0.60	-0.01
2,2,3-Trimethylpentane	iso-C_8	0.68	0.62	0.06
2,3,4-Trimethylpentane	iso-C_8	0.68	0.62	0.06
n-Decane	n-C_{10}	1.01	1.00	0.01
n-Tridecane	n-C_{13}	1.75	1.80	-0.04
n-Hexadecane	n-C_{16}	2.92	3.05	-0.14
n-Nonadecane	n-C_{19}	4.70	4.70	0.00

Table A.9. Results of the viscosity prediction model (Three molecular descriptors): Dataset 2 + 3 (Predicting subset 1).

Molecule	Carbon number	Kinematic Viscosity (cSt)	Predicted viscosity (cSt)	Literature - Predicted viscosity (cSt)
iso-Butane	iso-C_4	0.28	0.28	-0.01
n-Hexane	n-C_6	0.41	0.47	-0.06
2,2-Dimethylbutane	iso-C_6	0.47	0.45	0.02
2-Methylhexane	iso-C_7	0.48	0.51	-0.03
2,2-Dimethylpentane	iso-C_7	0.54	0.51	0.02
3,3-Dimethylpentane	iso-C_7	0.56	0.52	0.04
2-Methylheptane	iso-C_8	0.56	0.62	-0.06
3-Ethylhexane	iso-C_8	0.53	0.59	-0.05
2,4-Dimethylhexane	iso-C_8	0.71	0.59	0.11
2-Methyl-3-ethylpentane	iso-C_8	0.53	0.62	-0.09
2,3,3-Trimethylpentane	iso-C_8	0.70	0.70	0.01
2,2,3,3-Tertamethylpentane	iso-C_9	0.81	0.82	0.00
n-Dodecane	n-C_{12}	1.54	1.44	0.11
n-Pentadecane	n-C_{15}	2.49	2.57	-0.08
n-Octadecane	n-C_{18}	4.13	4.07	0.06
n-Pentane	n-C_5	0.34	0.33	0.01
2-Methylpentane	iso-C_6	0.39	0.43	-0.04
2,3-Dimethylbutane	iso-C_6	0.44	0.42	0.03
3-Methylhexane	iso-C_7	0.45	0.53	-0.09
2,3-Dimethylpentane	iso-C_7	0.53	0.52	0.01
2,2,3-Trimethylbutane	iso-C_7	0.69	0.57	0.12
3-Methylheptane	iso-C_8	0.55	0.64	-0.09
2,2-Dimethylhexane	iso-C_8	0.62	0.60	0.02
3,3-Dimethylhexane	iso-C_8	0.59	0.61	-0.02
2,2,3-Trimethylpentane	iso-C_8	0.68	0.65	0.03
2,3,4-Trimethylpentane	iso-C_8	0.68	0.65	0.03
n-Decane	n-C_{10}	1.01	0.95	0.06
n-Tridecane	n-C_{13}	1.75	1.74	0.02
n-Hexadecane	n-C_{16}	2.92	3.02	-0.10
n-Nonadecane	n-C_{19}	4.70	4.68	0.01
n-Butane	n-C_4	0.26	0.31	-0.05
2-Methylbutane	iso-C_5	0.32	0.36	-0.04
3-Methylpentane	iso-C_6	0.39	0.45	-0.05
n-Heptane	n-C_7	0.51	0.54	-0.03
3-Ethylpentane	iso-C_7	0.44	0.49	-0.05
2,4-Dimethylpentane	iso-C_7	0.53	0.51	0.01
n-Octane	n-C_8	0.64	0.66	-0.02
4-Methylheptane	iso-C_8	0.53	0.63	-0.10
2,3-Dimethylhexane	iso-C_8	0.58	0.62	-0.03
3,4-Dimethylhexane	iso-C_8	0.57	0.64	-0.07
2,2,4-Trimethylpentane	iso-C_8	0.60	0.62	-0.02
n-Nonane	n-C_9	0.81	0.76	0.05
n-Undecane	n-C_{11}	1.26	1.18	0.08
n-Tetradecane	n-C_{14}	2.25	2.09	0.17
n-Heptadecane	n-C_{17}	3.58	3.55	0.03
n-Eicosane	n-C_{20}	5.39	5.42	-0.02

Table A.10. Results of the viscosity prediction model (Three molecular descriptors): Dataset 1 + 3 (Predicting subset 2).

Molecule	Carbon number	Kinematic Viscosity (cSt)	Predicted viscosity (cSt)	Literature - Predicted viscosity (cSt)
n-Butane	n-C_4	0.26	0.26	0.00
2-Methylbutane	iso-C_5	0.32	0.32	-0.01
3-Methylpentane	iso-C_6	0.39	0.42	-0.03
n-Heptane	n-C_7	0.51	0.53	-0.02
3-Ethylpentane	iso-C_7	0.44	0.48	-0.04
2,4-Dimethylpentane	iso-C_7	0.53	0.50	0.03
n-Octane	n-C_8	0.64	0.66	-0.03
4-Methylheptane	iso-C_8	0.53	0.63	-0.10
2,3-Dimethylhexane	iso-C_8	0.58	0.61	-0.03
3,4-Dimethylhexane	iso-C_8	0.57	0.63	-0.06
2,2,4-Trimethylpentane	iso-C_8	0.60	0.61	-0.01
n-Nonane	n-C_9	0.81	0.78	0.03
n-Undecane	n-C_{11}	1.26	1.21	0.05
n-Tetradecane	n-C_{14}	2.25	2.13	0.12
n-Heptadecane	n-C_{17}	3.58	3.57	0.01
n-Eicosane	n-C_{20}	5.39	5.39	0.00
n-Pentane	n-C_5	0.34	0.30	0.04
2-Methylpentane	iso-C_6	0.39	0.40	-0.01
2,3-Dimethylbutane	iso-C_6	0.44	0.40	0.05
3-Methylhexane	iso-C_7	0.45	0.52	-0.07
2,3-Dimethylpentane	iso-C_7	0.53	0.51	0.03
2,2,3-Trimethylbutane	iso-C_7	0.69	0.54	0.15
3-Methylheptane	iso-C_8	0.55	0.64	-0.09
2,2-Dimethylhexane	iso-C_8	0.62	0.60	0.02
3,3-Dimethylhexane	iso-C_8	0.59	0.60	-0.02
2,2,3-Trimethylpentane	iso-C_8	0.68	0.64	0.04
2,3,4-Trimethylpentane	iso-C_8	0.68	0.64	0.05
n-Decane	n-C_{10}	1.01	0.98	0.03
n-Tridecane	n-C_{13}	1.75	1.78	-0.02
n-Hexadecane	n-C_{16}	2.92	3.04	-0.12
n-Nonadecane	n-C_{19}	4.70	4.68	0.02
iso-Butane	iso-C_4	0.28	0.24	0.04
n-Hexane	n-C_6	0.41	0.44	-0.03
2,2-Dimethylbutane	iso-C_6	0.47	0.42	0.05
2-Methylhexane	iso-C_7	0.48	0.50	-0.02
2,2-Dimethylpentane	iso-C_7	0.54	0.50	0.03
3,3-Dimethylpentane	iso-C_7	0.56	0.50	0.06
2-Methylheptane	iso-C_8	0.56	0.62	-0.06
3-Ethylhexane	iso-C_8	0.53	0.59	-0.06
2,4-Dimethylhexane	iso-C_8	0.71	0.59	0.11
2-Methyl-3-ethylpentane	iso-C_8	0.53	0.61	-0.08
2,3,3-Trimethylpentane	iso-C_8	0.70	0.68	0.03
2,2,3,3-Tertamethylpentane	iso-C_9	0.81	0.80	0.01
n-Dodecane	n-C_{12}	1.54	1.48	0.07
n-Pentadecane	n-C_{15}	2.49	2.60	-0.11
n-Octadecane	n-C_{18}	4.13	4.08	0.05

Appendix B

Table B.1. Statistics of the freeze point prediction model: Dataset 1 + 2 (Predicting subset 3).

Molecule	Carbon number	Freeze point (℃)	Predicted freeze point (℃)	Residual (℃) (Absolute)	Over/under predicted (%)
n-Butane	n-C_4	-138.4	-148.3	10.0	7.2
n-Hexane	n-C_6	-95.3	-97.8	2.5	2.6
2-Methylhexane	iso-C_7	-118.3	-121.1	2.8	2.4
2,2-Dimethylpentane	iso-C_7	-123.8	-126.9	3.1	2.5
n-Octane	n-C_8	-56.8	-62.1	5.3	9.4
4-Methylheptane	iso-C_8	-121.0	-107.8	13.2	10.9
2-Methyl-3-ethylpentane	iso-C_8	-115.0	-119.5	4.5	3.9
2,3,3-Trimethylpentane	iso-C_8	-100.9	-104.0	3.0	3.0
2-Methyloctane	iso-C_9	-80.4	-93.5	13.1	16.3
2,6-Dimethylheptane	iso-C_9	-102.9	-113.2	10.3	10.0
2,3,5-Trimethylhexane	iso-C_9	-127.8	-115.4	12.4	9.7
2,2-Dimethyl-3-ethylpentane	iso-C_9	-99.5	-104.8	5.3	5.3
2,3,3,4-Tetramethylpentane	iso-C_9	-102.1	-91.1	11.0	10.8
3-Methylnonane	iso-C_{10}	-84.8	-80.8	4.0	4.8
2,4-Dimethyl-3-isopropylpentane	iso-C_{10}	-81.7	-96.0	14.3	17.5
n-Tridecane	n-C_{13}	-5.4	-4.3	1.1	19.5
n-Hexadecane	n-C_{16}	18.6	17.5	1.1	5.7
n-Nonadecane	n-C_{19}	31.9	32.7	0.9	2.7
n-Pentane	n-C_5	-129.7	-118.9	10.8	8.3
2-Methylpentane	iso-C_6	-153.7	-138.7	15.0	9.7
3-Methylhexane	iso-C_7	-119.4	-121.1	1.7	1.4
2,4-Dimethylpentane	iso-C_7	-119.2	-133.4	14.2	11.9
2-Methylheptane	iso-C_8	-109.0	-108.1	0.9	0.8
2,2,-Dimethylhexane	iso-C_8	-121.2	-121.9	0.7	0.6
2,2,3-Trimethylpentane	iso-C_8	-112.3	-104.0	8.3	7.4
2,3,4-Trimethylpentane	iso-C_8	-109.2	-117.4	8.2	7.5
3-Methyloctane	iso-C_9	-107.6	-92.8	14.8	13.8
2,2,5-Trimethylhexane	iso-C_9	-105.8	-111.2	5.4	5.1
2,4,4-Trimethylhexane	iso-C_9	-113.4	-107.4	6.0	5.3
2,4-Dimethyl-3-ethylpentane	iso-C_9	-122.4	-116.2	6.2	5.1
n-Decane	n-C_{10}	-29.6	-34.4	4.8	16.1
5-Methylnonane	iso-C_{10}	-87.7	-80.0	7.7	8.7
n-Undecane	n-C_{11}	-25.6	-24.7	0.9	3.4
n-Tetradecane	n-C_{14}	5.9	3.1	2.8	47.7
n-Heptadecane	n-C_{17}	22.0	21.2	0.8	3.7
n-Eicosane	n-C_{20}	36.4	37.2	0.8	2.2
2-Methylbutane	iso-C_5	-159.9	-160.0	0.1	0.1
n-Heptane	n-C_7	-90.6	-80.2	10.4	11.5
3-Ethylpentane	iso-C_7	-118.6	-119.4	0.8	0.7
3,3-Dimethylpentane	iso-C_7	-134.5	-125.9	8.6	6.4
3-Methylheptane	iso-C_8	-120.5	-107.9	12.6	10.4
3,3-Dimethylhexane	iso-C_8	-126.1	-123.5	2.6	2.1
2,2,4-Trimethylpentane	iso-C_8	-107.4	-112.2	4.9	4.5
n-Nonane	n-C_9	-53.5	-47.5	6.0	11.2
2,2-Dimethylheptane	iso-C_9	-113.0	-117.7	4.7	4.1
2,3,3-Trimethylhexane	iso-C_9	-116.8	-106.2	10.6	9.1
3,3,4-Trimethylhexane	iso-C_9	-101.2	-105.5	4.3	4.3
2,2,4,4-Tetramethylpentane	iso-C_9	-66.5	-75.1	8.5	12.8
2-Methylnonane	iso-C_{10}	-74.7	-81.3	6.6	8.9
2,2,3,3-Tetramethylhexane	iso-C_{10}	-54.0	-72.6	18.6	34.5
n-Dodecane	n-C_{12}	-9.6	-13.5	3.9	40.8
n-Pentadecane	n-C_{15}	9.9	7.1	2.8	28.4
n-Octadecane	n-C_{18}	28.2	28.9	0.7	2.6

Table B.2. Statistics of the freeze point prediction model: Dataset 2 + 3 (Predicting subset 1).

Molecule	Carbon number	Freeze point (℃)	Predicted freeze point (℃)	Residual (℃) (Absolute)	Over/under predicted (%)
n-Pentane	n-C_5	-129.7	-125.5	4.2	3.3
2-Methylpentane	iso-C_6	-153.7	-145.0	8.7	5.7
3-Methylhexane	iso-C_7	-119.4	-126.7	7.3	6.1
2,4-Dimethylpentane	iso-C_7	-119.2	-137.3	18.0	15.1
2-Methylheptane	iso-C_8	-109.0	-112.3	3.3	3.0
2,2,-Dimethylhexane	iso-C_8	-121.2	-122.7	1.5	1.3
2,2,3-Trimethylpentane	iso-C_8	-112.3	-103.4	8.9	7.9
2,3,4-Trimethylpentane	iso-C_8	-109.2	-119.0	9.8	9.0
3-Methyloctane	iso-C_9	-107.6	-96.1	11.5	10.7
2,2,5-Trimethylhexane	iso-C_9	-105.8	-108.0	2.2	2.1
2,4,4-Trimethylhexane	iso-C_9	-113.4	-104.9	8.5	7.5
2,4-Dimethyl-3-ethylpentane	iso-C_9	-122.4	-115.6	6.7	5.5
n-Decane	n-C_{10}	-29.6	-36.8	7.1	24.0
5-Methylnonane	iso-C_{10}	-87.7	-82.1	5.6	6.4
n-Undecane	n-C_{11}	-25.6	-25.6	0.0	0.1
n-Tetradecane	n-C_{14}	5.9	4.8	1.0	17.5
n-Heptadecane	n-C_{17}	22.0	23.5	1.5	6.8
n-Eicosane	n-C_{20}	36.4	35.5	1.0	2.6
2-Methylbutane	iso-C_5	-159.9	-166.1	6.2	3.9
n-Heptane	n-C_7	-90.6	-85.4	5.2	5.7
3-Ethylpentane	iso-C_7	-118.6	-125.3	6.7	5.6
3,3-Dimethylpentane	iso-C_7	-134.5	-127.7	6.8	5.0
3-Methylheptane	iso-C_8	-120.5	-112.1	8.4	7.0
3,3-Dimethylhexane	iso-C_8	-126.1	-123.8	2.3	1.8
2,2,4-Trimethylpentane	iso-C_8	-107.4	-110.0	2.6	2.4
n-Nonane	n-C_9	-53.5	-51.0	2.5	4.7
2,2-Dimethylheptane	iso-C_9	-113.0	-117.3	4.3	3.8
2,3,3-Trimethylhexane	iso-C_9	-116.8	-103.8	13.0	11.1
3,3,4-Trimethylhexane	iso-C_9	-101.2	-103.2	2.0	2.0
2,2,4,4-Tetramethylpentane	iso-C_9	-66.5	-66.3	0.2	0.3
2-Methylnonane	iso-C_{10}	-74.7	-83.3	8.7	11.6
2,2,3,3-Tetramethylhexane	iso-C_{10}	-54.0	-64.3	10.3	19.1
n-Dodecane	n-C_{12}	-9.6	-13.5	3.9	40.6
n-Pentadecane	n-C_{15}	9.9	10.0	0.1	0.7
n-Octadecane	n-C_{18}	28.2	29.9	1.8	6.3
n-Butane	n-C_4	-138.4	-153.7	15.3	11.1
n-Hexane	n-C_6	-95.3	-104.0	8.7	9.1
2-Methylhexane	iso-C_7	-118.3	-126.8	8.5	7.2
2,2-Dimethylpentane	iso-C_7	-123.8	-128.6	4.8	3.9
n-Octane	n-C_8	-56.8	-66.7	9.9	17.5
4-Methylheptane	iso-C_8	-121.0	-111.9	9.0	7.5
2-Methyl-3-ethylpentane	iso-C_8	-115.0	-123.0	8.0	7.0
2,3,3-Trimethylpentane	iso-C_8	-100.9	-103.4	2.4	2.4
2-Methyloctane	iso-C_9	-80.4	-96.8	16.4	20.4
2,6-Dimethylheptane	iso-C_9	-102.9	-115.1	12.2	11.9
2,3,5-Trimethylhexane	iso-C_9	-127.8	-115.2	12.6	9.9
2,2-Dimethyl-3-ethylpentane	iso-C_9	-99.5	-102.7	3.2	3.2
2,3,3,4-Tetramethylpentane	iso-C_9	-102.1	-85.9	16.2	15.8
3-Methylnonane	iso-C_{10}	-84.8	-82.8	2.0	2.4
2,4-Dimethyl-3-isopropylpentane	iso-C_{10}	-81.7	-94.1	12.4	15.1
n-Tridecane	n-C_{13}	-5.4	-3.4	2.0	36.6
n-Hexadecane	n-C_{16}	18.6	19.7	1.1	5.7
n-Nonadecane	n-C_{19}	31.9	32.8	0.9	2.8

Table B.3. Statistics of the freeze point prediction model: Dataset 1 + 3 (Predicting subset 2).

Molecule	Carbon number	Freeze point (℃)	Predicted freeze point (℃)	Residual (℃) (Absolute)	Over/under predicted (%)
n-Butane	n-C_4	-138.4	-145.6	7.2	5.2
n-Hexane	n-C_6	-95.3	-98.9	3.6	3.8
2-Methylhexane	iso-C_7	-118.3	-122.8	4.5	3.8
2,2-Dimethylpentane	iso-C_7	-123.8	-126.1	2.3	1.8
n-Octane	n-C_8	-56.8	-63.5	6.7	11.8
4-Methylheptane	iso-C_8	-121.0	-108.5	12.4	10.3
2-Methyl-3-ethylpentane	iso-C_8	-115.0	-120.4	5.5	4.8
2,3,3-Trimethylpentane	iso-C_8	-100.9	-102.9	2.0	2.0
2-Methyloctane	iso-C_9	-80.4	-94.1	13.7	17.1
2,6-Dimethylheptane	iso-C_9	-102.9	-112.8	9.9	9.7
2,3,5-Trimethylhexane	iso-C_9	-127.8	-113.7	14.1	11.0
2,2-Dimethyl-3-ethylpentane	iso-C_9	-99.5	-102.4	2.9	2.9
2,3,3,4-Tetramethylpentane	iso-C_9	-102.1	-86.7	15.4	15.1
3-Methylnonane	iso-C_{10}	-84.8	-80.7	4.1	4.8
2,4-Dimethyl-3-isopropylpentane	iso-C_{10}	-81.7	-94.7	13.0	15.9
n-Tridecane	n-C_{13}	-5.4	-2.7	2.7	49.6
n-Hexadecane	n-C_{16}	18.6	19.4	0.8	4.0
n-Nonadecane	n-C_{19}	31.9	31.4	0.4	1.4
2-Methylbutane	iso-C_5	-159.9	-159.8	0.1	0.1
n-Heptane	n-C_7	-90.6	-81.2	9.4	10.3
3-Ethylpentane	iso-C_7	-118.6	-121.4	2.8	2.4
3,3-Dimethylpentane	iso-C_7	-134.5	-125.3	9.2	6.8
3-Methylheptane	iso-C_8	-120.5	-108.7	11.8	9.8
3,3-Dimethylhexane	iso-C_8	-126.1	-121.7	4.4	3.5
2,2,4-Trimethylpentane	iso-C_8	-107.4	-108.9	1.5	1.4
n-Nonane	n-C_9	-53.5	-48.5	5.0	9.4
2,2-Dimethylheptane	iso-C_9	-113.0	-115.6	2.6	2.3
2,3,3-Trimethylhexane	iso-C_9	-116.8	-103.4	13.4	11.4
3,3,4-Trimethylhexane	iso-C_9	-101.2	-102.9	1.7	1.7
2,2,4,4-Tetramethylpentane	iso-C_9	-66.5	-68.0	1.4	2.2
2-Methylnonane	iso-C_{10}	-74.7	-81.2	6.6	8.8
2,2,3,3-Tetramethylhexane	iso-C_{10}	-54.0	-66.7	12.7	23.4
n-Dodecane	n-C_{12}	-9.6	-12.4	2.8	29.2
n-Pentadecane	n-C_{15}	9.9	10.3	0.4	4.3
n-Octadecane	n-C_{18}	28.2	28.9	0.8	2.7
n-Pentane	n-C_5	-129.7	-119.3	10.5	8.1
2-Methylpentane	iso-C_6	-153.7	-140.0	13.7	8.9
3-Methylhexane	iso-C_7	-119.4	-122.7	3.3	2.8
2,4-Dimethylpentane	iso-C_7	-119.2	-133.8	14.5	12.2
2-Methylheptane	iso-C_8	-109.0	-108.9	0.1	0.1
2,2,-Dimethylhexane	iso-C_8	-121.2	-120.7	0.5	0.4
2,2,3-Trimethylpentane	iso-C_8	-112.3	-102.9	9.3	8.3
2,3,4-Trimethylpentane	iso-C_8	-109.2	-117.4	8.2	7.5
3-Methyloctane	iso-C_9	-107.6	-93.4	14.2	13.2
2,2,5-Trimethylhexane	iso-C_9	-105.8	-107.2	1.5	1.4
2,4,4-Trimethylhexane	iso-C_9	-113.4	-104.4	9.0	7.9
2,4-Dimethyl-3-ethylpentane	iso-C_9	-122.4	-114.1	8.3	6.8
n-Decane	n-C_{10}	-29.6	-34.8	5.2	17.5
5-Methylnonane	iso-C_{10}	-87.7	-80.0	7.7	8.7
n-Undecane	n-C_{11}	-25.6	-23.9	1.6	6.4
n-Tetradecane	n-C_{14}	5.9	5.2	0.6	10.5
n-Heptadecane	n-C_{17}	22.0	23.0	1.0	4.7
n-Eicosane	n-C_{20}	36.4	33.7	2.7	7.5